ROLE OF THE THERMODYNAMIC REGIME IN ECOSYSTEM SELF-ORGANIZATION AND ITS RESPONSE TO HUMAN PERTURBATIONS

BY

MEREDITH L. RICHARDSON

DISSERTATION

Submitted in partial fulfillment of the requirements
for the degree of Doctor of Philosophy in Civil Engineering
in the Graduate College of the
University of Illinois Urbana-Champaign, 2021

Urbana, Illinois

Doctoral Committee:

Professor Praveen Kumar, Chair
Associate Professor Ashlynn S. Stillwell
Professor Ximing Cai
Professor Andrew Leakey
Professor Jon Chorover, University of Arizona

ABSTRACT

As the rate and scale of human activities increase throughout the world, the structure and function of Earth systems are consequently altered. Human-induced direct and indirect perturbations, such as changes in atmospheric temperature or the burning or logging of vegetation, alter the thermodynamic environment in which ecosystems operate. Yet, the ecosystem-level vegetation response is coupled to its thermodynamic regime, and changes therein are still relatively unknown. Thus, a framework for characterizing and understanding self-organization of ecosystem vegetation from the thermodynamic perspective is needed to understand its emergent response to natural and human-induced perturbations.

The goals of this thesis are to (i) develop a thermodynamic framework to characterize the existence of emergent vegetation structure at any given location, and (ii) utilize this framework to gain insight about the thermodynamic response of ecosystem behavior to direct alteration of vegetation structure through human activities. Vegetation structure, which refers to the number and type of plant functional groups comprising an ecosystem, is the result of self-organization, or the spontaneous emergence of order from random fluctuations. By treating ecosystems as open thermodynamic systems, we use a multi-layer canopy-root-soil model to calculate their thermodynamic properties – such as energy, entropy, and work – for field sites across various climates, vegetation structures, and disturbance regimes.

We first ask the question: *Why do ecosystems exhibit a prevalence of vegetation structure consisting of multiple functional groups?* In other words, does the coexistence of multiple functional groups provide a thermodynamic advantage over the individual functional groups that each ecosystem comprises. From this work, we conclude that ecosystems self-organize towards the multiple functional group vegetation structure due to greater fluxes of entropy, work, and work efficiency. Together, these characteristics comprise the concept of thermo-

dynamic advantage.

Since multiple functional groups do not exist everywhere in nature, we study and analyze the thermodynamic basis for the existence of ecosystems with a single functional group vegetation structure – in particular, the region beyond the treeline in alpine and Arctic ecosystems. We therefore ask the question: *Since the existence of multiple vegetation groups provides a thermodynamic advantage, is the existence of only a single functional group a result of a thermodynamic limitation?* This analysis using counterfactual scenarios comprising of hypothetical trees existing beyond the treeline identifies two conditions of thermodynamic infeasibility. We find that existence of trees beyond the treeline would result in negative work, and in some cases, net leaf carbon loss from the ecosystem, both comprising a thermodynamic infeasibility condition.

Based on these two components, we conclude that an ecosystem will self-organize towards the most advantageous vegetation structure made possible by thermodynamic feasibility.

These concepts of thermodynamic feasibility and thermodynamic advantage are then applied to study ecosystems perturbed by human activities through logging and fire. Findings indicate that a forest that is consistently logged is held in a sub-optimal state with lower fluxes of entropy and work efficiency than an undisturbed forest, meaning that human activities prevent the ecosystem from reaching its most thermodynamically advantageous vegetation structure. However, for controlled burns on a tallgrass prairie the advantageous vegetation structure is dependent on the frequency of the burn. Overall, logging events force forests into a disadvantageous vegetation structure while the frequency of burn events determines and reinforces the resulting vegetation structure.

This thesis develops a novel framework for analyzing ecosystems as thermodynamic systems driven by thermodynamic feasibility and thermodynamic advantage. Further, by characterizing the behavior of vegetation upon direct alterations to its structure, this work provides foundation for understanding and predicting the thermodynamic response of vegetation structure to emergent climate scenarios that could impact the thermodynamic environment in which ecosystems operate.

This dissertation is dedicated in loving memory of my grandfather, Dr. Flavious Joseph Smith, Sr. (1929-2020), the former Chairperson of the Department of Exercise Science, Physical Education, and Wellness at Tennessee Technological University for 34 years, whose career in academia inspired me to pursue a PhD of my own.

ACKNOWLEDGMENTS

I would like to acknowledge to my outstanding advisor, Praveen Kumar, for his support and keen ability to continue to push me to improve, sometimes without my awareness. The advisor a student has through their graduate school can either make or break one's experience, and I cannot imagine how it could have been any better. I would also like to thank my committee members – Ashlynn Stillwell, Ximing Cai, Andrew Leakey, and Jon Chorover – for sharing their unique perspective and insights to broaden my thinking and enhance my research. I am grateful to the Kumar Hydrocomplexity Research Group through the years. Many thanks to former Kumarians, Allison Goodwell, Qina Yan, Phong Le, Dongkook Woo, Debsunder Dutta, and Peishi Jiang, for setting the bar high and sharing all the wisdom I could handle before you graduated. Thank you to Susana Roque-Malo, for fighting through this process with me since we started bright-eyed on day one in 2014. Many thanks to Esther Lee, Leila Hernández, and Kunxuan Wang for the advice, coding expertise, and guidance shared over the past spent five to seven years we have spent working together. Afeefa and Tarun, good luck, and keep the legacy going! Further, I am grateful for my PhD squad, Susana Roque-Malo, Lana Stekovic, and Gioella Chaparro, for the study sessions, encouragement, and shared celebrations necessary for completing the PhD.

Last but not least, thank you to my family. I cannot thank my parents, Dave and René Richardson, enough for instilling in me at a young age to expect greatness from myself and not to question it. Thanks, Dad, for convincing me that engineering was a good way to go! Thank you to my fiancé, Curtis Martin, who has continually pushed me to work harder since the day we met. This work was supported in part by the coffee you made for me every morning throughout the dissertation writing process. I cannot wait to take on life with you as The Drs. Martin.

With respect to funding, this work has been supported by NSF grant EAR 1331906 for the Intensively Managed Landscapes Critical Zone Observatory (IML CZO) with additional support from NSF grants EAR 1417444 and ICER 1440315, EAR 2012850, and OAC 1835834 and NASA Fellowship grant NNX13AO46H. Oliver Sonnentag from the Université de Montréal provided eddy covariance, precipitation, and leaf area index data as well as site expertise and data processing for the Western Canadian Taiga-Tundra sites, HPC and TVC. John Knowles of the University of Arizona provided site expertise in locating and processing of the various datasets for the United States Rocky Mountains sites, T-Van and NR1. Bryan Conrad from the University of Kansas provided insight into the vegetation and site dynamics of the Konza Prairie sites, KON and KFB.

TABLE OF CONTENTS

CHAPTER 1

INTRODUCTION

Together, water and energy availability have been utilized for decades to study ecohydrologic response through concepts such as the Budyko curve to capture the influence of various climates that exist throughout the world [1, 2]. However, vegetation itself has strong feedbacks with climate, and many researchers have argued that vegetation properties, such as above-ground biomass, rooting structure, and photosynthetic capacity, are vital in understanding the controls of the various climatic regimes [3–5]. Further, as the rate and scale of human activities increase throughout the world, the structure and function of Earth systems are being significantly altered. Human-induced perturbations, such as changes in atmospheric temperature or the burning or logging of vegetation, alter the thermodynamic environment in which ecosystems operate. Yet, the ecosystem-level vegetation response to thermodynamic regime changes is still relatively unknown. This thesis focuses on the thermodynamic behavior of ecosystems explicitly. We explore natural and human-induced self-organization of vegetation using model-based computation of thermodynamic properties of ecosystems at several field sites across the globe. By viewing ecosystems as open thermodynamic systems, we calculate their entropy produced and work performed, which can allow us to characterize thermodynamic variations among ecosystems and document trends of influence from human activities.

This thesis develops a novel framework for analyzing ecosystems as thermodynamic systems that self-organize to vegetation structure found in nature based on thermodynamic advantage and thermodynamic feasibility, two concepts developed as an outcome of this research. Here, we define vegetation structure in terms of the number and type of plant functional groups, i.e., sets of species that perform similar functions in an ecosystem [6], aggregated based on literature [7–10] to balance model accuracy with performance. Examples

of functional groups include evergreen needleleaf trees, shrubs, and grasses.

The fields of ecology and biology have established how plants grow, but have yet to comprehensively answer the questions: *What causes the spontaneous emergence of vegetation structure? What drives the existence of different vegetation structures?* The concepts of entropy, work, and work efficiency provide an answer to these questions in the form of thermodynamic advantage. We propose thermodynamic advantage and thermodynamic feasibility as an additional but critical dimension – along with resource availability pertaining to water and nutrients – to further our understanding of ecosystems with the goal that it will enable us to better characterize the non-stationary trajectory and feedback between vegetation and climate. Thermodynamic advantage indicates that a vegetation structure yields a thermal environment that is more favorable than that of another vegetation structure, deeming it more probable to exist through self-organized processes (see Section 1.2). On the other hand, thermodynamic feasibility indicates which vegetation structures are able to be supported by the thermal environment at a given location (see Section 1.3). Furthermore, this framework provides insight into trends in ecosystem behavior as a result of human perturbations, such as controlled burns or selective logging, which alter vegetation structure directly and thereby its resulting thermodynamic environment. The ability to anticipate these trends could have broad implications for the sustainability of ecosystems and their life-supporting services as anthropogenic modifications to landscapes continue to increase.

The components of this thesis are, therefore, grounded in these three interrelated concepts: open thermodynamic systems, thermodynamic advantage, and thermodynamic feasibility. Research in open thermodynamic systems forms the basis for capturing ecosystem response to external forcing and describing how ecosystems naturally self-organize into different structured forms, or stable states. The vegetation structure to which an ecosystem will self-organize is then determined through thermodynamic advantage if all structures considered are feasible. Lastly, the concept of thermodynamic feasibility is vital for determining the viable vegetation structure at a given location. These concepts lay the groundwork for the research presented in Chapters 2-4.

1.1 Ecosystem Thermodynamics

Ecosystems can be categorized as open thermodynamic systems held far from equilibrium. Far-from-equilibrium systems are maintained by the spatial imbalance of energy due to inputs and outputs of energy and mass from the external environment. The formation of internal system order in the form of dissipative structures (e.g., vegetation structure that dissipates the incident energy) enables energy to disperse more rapidly along gradients from high to low temperature throughout the system control volume [11, 12]. The formation of dissipative structures is a self-organized outcome, meaning that this organization emerges without external predetermination. The local emergence of order corresponds to establishment of low local entropy which results in overall greater spatial balance of energy throughout the control volume, and a higher release of entropy from the control volume to the surrounding environment [11]. *Entropy* – a function of the associated energy flux and the temperature of that energy flux's source [13–18] – is a measure of thermodynamic disorder, but can also be a measure of proximity to equilibrium in closed systems [12]. However, in far-from-equilibrium open systems, entropy's value has yet to be fully understood.

This thesis builds upon the work initiated by Quijano [18], who examined the entropy produced by an ecosystem through model simulations with canopy, roots, and soil included in the control volume. The entropy of multi-species ecosystems was compared through simulated stages of evolutionary development, ultimately finding that the most developed ecosystems resulted in the most entropy production. Rather than comparing the evolution or stages of development of an ecosystem, the present work seeks to identify a framework to understand to which preferred state an ecosystem will self-organize under different conditions. In this work, the organized state considered is the ecosystem's vegetation structure. Yet, we found that entropy alone cannot succeed in answering this question. Thus, we look to other thermodynamic properties to examine different developed vegetation structures and additional determinants of vegetation self-organization.

The concept of identifying an ecosystem's 'optimal' thermodynamic state has been studied in several different variations. Jørgensen approached the problem from the ecological and biological perspectives [19, 20], utilizing concepts such as exergy and eco-exergy to cat-

egorize the available free energy used by ecosystems such that an ecosystem will evolve to optimize its eco-exergy [21, 22]. Exergy is defined as the ability of a system to perform work upon returning to equilibrium, and eco-exergy is the equivalent of exergy with respect to ecosystems, defined as the ability of the ecosystem to perform work relative to the same ecosystem existing at thermodynamic equilibrium [21]. Thus, the estimation for eco-exergy (Ex) is defined as a relative difference in chemical energy associated with the biomass of components in the two ecosystems:

$$Ex = \sum_{c} (\mu_c - \mu_{c_0}) N_i \tag{1.1}$$

where c represents all of the components in the ecosystem, N_i are the moles of chemical compounds, and $(\mu_c - \mu_{c_0})$ is the difference in chemical potential between the ecosystem and its reference state in thermodynamic equilibrium [21]. The components included are those being directly compared. In terms of ecosystem vegetation structure, use of this formulation would only take into account the change in chemical energy associated with the total plant biomass in the ecosystem rather than considering the interactions among functional groups and their associated impact to the temperature profile or thermal environment within the ecosystem. Further, this computation requires the knowledge of an equivalent ecosystem in equilibrium – similar to an 'inorganic soup' [21] with no lifeforms – which is impossible to estimate. Therefore, this perspective does not allow for estimation of the eco-exergy of an ecosystem on a scale or level of detail beneficial for comparing changes in vegetation structure.

Schneider and Kay [11] presented an alternative interpretation of optimality in far-from-equilibrium systems, characterized by their ability to degrade their exergy. They presented the concept that all self-organized systems are formed to deplete their "applied gradients" of mass and energy from the external environment. Still, this perspective requires the quantification of exergy, which similar to eco-exergy is not feasible beyond orders of magnitude, deeming it not useful for the comparison of different vegetation structures [21, 22]. While Jørgensen's principle asserts that an ecosystem will evolve to increase its eco-exergy, or ability to perform work, Schneider and Kay assert that ecosystems will evolve by quickly

forming dissipative structures to rapidly and efficiently deplete their dominant gradients and degrade their exergy. We take into consideration these interpretations of the second law of thermodynamics but by quantifying the actual work performed by an ecosystem.

1.2 Thermodynamic Advantage

This work provides the first characterization of thermodynamic work performed by various ecosystems through site-specific model simulations. We present the concept of thermodynamic advantage to diagnose an ecosystem's thermodynamic behavior based on the self-organized structure and response to human-induced perturbations through calculations enabled by modeled ecosystem fluxes of energy. The concept of thermodynamic advantage – demonstrated through entropy, work, and work efficiency – is used as a means to diagnose the most probable self-organized vegetation structure at a given location.

The dominant gradient driving ecosystems is associated with the vertical temperature profile, which is a result of self-organized dynamics of vegetation and local environmental conditions in response to incoming radiation, where vegetation itself is the dissipative structure that disperses heat [11]. The temperature gradient in this case corresponds to the difference between the temperature of the earth surface and the temperature of the air just above the canopy. During photosynthesis, vegetation releases heat from the ecosystem as latent heat through evapotranspiration and temperature dependent sensible heat, decreasing outgoing radiation and resulting in a weaker temperature gradient. Thus, presence of vegetation results in a negative feedback between heat dissipation and temperature gradient in which heat dissipation leads to a reduction in temperature gradient.

In classical thermodynamics, *work* is defined as the energy associated with motion. In an ecosystem, the direct work from solar radiation is the energy used for photosynthesis, but other forms of motion also take place (e.g., diffusion, convection, advection). Since quantification of all internal motion within an ecosystem is infeasible, indicators of work from the ecosystem as a whole are required. As a consequence of internal work in the system, ecosystems transport and dissipate heat. Thus, in the context of ecosystems, we define *work* as the flux of energy through heat transported along a temperature gradient,

estimated as the net sum of latent and sensible heat fluxes throughout the ecosystem in the direction of the resultant temperature gradient (Equation 3.2). Since the ecosystem heat loss due to water infiltration below the root zone is negligible, it is ignored in calculations of work.

In Chapter 2, we coin the term *work efficiency* as the ratio of work performed by an ecosystem as a fraction of the incoming radiation. Greater work efficiency means that an ecosystem is better able to dissipate the incoming energy into useful forms of work, resulting in a weaker temperature gradient. Intuitively, we expect ecosystems with more plant functional groups – corresponding to more complex dissipative structures with greater capacity for latent and sensible heat transport – to produce more total entropy and perform more work, resulting in a higher work efficiency than ecosystems having only one plant functional group. However, we find that greater entropy or work efficiency does not always correspond to the most advantageous structure. Thus, the concepts of entropy, work, and work efficiency when analyzed altogether define a vegetation structure's thermodynamic advantage. Chapter 2 establishes thermodynamic advantage as a framework for vegetation structure emergence and the coexistence of multiple plant functional groups.

1.3 Thermodynamic Feasibility

While thermodynamic advantage provides a framework to explain the widely prevalent existence of multiple functional groups, there are some circumstances in which only one functional group exists in nature. For example, in an Arctic tundra or an alpine meadow above the treeline, trees are absent and shrubs or grasses dominate the landscape. The concept of thermodynamic feasibility, or more, the thermodynamic infeasibility that hinders the existence of multiple functional groups, arises. In Chapter 3, environments above and below Arctic and alpine treelines are explored, and findings indicate that multiple functional groups do not exist beyond a treeline due to thermodynamic infeasibility. These results indicate that if trees were to exist, they would create a thermal environment that would make their existence infeasible. Since vegetation consistently dissipates heat through evapotranspiration, these environments would result in negative work indicating that dissipative

structures in the form of trees dissipate more heat than is needed for the incoming radiation and create local imbalance of energy within the ecosystem. Thus, when trees are forced to exist in an alpine ecosystem through model simulations, the resulting temperature gradient becomes negative, such that (i) the vegetation would actually transport energy in the opposite direction of the vertical temperature gradient, and (ii) eventually there would be no more heat to dissipate, and the vegetation would not have the ability to transpire (release latent heat), both of which are thermodynamically infeasible.

Another way to capture this infeasibility is the concept of *potential dissipation capacity* – "the maximum possible heat dissipation rate supported by the thermodynamic environment of an ecosystem, determined by its incoming radiation and other local environmental conditions" (Chapter 4). A vegetation structure will only self-organize when its dissipation rate is equivalent to or below the potential dissipation capacity of an ecosystem. When the dissipation of the vegetation is larger than the potential dissipation capacity, due to greater leaf area or higher photosynthesis rates, the vegetation structure is then thermodynamically infeasible. Overall, we may conclude that the vegetation structure to which an ecosystem will self-organize will: first, be thermodynamically feasible, and second, exhibit a thermodynamic advantage over other feasible alternative vegetation structures.

1.4 Dissipation Deficit

Thermodynamic advantage and thermodynamic feasibility characterize how natural ecosystems will self-organize. However, when human activities impact ecosystems, self-organization is no longer the only determinant of vegetation structure. In particular, vegetation structure can be directly altered by removing vegetation through activities such as logging and controlled burns. After such a disturbance event occurs, the ecosystem no longer exists in a state governed by self-organization. Instead, it is forced to exist in a structure that may perform significantly below its optimal thermodynamically advantageous state. Ecologists have long asserted that natural ecosystems self-organize towards the state that optimizes their thermodynamic exchanges with their environment [11, 20, 22–25]. Thus, we consider a natural quasi-stable ecosystem as existing in an optimal thermodynamically advantageous

state. We demonstrate a loss in optimality due to human perturbation as resulting in a dissipation deficit. Presence of a one-time or recurring disturbance event can cause an ecosystem to perform sub-optimally, meaning vegetation has been removed, decreasing the leaf area and ability of the ecosystem to perform work and dissipate heat at its optimal rate (its potential dissipation capacity, D_p). An ecosystem's dissipation deficit (D_d) is defined as the difference between its potential dissipation capacity and its actual dissipation rate (D_a), the net sum of ecosystem latent and sensible heat fluxes, such that $D_d = D_p - D_a$ (see Section 4.2.3). Dissipation deficit allows for comparison and determination of how poorly a disturbed ecosystem performs work relative to its natural thermodynamically advantageous state, or vegetation structure.

Chapter 4 uses these concepts to explore the thermodynamic behavior of ecosystems that incur direct alteration to vegetation structure in the form of recurring selective logging in the Brazilian Amazon and varying frequencies of controlled burns in the Kansas Konza Prairie. These studies highlight the important feedback loops among vegetation structure, disturbance events, and the thermal environment that are useful for understanding the self-organization of vegetation structure in ecosystems that experience direct human-induced perturbations. Negative feedback loops among these components emerge in response to a recurring burn cycle and reinforce the existing vegetation structure. Alternatively, a forest experiencing recurring logging events yields significant dissipation deficits associated with thermodynamically disadvantageous vegetation structure compared to an undisturbed site. The forest is unable to recover from the disturbance event on the timescale equivalent its recurrence. Therefore, the feedback loops are out of sync, and the logged forest is held in a sub-optimal thermodynamic state.

1.5 Model Simulations

Throughout this thesis, a multi-layer canopy-root-soil model, MLCan [26–28], is used to calculate thermodynamic properties – such as energy, entropy, and work – for field sites across various climates, vegetation structures, and disturbance regimes. The use of this sophisticated model with multiple layers above and below ground is necessary to accurately

estimate the thermodynamic behavior throughout the ecosystem. As vegetation structure varies, the radiation regime through the canopy is consequently altered, resulting in variable temperatures throughout the canopy. Latent heat, sensible heat, work, and entropy are calculated based on the temperature of each layer within the canopy and on the soil surface. Therefore, resolving the thermal regime throughout the canopy in addition to the fluxes produced by each layer, is necessary for accurately characterizing thermodynamic advantage and feasibility of differing vegetation structures.

Additionally, MLCan is chosen because of its ability to capture multi-species or multiple functional group interactions [28]. Taller vegetation casts shade upon the shorter understory vegetation, thereby determining the understory's thermodynamic environment. This model enables characterization of the thermodynamic and mass balance interactions between functional groups, such that we can accurately estimate changes in thermodynamic properties for different vegetation structures. Since MLCan is a one-dimensional model that satisfies the vertical profile of an ecosystem, we assume an ecosystem's vegetation structure consists of spatially uniform composition and pattern on the landscape at a given location.

To apply MLCan to ecosystems in cold regions, such as an Arctic tundra or alpine meadow, additional parameterizations and formulations were incorporated. For example, soil thermal conductivity is typically computed based on its percentages of sand and clay. However, peat soils that are found above permafrost in Arctic regions do not behave as other soils do with respect to thermal and hydraulic conductivity. Therefore, new parameterizations were incorporated into the model for peat soil [29–31]. Extremely cold temperatures also required a new formulation to prevent plant and soil water uptake when soils were considered frozen. Furthermore, alpine and Arctic vegetation hibernate during winter months and do not photosynthesize below certain temperatures, when the soil is completely frozen, or when snowpack is deeper than the height of the canopy (as is the case in an Arctic tundra or alpine meadow) [32–34]. Additional model adjustments were made to emulate this behavior. Further information pertaining to model updates can be found in Appendix A.2.2. These modeling advances enabled the comparisons of alpine and Arctic ecosystems with subalpine and sub-Arctic ecosystems, such that the existence of trees beyond a treeline was identified as thermodynamically infeasible.

Through model simulations that enable comparisons of vegetation structure across the globe, we accomplish the following goals of this thesis: (i) develop a thermodynamic framework to characterize the existence of emergent vegetation structure at any given location, and (ii) utilize this framework to gain insight about the thermodynamic response of ecosystem behavior to direct alteration of vegetation structure through human activities.

1.6 Research Contributions

This thesis addresses the following questions related to the self-organization of vegetation structure:

1. Does the existence of multiple functional groups offer a thermodynamic advantage?
2. Is the non-existence of trees beyond the region demarcated as a treeline a reflection of thermodynamic infeasibility associated with the presence of trees?
3. How does the act and frequency of vegetation structural alteration from human activities affect ecosystem thermodynamic behavior?

Through these questions, this study presents the following original contributions:

1. This work provides the first characterization of thermodynamic work performed by various ecosystems through site-specific model simulations for direct comparison of vegetation structure.
2. Thermodynamic advantage is presented as a framework and explanation for the existence and prevalence of multiple functional groups in nature.
3. Thermodynamic feasibility is identified as a mechanism for understanding the existence of individual functional groups (or non-existence of multiple functional groups) in nature.
4. Thermodynamic feasibility is established as an important and complementary condition to resource availability for vegetation self-organization.

5. Thermodynamic feasibility constraints, such as temperature inversions and sustained negative work, are presented as examples of expressions that arise when modeling an infeasible vegetation structure at a given site.

6. Modeling and observation of burned and logged ecosystems identify feedback loops between disturbance events and vegetation as important expressions of thermodynamic behavior following direct alteration to ecosystem vegetation structure.

7. Modeling advances are identified such that the multi-layer-canopy model, MLCan, could be applied to cold region processes and ecosystems.

1.7 Organization

The chapters of this thesis are arranged as follows:

- In Chapter 2, the coexistence of multiple functional groups is explored. Thermodynamic advantage is defined as a vegetation structure that produces larger fluxes of entropy, performs more work, and yields higher work efficiency. From this work, we conclude that ecosystems will self-organize towards the multiple functional group vegetation structure due to its thermodynamic advantage, given local availability of energy, water, and nutrients.

- In Chapter 3, alpine and Arctic ecosystems in which only one functional group exists are explored. Counterfactuals are constructed such that forest vegetation is modeled on alpine and Arctic study sites. Two conditions of infeasibility are identified for this counterfactual, both of which arise due to insufficient energy availability in the lower canopy and earth surface through much of the year. This chapter portrays thermodynamic feasibility as an important constraint on vegetation structure that must be considered amongst resource availability and thermodynamic advantage. Further, the implications of negative work on thermodynamic advantage is discussed, and the idea that a vegetation structure can be a stronger dissipator than needed by a given ecosystem is introduced.

- In Chapter 4, we compare two cases in which vegetation structure is manually perturbed. These two cases impact the stability of the current vegetation structure of their respective ecosystems very differently. Logging events force forests into a disadvantageous vegetation structure while the frequency of burn events determines and reinforces the resulting vegetation structure. This chapter presents a novel analysis of the thermodynamic response of ecosystem vegetation structure at the site level, providing a foundation for understanding ecosystem thermodynamic response in future emergent climate scenarios.

- In the Appendix, supplementary information is provided for Chapters 2 and 3 pertaining to model implementation, including additional results, validation, and model parameters.

CHAPTER 2

DISCERNING THE THERMODYNAMIC FEASIBILITY OF THE SPONTANEOUS COEXISTENCE OF MULTIPLE FUNCTIONAL VEGETATION GROUPS

2.1 Introduction[1]

Presence of vegetation on our planetary surface, when resources of water and nutrients are not limiting, is a ubiquitous feature. Often different plant species utilize niche space to create a plurality of simultaneous existence through competitive and/or symbiotic sharing of resources. The spontaneous emergence of such complexity across a range of climates suggests that this self-organization should be thermodynamically viable. We propose that thermodynamics can provide insights that can bolster scientific understanding of the coexistence of multiple vegetation species or functional groups within an ecosystem. By viewing ecosystems as open thermodynamic systems, we are able to calculate their entropy, which can allow us to identify possible thermodynamic drivers for the spontaneous emergence of complex vegetation structure.

The concept of viewing organisms and other natural phenomena as webs of open thermodynamic systems has been utilized across scientific disciplines for several decades. Prigogine [36, 37] and other chemists, physicists, and biologists studied and developed the ideas of open thermodynamic systems in the early twentieth century with the goal of conceptualizing the growing complexity of organisms and other biological systems. They discovered that this complexity comprises of a hierarchy of irreversible processes leading to systematic organization which maintains the system in a state far from thermodynamic equilibrium [36–41]. Soon the idea of system theory was extended to other natural systems including ecological and earth systems [42–44]. It became understood that ecosystems can be categorized as open thermodynamic systems existing far from thermodynamic equilibrium maintained

[1]This chapter is published as an article in *Nature Scientific Reports*: Richardson & Kumar, 2020 [35]

by the spatial imbalance of energy in the form of state variables, such as temperature or geopotential height [11, 45]. Energy and mass naturally flow along gradients from high to low concentrations, and more rapid dissipation of these gradients is made possible by the formation of structures [11, 25, 44]. These so-called dissipative structures give the system a form of organization that emerges without external directive or predetermination, called self-organization [12]. This local self-organization results in low local entropy and greater overall system entropy due to the dissipation of the driving gradient and the decreasing spatial heterogeneity of the associated state variables [11, 36]. Such dissipative structures spontaneously emerge through self-organization, which can be exemplified in Earth systems from convection cells on the global scale to vegetation on the local scale [11, 45].

Ecologists further expanded these ideas to understand the direction of ecosystem evolution and quantify the distance of a system from equilibrium [46–48]. Concepts such as exergy and eco-exergy have been fruitful for the understanding of relative stages of ecosystem development and developing thermodynamic principles of ecology, such as the irreversible nature of ecosystem processes and the increasing disequilibrium of ecosystems [19–21, 49–51]. However, exact quantifications of exergy are not feasible due to the requirement of the knowledge of the equivalent ecosystem in equilibrium – similar to an 'inorganic soup' [21] with no life-forms. Thus, when comparing differences in similar ecosystems based on the composition of functional groups, a new framework must be developed.

While growth and development of ecosystems has been studied from the thermodynamic perspective, the thermodynamic basis for the self-organization towards one dissipative structure over another remains unexplored. This chapter seeks to fill this gap in understanding by comparing the thermodynamic behavior of different possible vegetation structures for a given ecosystem to identify if one results in a thermodynamic advantage over others.

We characterize ecosystem composition and vegetation structure in terms of the number and type of plant functional groups present. A plant functional group corresponds to a set of species that perform similar functions [6]. We accept the existence of an observed vegetation structure as a probabilistic, self-organized outcome. However, little has been done to compare the prospects of other vegetation scenarios that do not emerge. The probabilistic set of possible vegetation structures at a given site is based on the available energy, nutrients,

and water. We seek clarity on this topic by adding an additional parameter – thermodynamic advantage. We utilize work and entropy flux as metrics to compare thermodynamic behavior and determine if a certain vegetation structure has a thermodynamic advantage over others, thereby making it more probable. In classical mechanics, work is defined as the energy required for motion or the "the flow of heat" for heat engines in particular [12]; for ecosystems, we interpret this existing definition to estimate work as the sum of the latent and sensible heat leaving the system (i.e., the energy leaving the system through molecular motion of water vapor and air molecules). In these systems, self-organization in the form of vegetation emerges as a result of the heat dissipation throughout the vertical temperature gradient between the atmosphere at the top of the canopy and the soil-surface. Work is a measure of the ability of an ecosystem (by way of vegetation) to diminish this temperature gradient through the redistribution of heat. The entropy flux leaving an ecosystem – calculated from its temperature and outgoing energy flux – is a measure of the disorder of the outgoing energy, or the inability of this energy to perform work. However, high outgoing entropy flux does not always mean that more work has been performed. Longwave radiation has high entropy, but it is not a component of work; it is a form of radiative energy that is a passive response to the temperature state of its source and leaves the control volume without directly affecting the distribution of heat throughout the vertical profile. Thus, it is wasted energy. To distinguish between work and wasted energy, we introduce the concept of work efficiency as the work performed for the amount of radiation entering the ecosystem. Work efficiency measures an ecosystem's ability to effectively dissipate the incoming energy throughout the ecosystem through conversion of energy into alternate forms. Ecosystems with greater work efficiency more effectively decrease the temperature gradient imposed on the ecosystem, giving the ecosystem a thermodynamic advantage. Since entropy flux and work efficiency are not equivalent, both metrics are important for the interpretation of thermodynamic advantage.

Our premise is that ecosystems with more plant functional groups – corresponding to more complex dissipative structures – produce more total entropy and perform more work, resulting in a higher work efficiency than ecosystems having only one plant functional group. This leads to our main research question: *Does the existence of multiple functional groups*

offer a thermodynamic advantage?

To address this question, we model and compare the thermodynamic behavior of representative ecosystems consisting of multiple functional groups with that of hypothetical single-functional-group scenarios comprising of the individual native functional groups that make up the coexisting multiple functional groups. This is with the acknowledgement that the energy, water, and nutrients at each site support the existing functional groups. We do not alter the biomass or any additional parameters of these individual functional groups when modeled individually because we do not know how the energy, nutrients, and water of the ecosystem would support additional growth of these species if the others did not exist. Self-organization is non-linear, subject to chance outcomes to which we cannot predict how the alternative ecosystem would be structured. Thus, we compare the multi-group scenario with the known composition of the individual functional groups as they are observed to discern if there are advantages that promote the thermodynamic feasibility, or drivers towards the existing multi-group scenario. Using an open thermodynamic system framework and a 1-dimensional multi-layer canopy model (MLCan) which has been widely used and validated [26–28, 52–55], we simulate three climatologically-different natural ecosystems to determine the energy and entropy fluxes across the ecosystem control volume consisting of the canopy, roots, and soil (Fig. A.1). Energy fluxes considered are shortwave and longwave radiation, and sensible and latent heat. The model calculates the energy and entropy fluxes in each layer over a two-year study period, 2004-2005. These years were chosen based on continuous data availability in order to use the same study period across all study sites. Entropy flux, work, and work efficiency at each timestep (half-hourly or hourly) are then calculated as the net sum over all 21 layers (20 canopy layers and 1 layer for the ground surface) to complete the ecosystem level analysis, providing a description of thermodynamic behavior that is able to capture the subtle differences among different simulation scenarios.

Three sites from the FLUXNET2015 dataset [56] are modeled: Santa Rita Mesquite (SRM) in Arizona, Willow Creek (WCR) in Wisconsin, and Tapajos National Forest (TAP) in Pará, Brazil (Fig. A.2) [57–59]. The SRM and WCR sites are modeled with two functional groups based on the composition of their dominant vegetation, and the TAP vegetation is divided into four functional groups (based on the details in Domingues et al. [7]). For sim-

plicity, the functional groups are abbreviated as: understory (UN), mid-canopy trees (MT), overstory trees (OT), and lianas (L). The scenario with multiple functional groups is abbreviated as MG. Site-specific classifications can be found in Table A.1 of Appendix A.1. At each location we compare the existing scenario of vegetation consisting of multiple functional groups with hypothetical scenarios of each one of the individual functional groups present. For all scenarios, we calculate the entropy flux (J_{eco}; see Equation 2.7), work (W; see Equation 2.11), and work efficiency (WE; see Equation 2.13). We define thermodynamic advantage as the production of larger entropy fluxes as well as greater work efficiency by the ecosystem as a whole. *We hypothesize that the multiple-functional-group systems are more thermodynamically advantageous than or similar to their respective single-group scenarios.*

2.2 Methods

2.2.1 Experimental design

A multi-layer canopy-root-soil model (MLCan) [27, 52, 53] is used to calculate the energy and entropy fluxes for three climatologically-different ecosystems containing multiple functional groups: water-limited Santa Rita Mesquite (SRM), energy-limited Willow Creek (WCR), and nutrient-limited Tapajos National Forest (TAP) [60].

MLCan takes site-specific parameters and weather forcing data and computes the energy and entropy fluxes and temperatures for each of the ecosystem layers. Entropy calculations are based on both the energy fluxes and temperature of soil, air, and leaves (see *Entropy Calculations*). The model is run for a simulation period of two years (2004-2005) at a half-hourly timescale for SRM and WCR and an hourly timescale for TAP due to data availability. Weather forcing data were downloaded from FLUXNET2015: air temperature, air pressure, global radiation, precipitation, wind speed, friction velocity, and relative humidity [57–59]. Additional model input parameters can be found in Table A.2 of the *Supplementary Information*.

The initial soil moisture and temperature profiles for each of the sites – and snow properties for WCR – were produced from a spin-up of the model. The WCR and TAP sites used 2004

LAI with 2003 forcing data for a spin-up of two years to provide the initial conditions for the beginning of the 2004 simulation. For the SRM site, the FLUXNET2015 data were not available for 2003, so 2004 data were used instead.

At each site, the model splits up the vegetation into plant functional groups. Domingues et al. [7] demonstrates the importance of modeling ecosystems based on functional groups. For WCR and SRM, the vegetation is represented by understory herbaceous species and overstory trees. For TAP, a high biodiversity ecosystem in Amazonia, the vegetation is further divided and represented by four groups: understory tree, mid-canopy tree, upper-canopy tree, and upper-canopy liana [7]. See Table A.1 of the *Supplementary Information* for functional group abbreviations.

The LAI data for all sites are taken from MODIS [61] and calibrated based on site documentation (Fig. A.4 of the *Supplementary Information*). The LAI is then partitioned into two or four components based on the number of functional groups at each site. Additional LAI information can be found in Appendix A.1.

MLCan has been previously validated for each of the sites considered [55, 62]. Since entropy cannot be directly measured, we provide a comparison of the model outputted latent heat fluxes with the observed fluxes at each site in Fig. A.5 of the *Supplementary Information* for additional validation.

2.2.2 Site descriptions

The SRM site is located on the Santa Rita Experimental Range in southern Arizona (31.8214°N, 110.8661°W). SRM has a hot semi-arid climate and consists of woody savannas with mesquite trees (*Prosopis velutina* Woot.) and C4 grasses and subshrubs [62, 63].

The WCR (Willow Creek) site is located within the Chequamegon-Nicolet National Forest in northern Wisconsin (45.8059°N, 90.0799°W) with a northern continental climate. It is a deciduous broadleaf forest dominated by sugar maple (*Acer saccharum* Marsh.) with understory shrubs, including bracken ferns (*Pteridium aquilinum*), and overstory seedlings and saplings [64–66].

The TAP (Tapajos National Forest) site data is taken from the Santarem Km 67 Primary

Forest site located in Belterra, Pará, Brazil (2.8567°S, 54.9589°W). This evergreen broadleaf forest in Amazonian Brazil has a tropical monsoon climate with vegetation consisting of dozens of known tree species and lianas [7, 55].

2.2.3 Entropy calculations

Entropy calculations are based on model-simulated temperature and energy at each of the 20 canopy layers and the soil-surface layer, and results are scaled up to the ecosystem level. No lateral exchange of fluxes are considered. The net sum of energy fluxes from all layers of the ecosystem is equivalent to the total flux of energy across the boundary of the control volume (Fig. A.1 of the *Supplementary Information*). These energy fluxes include shortwave radiation (SW), longwave radiation (LW), latent heat (LE), and sensible heat (H). All results are categorized as the flux of energy at the boundary entering (SW_{in}, LW_{in}) or leaving (SW_{out}, LW_{out}, LE, H) the ecosystem. Because the total energy flux across the ecosystem boundary is equal to the sum across the canopy layers in the model, the total entropy flux across the boundary can also be taken as the cumulative sum of the entropy fluxes from all layers of the ecosystem.

Entropy flux calculations are summarized in Table 2.1. All energy variables have units of W/m^2, entropy variables are in W/m^{2}K, and temperatures are in K.

Entropy for LE and H calculations are based on simple heat transfer. The change in entropy is:

$$dS = \frac{dQ}{T} \tag{2.1}$$

where dQ is change in heat and T is temperature [13]. Thus, the flux of entropy for a given energy flux (E) across a boundary is:

$$J = \frac{E}{T}. \tag{2.2}$$

However, thermal radiation (SW and LW) cannot be treated this simply. The entropy flux for blackbody radiation is:

$$J_{BR} = \frac{4}{3}\sigma T^3 = \frac{4}{3}\frac{E_{BR}}{T} \tag{2.3}$$

where σ is the Stefan-Boltzmann constant, and E_{BR} is the blackbody radiation flux defined

Table 2.1: Entropy Calculations

Energy Category	Symbol	Entropy Equation
Latent Heat	J_{LE}	$\frac{E_{LE}}{T_{eq,LE}}$
Sensible Heat	J_H	$\frac{E_H}{T_{eq,H}}$
Direct Shortwave	$J_{SWdirect}$	$\frac{4}{3}\frac{E_{SWdirect}}{T_{sun}}$
Incoming Longwave	J_{LWin}	$\frac{4}{3}\frac{E_{LWin}}{T_{atm}} \times X(\epsilon)$
Outgoing Longwave	J_{LWout}	$\frac{4}{3}\frac{E_{LWout}}{T_{eq,LWout}} \times X(\epsilon)$
Diffuse Shortwave	$J_{SWdiffuse}$	$\frac{4}{3}\frac{E_{SWdiffuse}}{T_{sun}} \times X(\xi)$

X: reflection factor as a function of ξ or ϵ from Landsberg and Tongue [15] and Wright et al. [16].
ξ: dilution factor based on scattering [14, 15, 17, 18]
ϵ: emissivity
T_{sun}: temperature of the sun (5760K)
T_{atm}: observed atmospheric temperature
$T_{eq,j}$: equivalent temperature of the system for energy category $j \in \{LW_{out}, LE, H\}$; see Equation 2.5

as σT^4 from the Stefan-Boltzmann Law [13, 14].

SW is considered blackbody radiation, and entropy fluxes for direct shortwave radiation ($J_{SW\,direct}$) can be obtained by Equation 2.3. However, LW is considered non-blackbody radiation, also called 'diluted blackbody radiation', which must include an additional factor $X(\epsilon)$ to account for the entropy produced during the 'diluted emission' of radiation given by an object's emissivity, ϵ. This factor is defined as [15, 16]:

$$X(\epsilon) = 1 - \Big[\frac{45}{4\pi^4}\ln(\epsilon)(2.336 - 0.26\epsilon)\Big]. \tag{2.4}$$

Although $SW_{diffuse}$ is still a blackbody radiation, it has been demonstrated [17] that the entropy flux due to $SW_{diffuse}$ can be treated similarly to non-blackbody radiation with a new variable, ξ, in place of emissivity. ξ is the 'dilution factor' of radiation due to scattering, meaning it is the ratio of diffuse solar radiance on Earth's surface to solar radiance in extraterrestrial space [17]. Since diluted blackbody radiation ($SW_{diffuse}$) is mathematically equivalent to non-blackbody radiation (LW) when the dilution factor is equal to the emissivity, ξ can also be plugged into Equation 2.4 to solve for the amplifying factor of entropy production due to scattering, $X(\xi)$ [14–16, 18].

Each of the entropy calculations in Table 2.1 have a temperature value corresponding to the temperature of the energy's source. For instance, shortwave radiation originates from the sun, so the source temperature in its equations is T_{sun}. Likewise, longwave radiation is assumed to originate from the atmosphere, leading to a corresponding temperature of T_{atm}. However, LW_{out}, LE, and H do not have a single source location, so we must calculate an equivalent temperature (T_{eq}) for each energy category based on the modeled temperatures and weighted contribution of each layer to the total energy flux at the ecosystem boundary. The equivalent temperatures for these three energy categories are calculated as follows:

$$T_{eq,j} = \sum_{k=1}^{21}[T_k \times \omega_{j,k}] \tag{2.5}$$

where $T_{eq,j}$ is the equivalent temperature of energy category j such that $j \in \{LW_{out}, LE, H\}$. k refers to the layer in the ecosystem such that layers 1-20 are the canopy layers, and layer

21 refers to the ground surface. T_k is the temperature of layer k, and $\omega_{j,k}$ is the weight of energy category j coming from layer k given by:

$$\omega_{j,k} = \frac{E_{j,k}}{E_{j,eco}} \tag{2.6}$$

where $E_{j,k}$ is the energy j leaving layer k, and $E_{j,eco}$ is the total energy j leaving the ecosystem.

The total entropy flux of the ecosystem (J_{eco}) is calculated by summing the energy categories:

$$J_{eco} = \sum J_j + J_{SWout} \tag{2.7}$$

where J_{SWout} is the entropy flux of diffuse shortwave radiation leaving the ecosystem. The entropy flux per unit energy (EUE) is another way to view the thermodynamic state of ecosystem vegetation. EUE is calculated as:

$$EUE_j = \frac{J_j}{E_j} \tag{2.8}$$

where EUE_j is the entropy per unit energy in 1/K of energy category j. It follows that the corresponding $EUE_{SWout} = J_{SWout}/E_{SWout}$, and the total ecosystem EUE is:

$$EUE_{eco} = \frac{\sum J_j + J_{SWout}}{\sum E_j + E_{SWout}} \tag{2.9}$$

2.2.4 Work calculations

Work in an ecosystem represents the energy required to directly perform motion in the form of heat, effectively decreasing the temperature gradient within the ecosystem. We assume that LE and H are the primary regulators of temperature within a natural ecosystem, and LW_{out} is wasted energy. Additionally, we assume that the bottom of the control volume is sufficiently deep that at the boundary the temperature is consistent and there is no loss of heat (i.e., ground heat flux is ignored). Thus, work is estimated and calculated directly from

LE, H, and change in internal energy due to photosynthesis, ΔQ:

$$W = LE + H + \Delta Q \tag{2.10}$$

where ΔQ is significantly less than LE and H and can be ignored. So work can be simplified to:

$$W = LE + H \tag{2.11}$$

Since work represents the ability of an ecosystem's vegetation to deplete the driving temperature gradient imposed upon the ecosystem, our analysis compares work with temperature gradient. We define temperature gradient as:

$$\frac{\Delta T}{\Delta z} = \frac{T_{surf} - T_{air}}{h_e} \tag{2.12}$$

where T_{surf} is the temperature of the soil surface, T_{air} is the temperature of the air in the top layer of the ecosystem, and h_e is the ecosystem height (see Table A.2 in the *Supplementary Information*).

Work efficiency is the work performed for the amount of radiation entering the ecosystem defined as:

$$WE = \frac{LE + H}{E_{SWin} + E_{LWin}} = \frac{W}{E_{in}} \tag{2.13}$$

Since each vegetation functional group partitions energy differently among the energy categories, work efficiency is a good way to compare thermodynamic behavior across model scenarios at each site in a normalized way.

2.3 Results

The distributions of entropy fluxes at each timestep and the distributions of daily work efficiency for the two-year study period are shown in Fig. 2.1. The three sites have different ranges of entropy fluxes and work efficiencies due to distinctions in the local availabilities of water, energy, and nutrients. WCR, SRM, and TAP have relatively energy-limited,

water-limited, and nutrient-limited environments, respectively. Thus, the entropy and work efficiencies should not be directly compared across sites. However, within each site the ranges gradually change as we look across the different functional group scenarios. SRM has the least variability amongst its functional groups, and TAP has the most. Considering the entropy fluxes and work efficiencies, the multi-group scenarios all appear to have distributions similar to or consisting of larger values than the other scenarios for each site.

Using the Miller Jacknife and Kolmogorov-Smirnov tests, the distributions of entropy fluxes and work efficiency for the multiple functional group scenarios at each site are compared for statistical significant differences with each of their individual functional groups. Overall, the results indicate that multiple-functional-groups either have a thermodynamic advantage over single-groups or they are not at a disadvantage due to greater or similar values of entropy flux and work efficiency. There was a statistically significant difference in the distributions of entropy and work efficiency between the MG scenarios and each of individual functional groups except for WCR-OT. This case is unique since WCR-UN only contributes to 3% of the total leaf area of WCR-MG, meaning that the WCR-OT and WCR-MG are very similar in vegetation composition. For all other cases, the values of entropy and work efficiency were significantly larger in the MG scenarios, indicating thermodynamic advantage. The following section lays out the statistical tests and related analyses for comparing these entropy flux and work efficiency distributions.

2.3.1 Statistical analysis

To determine if the differences of entropy flux and work efficiency among scenarios at each site are statistically significant, we perform two separate tests for entropy flux and work efficiency. Since entropy flux distributions are positively skewed (Fig. 2.1a), we use the variance as an indicator of the difference between them. To this end we use the distribution-free Miller Jackknife (MJ) significance test [67, 68] for variance that does not assume that the distributions come from populations with the same median. However, the work efficiency distributions exhibit no such pattern (Fig. 2.1b), and, therefore, we use the two-sample Kolmogorov-Smirnov (KS) test, which measures the maximum absolute difference between

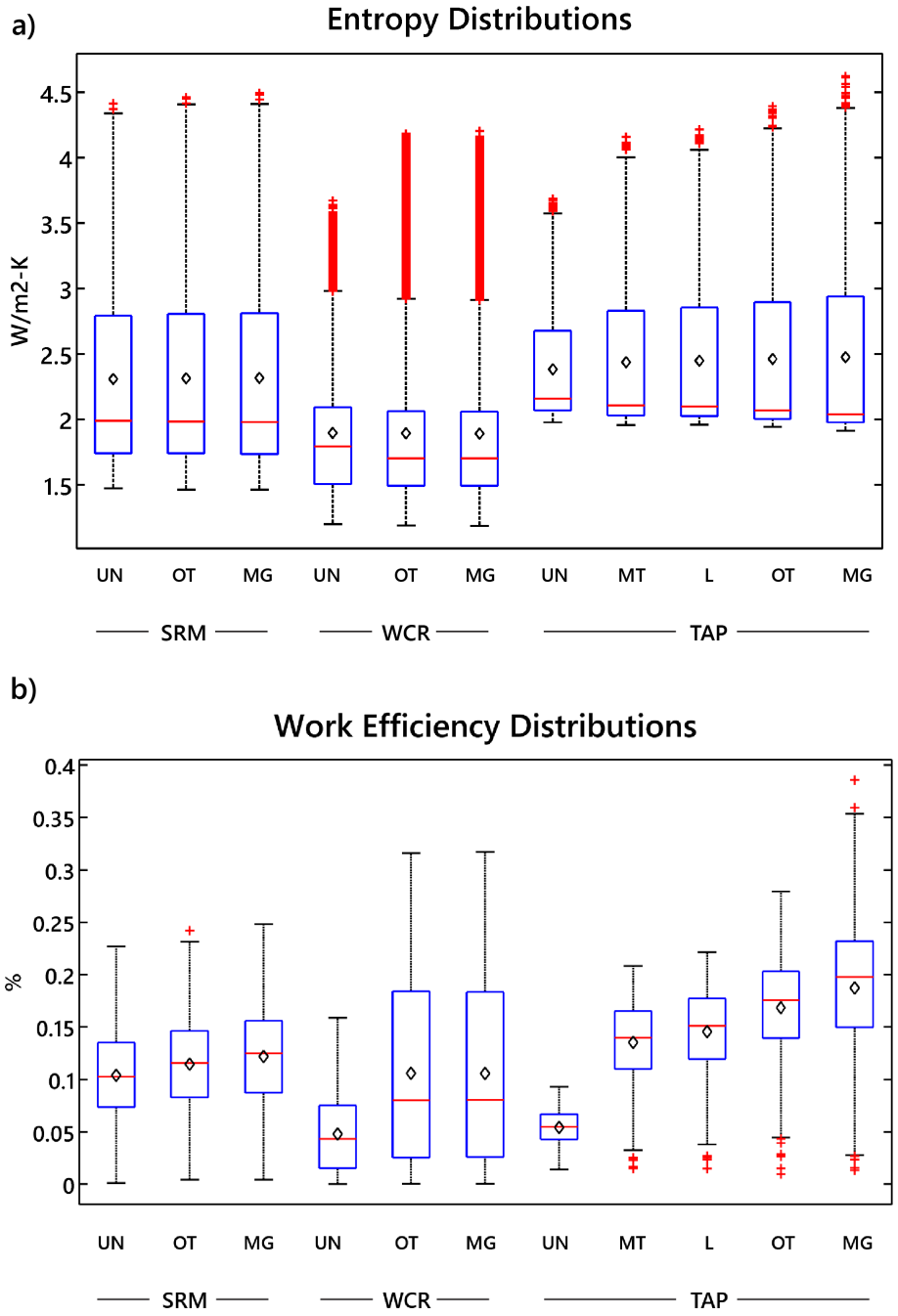

Figure 2.1: Entropy and work efficiency flux distributions. Illustration of the variability of (a) entropy flux, and (b) work efficiency associated with each functional group and coexisting multi-functional vegetation groups (see Table A.1). The distributions of entropy fluxes are developed based on each time step of simulation for the two-year study period, and the distributions of work efficiency are calculated based on daily energy fluxes (see Equation 2.13). Means are shown as black diamonds.

two empirical cumulative distribution functions (CDF) [69–71].

First, the entropy flux variances are compared with the MJ test. Because functional group scenarios at each site are bounded on the lower end by similar values, if a distribution has a larger variance than another, then the two populations cannot be considered as coming from the same continuous distribution, and the distribution with a larger variance generally consists of larger values. For each site we test the null hypothesis, H_0, that the distribution of multiple-functional-group entropy fluxes and the distribution for each of its single-functional-groups have the same variance. This is done with each functional group present at each site (Table A.1). The alternate hypothesis, H_{A1}, states that the distribution of entropy fluxes from the multiple-functional-group has a larger variance than that of the corresponding single-functional-group, meaning that the two populations do not belong to the same distribution and the multi-group scenario consists of larger values than the single-group scenario. The results from this test, shown in Table 2.2, indicate that H_0 is rejected in favor of H_{A1} at the 5% level ($p < 0.05$) for all scenarios except for the WCR-OT scenario. This indicates that for these ecosystems the distributions of entropy fluxes consist of larger values when multiple functional groups are present.

Using the KS test to compare work efficiency distributions for each site, we test the null hypothesis, H_0, that the multiple-functional-group measures of work efficiency and those for each of its single-functional-groups are from the same continuous distribution, or population. The alternate hypothesis, H_{A3}, states that the CDFs of the entropy flux from the multi-group scenario are smaller than those from the corresponding single-groups, meaning that the multi-group scenarios consist of values that are larger than their associated single-group scenarios. The results from this test, shown in Table 2.2, indicate that H_0 is rejected in favor of H_{A3} at the 5% level ($p < 0.05$) for all scenarios except for the WCR-OT scenario. This indicates that the distributions for work efficiency are indeed larger when multiple functional groups are present in these ecosystems, as indicated by a smaller CDF (Fig. A.3 of the *Supplementary Information*).

However, the tests of comparison for the WCR-OT scenario for both work efficiency and entropy flux distributions have p-values larger than 0.05 (i.e., H_0 cannot be rejected at the 5% level). This means that we cannot say that the WCR multi-group entropy flux distribution

Table 2.2: Significance Tests

Site	**Funct. Group**	H_{A1} **p-value**	H_{A1} **Reject** H_0?	H_{A2} **p-value**	H_{A2} **Reject** H_0?	H_{A3} **p-value**	H_{A3} **Reject** H_0?	H_{A4} **p-value**	H_{A4} **Reject** H_0?
SRM	UN	0.004	yes			$\sim$0	yes		
	OT	0.017	yes			0.002	yes		
WCR	UN	$\sim$0	yes			$\sim$0	yes		
	OT	0.606	no	0.394	no	0.934	no	0.915	no
TAP	UN	$\sim$0	yes			$\sim$0	yes		
	MT	$\sim$0	yes			$\sim$0	yes		
	OT	$\sim$0	yes			$\sim$0	yes		
	L	$\sim$0	yes			$\sim$0	yes		

H_0 is rejected if $p < .05$ at the 5% significance level.

Entropy – Miller Jackknife Test of Variance

H_{A1}: The entropy flux results from multiple functional groups have a variance **larger than** the single-functional-group.

H_{A2}: The entropy flux results from multiple functional groups have a variance **smaller than** the single-functional-group.

Work Efficiency – Two-sample Kolmogorov-Smirnov Test

H_{A3}: The work efficiency results from multiple functional groups have a CDF **smaller than** the single-functional-group (i.e., values are generally larger).

H_{A4}: The work efficiency results from multiple functional groups have a CDF **larger than** the single-functional-group (i.e., values are generally smaller).

has a variance larger than the OT single-group distribution or the multi-group work efficiency scenario comes from a larger distribution than the OT single-group scenario. This is not entirely surprising, as there is very little difference in LAI between these two scenarios; the maximum difference in LAI is about 0.2 (Fig. A.4 in the *Supplementary Information*), only 3% compared to the total WCR-MG LAI. This small increase in LAI from the single to the multi-group scenario provides less opportunity for increased energy dissipation and hence entropy production due to the smaller understory. Thus for completeness, we also perform the MJ and KS tests in the opposite direction for the WCR-OT scenario with the following alternative hypotheses. For the MJ test on entropy flux variances, H_{A2} states that the distribution of entropy fluxes from the WCR multiple-functional-group has a smaller variance than that of the OT single-functional-group, meaning that the two populations do not belong to the same distribution and the multi-group scenario consists of smaller values than the single-group scenario. For the KS test on work efficiency, H_{A4} states that the CDF of the entropy fluxes from the WCR multiple-functional-group is larger than the CDF from the OT single-functional-group, meaning that the multi-group scenario consists of values that are smaller than the single-group scenario. The results from both tests, shown in Table 2.2, indicate that we again cannot reject H_0 at the 5% significance level for WCR-OT. Thus, although the WCR multi-group scenario compared to the OT scenario does not have a significantly greater entropy flux variance or a greater work efficiency distribution, it also does not have less variance or a smaller distribution. Overall, the test results indicate that multiple-functional-groups have either greater or similar values of entropy flux and work efficiency than the modeled scenarios of their individual functional groups.

2.3.2 Factors impacting entropy flux

The behavior of an ecosystem's entropy is determined by the combined variation of its individual energy fluxes leaving the system, such as: shortwave radiation (SW), longwave radiation (LW), latent heat (LE), and sensible heat (H). For each scenario at each site, an entropy per unit energy (EUE) value is computed for all energy fluxes (see Equation 2.8) and reported as an average over the simulation period in Fig. 2.2a. Each ecosystem has its

own partitioning of energy among these categories, leading to differences in total entropy per unit energy leaving the ecosystem (EUE_{eco}), corresponding to "Total Out" in Fig. 2.2a.

The EUE for each energy category can be explained by the temperature of its source. SW originates from the sun, so its EUE is based on the temperature of the sun. However, outgoing longwave radiation (LW_{out}), LE, and H originate from the leaves as well as the soil surface. The total outgoing energy of the ecosystem is a resultant of the energy leaving each of the canopy layers including the soil surface within MLCan, each with its own temperature. Therefore, we calculate temperature equivalences (T_{eq}) for each of these energy categories based on the weighted average of the temperature of each leaf and soil layer contributing to the overall energy flux of that category (Fig. 2.2b, Equation 2.5). Entropy is calculated directly from temperature (Table 2.1), leading to an important inverse relationship between EUE and T_{eq}.

Figure 2.2b shows that for each of the sites, across almost all energy categories the UN scenario has the highest T_{eq} and the multi-group scenario has the lowest. Due to the inverse relationship between T_{eq} and EUE, all of the EUE averages for each category in Fig. 2.2a are smallest for the UN scenarios and largest in the multi-group scenarios, though some of these differences are marginal. From this pattern, one would expect that this would lead to a clearly greater overall EUE_{eco} for all multi-group scenarios ("Total Out" in Fig. 2.2a). Yet, this is not the case for all sites, as TAP is the only one in which the average EUE_{eco} varies considerably among functional group scenarios.

Although EUE averages tend to increase with leaf area index (LAI) and when multiple functional groups coexist, each energy category has different relative values of EUE. Further, EUE can be interpreted as an indicator of how degraded a particular form of energy is and the ability of that energy to perform additional work. SW has the least EUE across all sites and scenarios (Fig. 2.2a), so it has the greatest capacity for work to be done; plants are able to use this energy to perform work. Yet, SW is still radiative energy, so it does not perform work itself. On the other end, LW_{out} has the highest EUE of the energy categories studied here, meaning it is the most degraded with little capacity for additional work to be performed from it. In the middle, LE and H are more degraded than SW, but they are still able to perform physical work in the ecosystem through convection and conduction

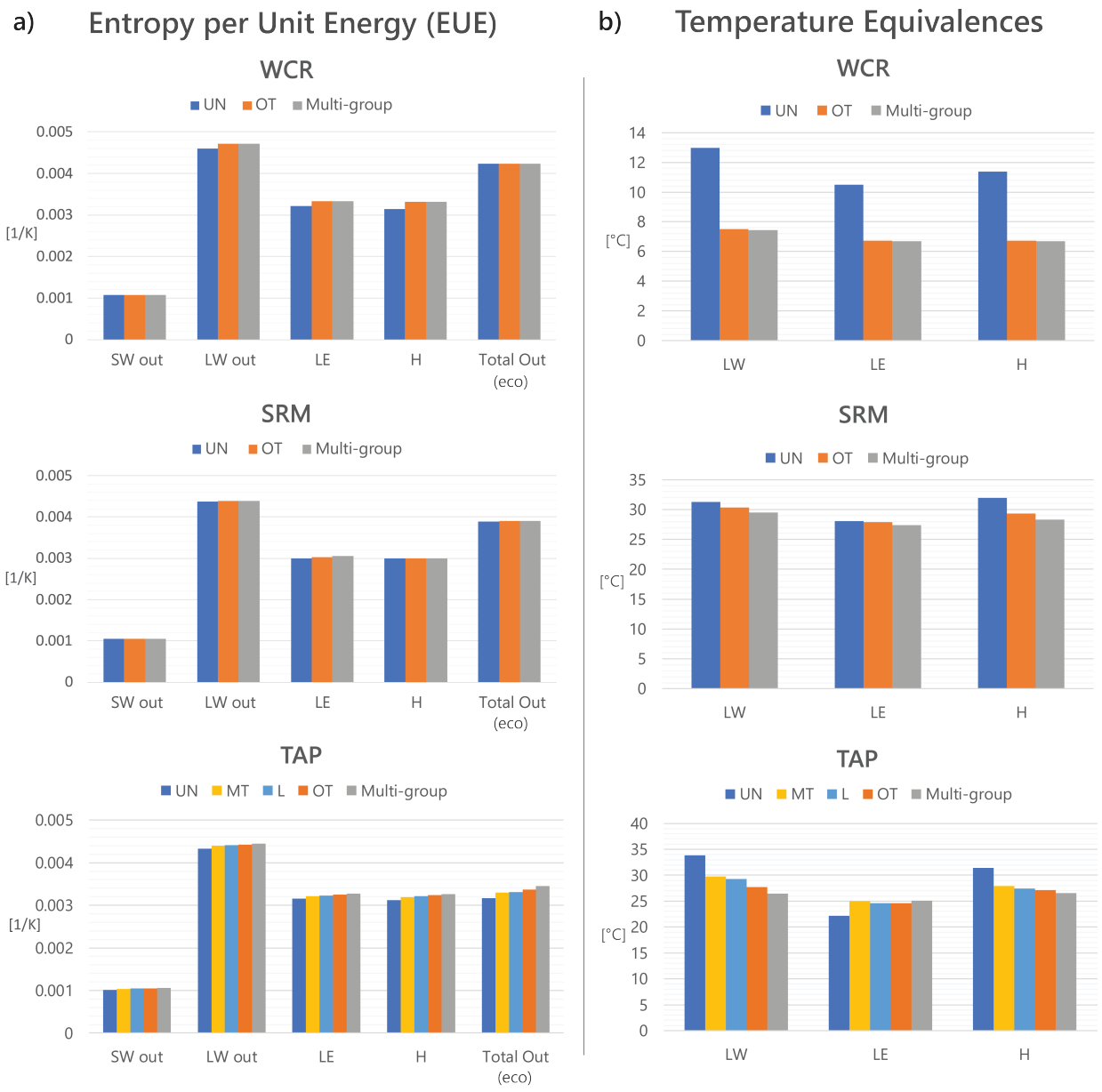

Figure 2.2: Entropy per unit energy and temperature equivalences. (a) Entropy per unit energy (EUE) by energy category for all sites (see Equation 2.8). Colors refer to vegetation functional groups: understory (UN), mid-trees (MT), overstory trees (OT), lianas (L), and multi-group consisting of all functional types observed in the ecosystem. In general for each energy category, more EUE is associated with increasing leaf area index (LAI). (b) Temperature equivalences (T_{eq}) by energy category for all sites. In general for each energy category, temperatures are cooler with increasing LAI. Despite similar equivalent temperatures for emitted longwave radiation (LW_{out}), latent heat (LE), and sensible heat (H), LW_{out} is by far the greatest contributor to EUE_{eco} (see Equation 2.9). [The weather forcing for all model simulations is the same across scenarios for each site.]

and contribute to the redistribution of heat throughout the vertical profile of the ecosystem. Since we are only considering the fluxes that enter and leave the ecosystem control volume in this analysis and all irreversible work releases heat, LE and H are also proxies for the work performed within the ecosystem internally (i.e., by the vegetation itself). Overall, when an ecosystem has low thermodynamic efficiency and high LW_{out}, it degrades the incoming SW quickly without performing much work within the ecosystem and constitutes wasted energy. However, higher values of LE and H leaving the ecosystem mean that more work has been performed.

Since each scenario partitions the incoming energy differently throughout the ecosystem, the considerably higher overall EUE for LW_{out} has important implications for overall EUE_{eco} and entropy fluxes, yielding larger values when more outgoing energy is allocated towards LW_{out}. Figure 2.3a displays the average partitioning of incoming radiation among the various energy categories at TAP, and Fig. 2.3b indicates the corresponding entropy fluxes presented as percentages of the incoming entropy flux and disaggregated into different energy categories. The energy and associated entropy entering the ecosystem are the same for all functional groups, but the outgoing fluxes vary significantly among them. Due to conservation of energy, the outgoing energy for all scenarios corresponds to 100% of the incoming radiation. Alternatively for entropy, this percentage is greater than the 100%, indicating entropy production (shaded in grey). At TAP and similarly at the other two sites, the multi-group scenario produces more total entropy on average than the other two scenarios.

However, the contribution of each energy category towards the total entropy differs among functional groups. As LAI increases from UN to OT and with the addition of multiple functional groups, the proportion of LE and H, or work, increases while the outgoing radiation decreases (Fig. 2.3). The UN scenario partitions more energy towards LW_{out} than the OT and multi-group scenarios. Since LW has the largest EUE of all the energy categories (Fig. 2.2a), its percentages in Fig. 2.3b are larger than in Fig. 2.3a. This observation, consistent across all sites, indicates that UN scenarios are able to make up for lower performing EUE values by partitioning more energy towards the higher entropy-producing energy category, LW_{out}. Thus, even though the UN scenario has the lowest EUE for all energy categories, its total EUE_{eco} – and overall ability to degrade the incoming SW –

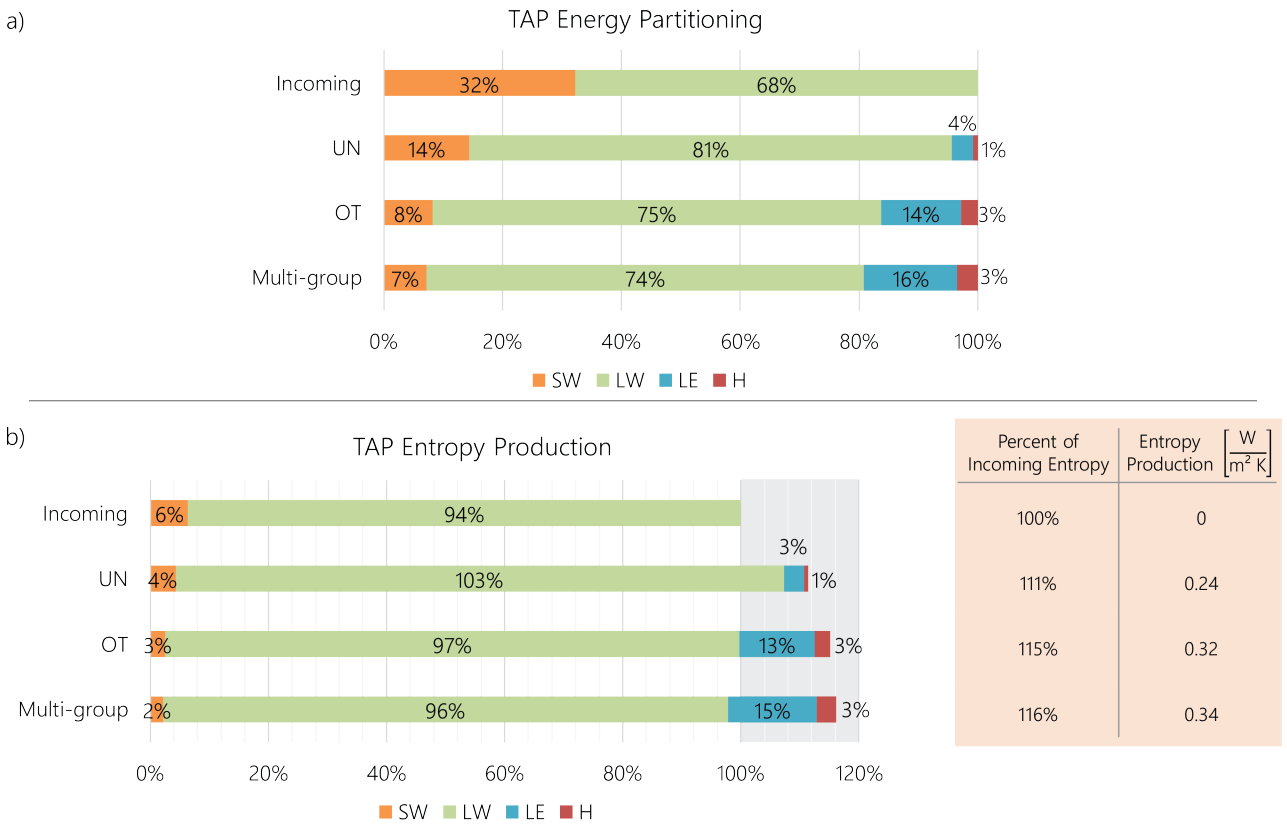

Figure 2.3: Energy and entropy partitioning by scenario for TAP. (a) Partitioning of incoming radiation into outgoing shortwave radiation (SW), longwave radiation (LW), latent heat (LE), and sensible heat (H) for three scenarios at TAP. From UN to OT to Multi-group, the percentage of LW_{out} decreases as the sensible and latent heat increases. A larger partitioning towards LW_{out} (i.e., UN) leads to greater weight towards a higher EUE value for an ecosystem's dissipation efficiency (Fig. 2.2a). (b) The corresponding entropy fluxes for the incoming radiation and outgoing energy fluxes of three TAP scenarios presented as a percentage of the total incoming entropy flux. Unlike energy, entropy is not conserved, but produced – indicated by a percentage greater than 100 and shaded in grey. The table displays the percent of the scenarios' outgoing entropy flux relative to the incoming entropy flux, indicating a 11-16% increase in entropy produced by the functional groups. Since LW has the largest EUE of all the energy categories (Fig. 2.2a), its percentages in (b) are larger than in (a).

and entropy production are similar to the other scenarios since it has more outgoing energy partitioned towards the largest EUE category, LW_{out}. However, EUE_{eco} is an indication of energy degradation, not work performed. Thus, the additional assessment of work and work efficiency is necessary for the interpretation of thermodynamic advantage.

2.3.3 Work as an indicator of self-organization

As discussed in the previous section, partitioning of energy and entropy fluxes are important for understanding the overall thermodynamic behavior of ecosystems. Energy fluxes with large EUE values result in greater entropy production for an ecosystem but do not always yield more work performed. Work – estimated as the sum of the ecosystem's latent and sensible heat fluxes (W; Equation 2.11) – represents the ability of an ecosystem to diminish the temperature gradient through the ecosystem. Despite having the largest EUE value, LW_{out} is not a component of work since it is a passive response to the temperature state. Figure 2.4 displays the relationships of work versus temperature gradient between the atmosphere and land surface ($\Delta T/\Delta z$; Equation 4.4) for the functional group scenarios at each site. Work performed within an ecosystem has a positive nonlinear relationship with temperature gradient across all scenarios. Further, each functional group scenario is fitted to a power function: $W = a(\Delta T/\Delta z)^b$. At each site a power law is observed; higher powers (b) correspond to functional groups with larger LAI, and except for the SRM-UN scenario, the highest power at each site corresponds to the multiple-functional-group scenario. This means that the work performed by the ecosystems with multiple functional groups has an exponentially greater response to marginal changes in temperature gradient as it increases.

To better understand the relationship between work and temperature gradients, we refer to the 1994 paper in which Schneider and Kay [11] theoretically explored Silveston's [72] Bénard cell experiments of heating an enclosed fluid from below. They demonstrated that without self-organization, a system's work performed from conduction alone has a linear relationship with the temperature gradient. However, when self-organization in the form of convection occurs at a critical point, Bénard cells form, the relationship becomes nonlinear, and more work is performed for each additional unit increase in gradient [11].

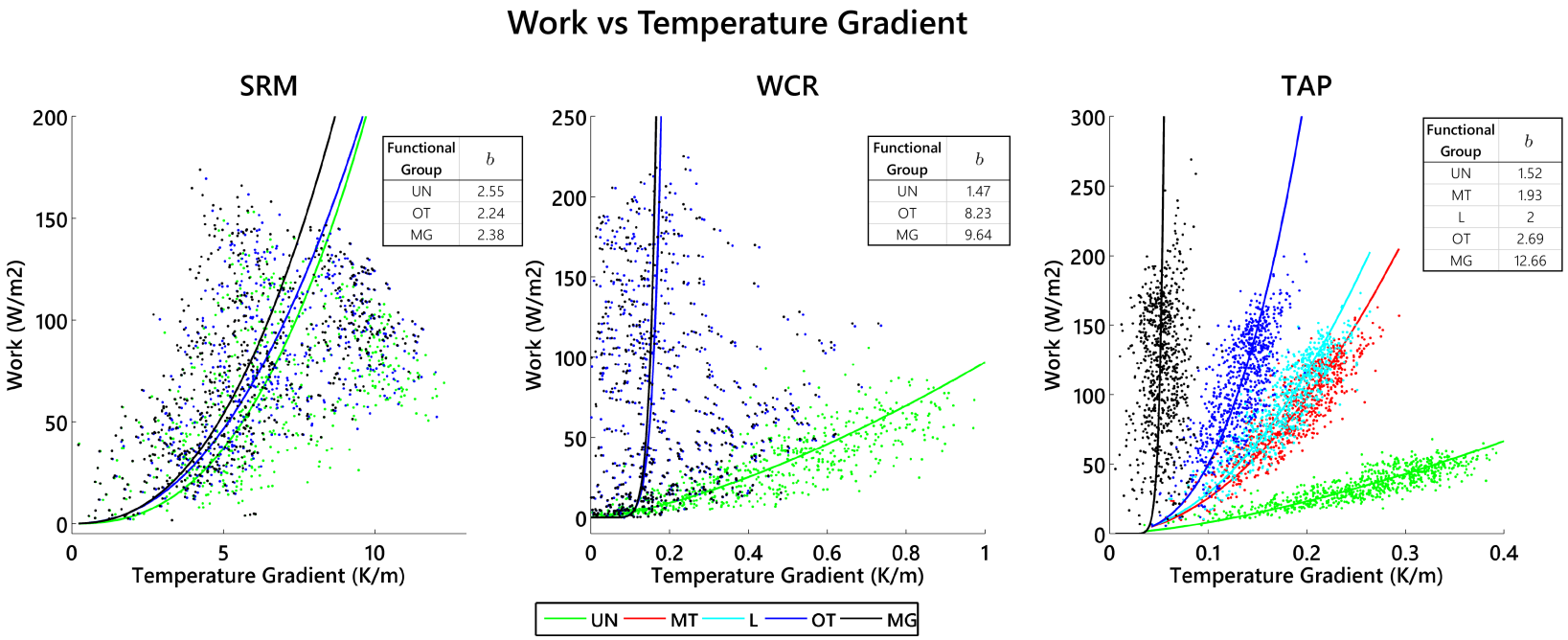

Figure 2.4: Plots of work versus temperature gradient for all functional groups and sites. Power functions are fit to the data: $W = a(\Delta T/\Delta z)^b$. a and b are reported in the upper right corner of each plot. For each site LAI increases in each functional group scenario from left to right in the legend at the bottom (i.e., UN has the smallest LAI and MG has the largest – see Fig. A.4 in the *Supplementary Information*). Trends in b indicate that power increases with LAI among functional groups and is the largest in the MG scenario for all sites except the SRM-UN scenario. A few values corresponding to negative temperature gradients are removed from the WCR scenario since it is a function of the presence of snow rather than self-organization.

In this experiment, analysis of data in which no self-organization occurred at all demonstrated a linear relationship between work and gradient. Alternatively, when Bénard cells formed (i.e., self-organization occurred) power law relationships between work and gradient emerged with higher-degree powers corresponding to greater dissipation rates due to increased convection. We give this example not to study the emergence of the phenomena, but as a means of comparing the behavior of possible end states: with and without self-organization. If we take the functional group scenarios as possible end states with various levels of self-organization, the interpretation for each of our sites is consistent with those of the Bénard cells: with self-organization, there is a nonlinear relationship between work and gradient with larger exponents in the power law relationship corresponding to more advanced levels of self-organization. This yields exponentially more work performed in the more highly organized multiple-functional-group ecosystem scenarios. From the combined results of Schneider and Kay and Fig. 2.4, we infer that self-organization is the leading driver of the nonlinearity shown in work-gradient plots. This supports the proposition that the existence of multiple functional groups reflects a higher degree of self-organization that results in nonlinear increases of work performed in response to marginal increases in temperature gradient, reflecting thermodynamic advantage.

2.4 Discussion

Through the concepts of entropy and work efficiency, this chapter establishes a framework for identifying thermodynamic advantage for the spontaneous self-organization of ecosystems towards a vegetation structure that includes multiple functional groups. We identify decreased canopy temperature, increased LAI, and greater partitioning of energy towards LW_{out} as important factors amplifying the entropy production of an ecosystem. From these factors, one can deduce the relative changes in entropy flux and, thus, changes in thermodynamic behavior of an ecosystem. Entropy provides insights into the total disorder of a system. The second law of thermodynamics requires that closed systems yield increases in entropy over time. Although, ecosystems are open thermodynamic systems, scientists have correlated greater entropy production as a driver of self-organization [18, 45]. However, not

all energy and hence entropy is productive in terms of thermodynamic advantage. Thus, we provide work efficiency as another important component of thermodynamic advantage and the directionality of self-organization.

Work efficiency captures the ability of an ecosystem to perform work based on the energy throughflow of the system. Work without context of incoming radiation does not tell much about the performance of an ecosystem relative to others. Since all functional group scenarios at each site receive the same incoming radiation in this study, either work or work efficiency can be used as metrics of thermodynamic advantage. However, work efficiency is a more attractive metric for further study as it normalizes an ecosystem based on its local availability of energy, allowing for comparison of ecosystems across multiple climates. Thus, work efficiency provides promise for future research to compare ecosystems with varying energy availabilities and external environments directly.

Additionally, work efficiency measures an ecosystem's ability to rapidly convert incoming radiation into alternate forms of energy that disperse throughout the ecosystem control volume and diminish the imposed temperature gradient. Work efficiency helps us understand the reorganization of available energy entering an ecosystem towards thermodynamically-productive uses – meaning depleting the imposed temperature gradient. According to thermodynamic theory, all systems work to decrease gradients of their state variables, which in turn drive the movement of the energy and mass from high concentrations to low concentrations (i.e., high to low temperatures) [12]. In this study, work exhibits a nonlinear power law relationship with temperature gradient. This means that exponentially more work is performed to combat the greater temperature differences from the earth surface to the atmosphere above the canopy. For the sites studied here, scenarios with multiple functional groups exhibit the highest power law, meaning that the MG structure is more efficient at depleting the driving temperature gradient. This is a demonstration of high work efficiency. Since structures that perform more work for a given temperature gradient have a thermodynamic advantage over those with lower efficiencies, ecosystems have a natural tendency to self-organize to this MG structure.

Because ecosystems are formed and evolve through a process of random fluctuations, there is a nonzero statistical probability for the existence of any possible vegetation structure or

state. The state exhibiting thermodynamic advantage identifies the state with the highest probability of occurrence. This does not mean that the advantageous structure will always result. In all of our sites, the highest work efficiency corresponds to the existing MG scenario. Thus, the ecosystems exist in the highest probability thermodynamically-advantageous state.

The outcomes of this work provide valuable insight into the self-organization of natural ecosystems. Thus far, we have identified that when multiple functional groups coexist this structure exhibits a thermodynamic advantage over other possible individual functional group scenarios. Thus, ecosystems will have a higher probability of self-organizing towards this greater work efficiency state. Additionally, this work highlights new areas for further study. The framework of thermodynamic advantage through greater entropy production and work efficiency could be applied to other ecosystem structures, such as the existence of individual functional groups in nature. Further, this framework could help scientists understand how human-induced perturbations could impact the thermodynamic behavior and alter the most advantageous state. Thus, we propose the concepts of entropy and work efficiency as valuable contributions to the basic understanding of the existence of a particular vegetation structure and present thermodynamic advantage as a tool for future use in understanding and studying the stability and behavior of ecosystem self-organization.

2.5 Additional Information

Supplementary information is available for this chapter in Appendix A.1.

CHAPTER 3

THERMODYNAMIC BASIS FOR THE DEMARCATION OF ARCTIC AND ALPINE TREELINES

3.1 Introduction

Explaining the heterogeneous organization of vegetation across landscapes has proved both a puzzling and an inspiring concept as patterns have formed naturally across the world – one such pattern being the existence of a treeline, i.e., the demarcation zone between forestland and vegetation without trees [73, 74]. After decades of study, there is still debate among ecologists and biologists over the mechanisms that limit the presence of trees beyond treelines. Current explanations are rooted in, but not limited to, consideration of factors such as excessive light and wind, limited CO_2, and low temperatures [73, 75–77]. While these explanations are based on ideas of limited resources, we instead examine the question of what determines the existence of a treeline from the perspective of thermodynamic feasibility.

It is now generally accepted that observed patterns of vegetation composition and its organization are a result of self-organization, or the spontaneous emergence of pattern without external predetermination [78, 79]. By framing ecosystems as open thermodynamic systems, we explore further the concept of thermodynamic feasibility and its role in the self-organization of vegetation structure. Vegetation structure consists of composition (i.e., the number and type of functional groups) and organizational patterns on the landscape. We refer to this generally as vegetation structure and utilize a one-dimensional model with no lateral transport of energy or matter under the assumption that the composition and pattern remain spatially uniform. To balance model performance and accuracy, standing plant species are aggregated into functional groups (i.e., evergreen needleleaf trees, shrubs, grasses; see Table 3.1) based on literature [7–10]. We present the case that observed organization reflected in the demarcation of differing vegetation structures on either side of a

treeline is established in tandem with vertical thermodynamic gradients at a given location, driven by the incoming energy into an ecosystem. In other words, *we hypothesize that beyond a treeline, the existence of trees is prevented by conditions of thermodynamic infeasibility.*

The application of thermodynamic theory to ecology has been studied for the better part of the last century through the introduction of theoretical thermodynamic properties, such as entropy and exergy, into environmental systems. Exergy, similar to free energy, is defined as the maximum work capacity of energy and has been used in the context of ecosystems (eco-exergy) to define their thermodynamic efficiency, or the ability of an ecosystem to perform work through greater exergy storage [21, 22, 80]. Subsequently, the concept of exergy degradation was developed, asserting that open thermodynamic systems will evolve based on the strength of the applied gradient of exergy on the system and will undergo irreversible processes to dissipate energy and destroy the gradient through all means available [11, 25]. As this theory applies to ecosystems, fluxes of mass or energy from the external environment (i.e., above the canopy) result in concentration gradients within the system itself. State variables will transition along these gradients according to the second law of thermodynamics. When the magnitude of incoming energy and consequent spatial imbalance of energy becomes great enough, dissipative structures spontaneously emerge, or self-organize, and establish temperature gradients consistent with the dissipative need of the ecosystem [11, 12].

This work has been vital for establishing the applicability of thermodynamic theory to ecological systems. However, a major challenge, as it applies to ecosystems, has been the quantification of these thermodynamic properties. The calculation of exergy for an ecosystem requires knowledge of the equivalent ecosystem in thermodynamic equilibrium, which is currently infeasible to estimate [21]. Without this reference state, exergy estimates are not possible beyond orders of magnitude for an ecosystem. Further, eco-exergy is calculated solely based on the chemical energy of the biomass in the ecosystem [21]; thus, it does not take into account interactions among functional groups. Therefore, these quantification techniques are not applicable at the scale or level of detail needed to compare variations in vegetation structure. Thus, in this chapter rather than quantifying an ecosystem's exergy – the ability of an ecosystem to perform work – we estimate the actual work performed by an

ecosystem. This is estimated as the 1-D transport of heat in the form of latent and sensible heat, driven by the vertical imbalance of energy structured by both the incoming energy and the vegetation structure.

Ecosystem functions are driven, in part, by vertical temperature gradients, from the earth surface to the air above the canopy, resulting from the incoming solar radiation and subsequent dissipation of this energy by the self-organized vegetation structure [11, 35]. This creates a directionality of dissipation of incident radiation as heat out of the ecosystem from higher surface temperatures to lower air temperatures. Throughout this chapter, we measure work through the net sum of heat leaving the ecosystem as latent and sensible heat – which can either be positive or negative depending on the direction of the resultant temperature gradient. This temperature gradient (Equation 4.4) emerges as a result of self-organization through feedback between the incoming radiation, both shortwave and longwave, and local environmental conditions and the heat dissipation and work performed by the vegetation. The presence of ground cover, such as snow, is impacted by vegetation structure and further influences the thermal environment and temperature gradient.

A recent study concluded that at sites where multiple functional groups exist (e.g., forests), the vegetation structure in which all groups co-exist and are modeled together with interactions is more thermodynamically advantageous and, thus, more likely to occur than each of the individual functional groups that the forest comprises modeled separately [35]. Thermodynamic advantage is defined by the production of larger fluxes of entropy, more work performed, and higher work efficiency – a quantity that captures how much of the incoming energy is converted into forms useful for actively dissipating heat. It is possible to envision that under certain environmental conditions, the thermodynamic advantage, or the thermodynamic feasibility, offered by the existence of multiple functional groups is not tenable. The demarcation exhibited by treelines presents an ideal case to explore this scenario, in that there is a distinct transition from multiple functional groups below the treeline to a single functional group above it. In this chapter, we examine vegetation above and below Arctic and alpine treelines to determine whether the absence of trees in ecosystems above treelines are thermodynamically infeasible. Simply, we seek to answer the following research question: *Is the non-existence of trees beyond the region demarcated as a treeline a reflection*

of thermodynamic infeasibility associated with the presence of trees, and if so, how is this infeasibility exhibited?

To address this question, we use an extensively validated multi-layer 1-D physics-based model, MLCan [27, 28, 35, 52–55, 62], consisting of 20 above-ground layers, 1 ground surface layer, and 12 below-ground layers (see *Supplementary Information*). This model is chosen because of its ability to capture interactions among functional groups, such as the impact of shading on understory vegetation and the resulting thermal environment within the canopy [28]. The model output is used to compare the thermodynamic work performed at paired sites above and below the respective treelines for three different locations: the Italian Alps (IT), the United States Rocky Mountains (US), and the Western Canadian Taiga-Tundra (CA) (Fig. 3.1; see *Site Descriptions*). For each site pair, four scenarios are performed (Table 3.1): 1) The subalpine/sub-Arctic forest ecosystems are modeled as they exist with multiple functional groups (Fig. 3.2a, *left*). 2) The alpine/Arctic ecosystems are modeled as they exist with one functional group (i.e., shrubs or grasses; Fig. 3.2a, *right*). 3) We construct counterfactual scenarios above the treeline in which the vegetation of the subalpine or sub-Arctic forest is simulated with the environmental conditions and parameters of the alpine meadow or Arctic tundra (i.e., adding hypothetical trees where none exist; Fig. 3.2b). 4) As a control, a final counterfactual scenario is constructed below the treeline in which we model the understory of the subalpine/sub-Arctic forest individually (i.e., removing trees from the existing ecosystem).

The simulation of these four scenarios facilitates comparison of the existing vegetation structure of each site with the corresponding counterfactual scenarios. By varying the model inputs of vegetation present at each site while holding the environmental conditions and site specific-parameters consistent, we are able to directly compare thermodynamic outcomes as a result of varying vegetation structure and determine whether the simulated forest counterfactual scenario is thermodynamically feasible. The analysis supports the conclusion that thermodynamic feasibility is an important and complementary condition to the usual considerations of resource availability, such as water and nutrients, which determines the organizing form and function of ecosystems.

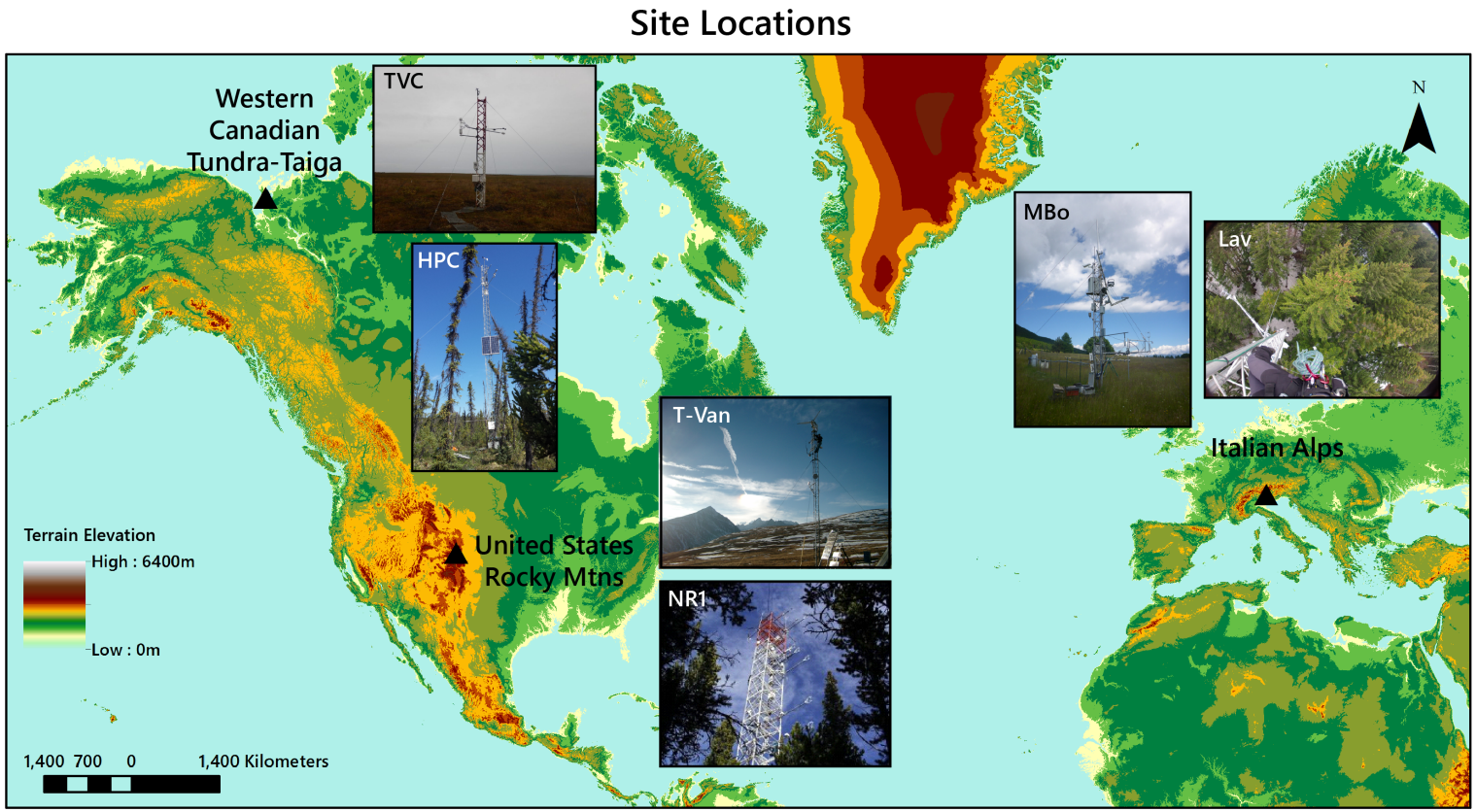

Figure 3.1: Site locations for the three pairs of sites (Table 3.1) above and below Arctic and alpine treelines. The background topographic map is from NASA space-based elevation data (https://visibleearth.nasa.gov/images/73934/topography#). Fluxtower site images were obtained from the following: TVC & HPC – Oliver Sonnentag (https://atmosbios.com/); T-Van – UCAR Earth Observing Lab (https://archive.eol.ucar.edu/homes/stephens/RACCOON/NWRsite.html); NR1 – Sean Burns, 10/07/2014, (https://ameriflux.lbl.gov/sites/siteinfo/US-NR1); MBo & Lav – Roberto Zampedri, Fondazione Edmund Mach.

Table 3.1: Simulation scenarios with observed and hypothetical vegetation

Abbrev.	UN FG	OT FG	Counterfactual?	Site ID
Italian Alps				
IT-Alp	grasses	–	no	MBo
IT-Tr	suppr DT	ENT	yes	MBo
IT-For	suppr DT	ENT	no	Lav
IT-Un	suppr DT	–	yes	Lav
United States Rocky Mountains				
US-Alp	sedge	–	no	T-Van
US-Tr	shrubs	ENT	yes	T-Van
US-For	shrubs	ENT	no	NR1
US-Un	shrubs	–	yes	NR1
Western Canadian Taiga-Tundra				
CA-Arc	shrubs	–	no	TVC
CA-Tr	shrubs	ENT	yes	TVC
CA-For	shrubs	ENT	no	HPC
CA-Un	shrubs	–	yes	HPC

The simulation abbreviations are defined as 'location'-'scenario', where the locations are the Italian Alps (IT), United States Rocky Mountains (US), and the Western Canadian Taiga-Tundra (CA); and the scenarios are defined as follows: Alp – alpine meadow or fellfield, Arc – Arctic tundra, Tr – alpine/Arctic site with simulated trees, For – subalpine/sub-Arctic forest, Un – subalpine/sub-Arctic forest understory simulated without overstory trees. Throughout this chapter, 'X-' is used to represent all locations (e.g., X-Un encompasses IT-Un, US-Un, and CA-Un). The understory (UN) and overstory (OT) functional groups (FG) for each modeled scenario are identified based on the Site IDs described in the *Site Descriptions* section of the *Materials and Methods*. 'suppr DT' refers to suppressed deciduous trees, and 'ENT' refers to evergreen needleleaf trees. The 'Counterfactual' column indicates whether synthetic vegetation was simulated.

3.2 Materials and Methods

We use the extensively validated multi-layer canopy-root-soil model, MLCan [27, 28, 35, 52–55, 62], to simulate and study three pairs of sites, each pair corresponding to ecosystems above and below the treeline. We vary the model inputs of vegetation present at each of the sites while holding the environmental conditions and site specific-parameters consistent to directly compare thermodynamic changes and determine the most advantageous scenario. The site descriptions are documented below. Additional information on MLCan, including model updates and site-specific validation and parameterization can be found in the *Supplementary Information* (Appendix A.1).

3.2.1 Site Descriptions

The eddy covariance data for the IT sites are taken from the Lavarone (Lav) and Monte Bondone (MBo) sites in the FLUXNET2015 network [81, 82], located in the Trento province in the Eastern Italian Alps, with a 200m elevation difference. The LAV site is an evergreen needle-leaf subalpine forest at 1300m above mean sea level (MSL) (45.95620°N, 11.28132°E), consisting of predominantly European silver fir (*Abies alba* Mill.) with a suppressed beech (*Fagus sylvatica* L.) understory [83]. The MBO site is an alpine meadow located on a mountain karst plateau at 1500m above MSL (Viote del Monte Bondone; 46.01468°N, 11.04583°E), dominated by perennial bunchgrass (*Nardus stricta* L.) [84, 85].

The eddy covariance data for the US sites are taken from the Niwot Ridge (NR1) site in the AmeriFlux network [86] and the "T-Van" location in Knowles et al. [87, 88], located 5km apart in distance with a 430m elevation difference near the Continental Divide in the United States Rocky Mountains in Colorado. The NR1 site (40.0329°N, 105.5464°W; 3050m elevation) is an evergreen needleleaf forest dominated by subalpine fir (*Abies lasiocarpa* var. *bifolia*) and Englemann spruce (*Picea engelmannii*) with sparse understory vegetation comprised of wild blueberry (*Vaccinium myrtillus*) [33, 89, 90]. The T-Van site (40.05305°N; 105.58639°W; 3480m above MSL) is an alpine fellfield consisting of curly sedge (*Carex rupestris*) [87, 91].

The eddy covariance data for the CA sites are taken from the Havikpak Creek (HPC) and Trail Valley Creek (TVC) AmeriFlux sites [92, 93], located 50km apart on either side of the Arctic treeline in Northwest Territories along the Western Canadian Taiga-Tundra interface. The sites consist of peat soil above mineral soil and continuous permafrost [31]. HPC (68.32029°N, 133.51878°W; 80m above MSL) exists in the forest-tundra ecotone in the Taiga. It is a sparse needleleaf boreal forest dominated by black spruce (*Picea mariana*) with small shrub species (*Ledum sp.*, *Ledum groenlandicum*) at 80m elevation [94]. TVC (68.7462°N, 133.5017°W; 85m above MSL) is an Arctic tundra site consisting of short grasses and berry species (*Ledum groenlandicum*) [95–97].

Additional information for all sites, including leaf area index and data pre-processing, can be found in the *Supplementary Information* (Appendix A.1).

3.3 Results

Model simulations from the three site pairs highlight two primary conditions of thermodynamic infeasibility that could help explain the non-existence of trees beyond a treeline. The first thermodynamic infeasibility is associated with alpine/Arctic temperature inversions (i.e., negative temperature gradients), which result in prolonged periods of negative work for the counterfactual tree scenarios for all three locations. The second manifests in the counterfactual alpine tree scenarios, (IT-Tr and US-Tr) as temperature-driven feedbacks lead to a decrease in net carbon gain or unsustainable net carbon loss from the vegetation's leaves for the two alpine sites.

In this section, we elucidate the relationship of work with temperature gradient; highlight the two conditions of thermodynamic infeasibility through site examples; and illustrate how these conditions of infeasibility translate into thermodynamic limits that explain the self-organization of differing vegetation structure on either side of a treeline.

3.3.1 Thermodynamic Behavior

Temperature gradient and work are key concepts for understanding thermodynamic behavior and the self-organization of ecosystem vegetation. For our study we calculate the resultant temperature gradient, arising as a result of self-organization of the thermal environment surrounding the canopy, as:

$$\frac{\Delta T}{\Delta z} = \frac{T_{surf} - T_{air}}{h_e} \tag{3.1}$$

where T_{surf} is the temperature of the soil surface in Kelvin, T_{air} is the temperature of the air above the canopy in Kelvin, and h_e is the ecosystem height determined by the height of the subalpine or sub-Arctic trees at each location (see Table A.3 in the *Supplementary Information*) [35].

In our 1-D model simulations, heat fluxes are assumed positive in the positive z direction, leaving the ecosystem control volume into the atmosphere above the canopy. However, work is defined based on the direction of the temperature gradient. When the work performed by the ecosystem, as measured by the sum of latent and sensible heat, is consistent with the temperature gradient it is designated as positive work, otherwise as negative work. To demonstrate this relationship, work is augmented from a prior formulation [35] as follows:

$$Work = (LE + H) \times sign(\Delta T) \tag{3.2}$$

in which work, latent heat (LE), and sensible heat (H) are in units of W/m^2, and $\Delta T = T_{surf} - T_{air}$. Since work considers total net fluxes of heat, internal ecosystem energy dynamics are taken into account in this formulation through signatures, such as heat loss, across the control volume. Further, the heat leaving the bottom of the control volume due to water loss is negligible, and thus ignored.

Based on these calculations, an ecosystem's ability to perform work manifests into four distinct cases depending on the sign of the resultant temperature gradient and the net loss or gain of heat driven by the thermal environment derived from present ground cover, such as vegetation or snow: 1) First and most common during the day when photosynthesis is

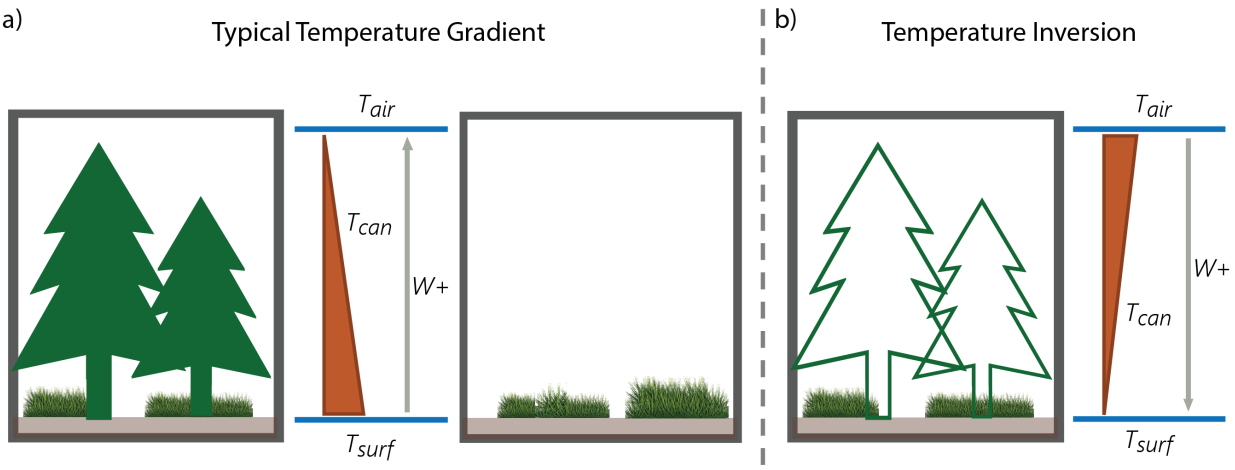

Figure 3.2: Conceptual diagram of temperature gradients. The $W+$ arrow indicates the positive direction of work performed through heat transport. Although in different directions, in both cases (a) and (b), the work performed is positive because heat moves from high to low temperatures. (a) Typical summertime temperature gradients are positive for the two real scenarios: subalpine/ sub-Arctic forest (*left*) and alpine tundra/Arctic meadow (*right*). (b) A conceptual temperature inversion, or negative temperature gradient, which arise when alpine/Arctic forest are simulated as counterfactuals.

occurring, the temperature of the earth surface is typically warmer than the air above the canopy, and heat leaves the ecosystem upward along the temperature gradient, corresponding to positive work (Fig. 3.2a). 2) The temperature of the earth surface is warmer than the air above the canopy, but there is a net heat gain within the ecosystem, meaning that the heat moves into the ecosystem against the direction of the temperature gradient. This case is rare and corresponds to negative work. 3) Common during the night, a phenomena called a temperature inversion emerges. In this case, the temperature gradient can become negative, meaning that the temperature of the air above the canopy is greater than the temperature of the earth surface. As heat enters the ecosystem to warm the surface, positive work is performed since the heat is still moving along the temperature gradient (Fig. 3.2b). 4) During snowmelt conditions, particularly for Arctic and alpine ecosystems, temperature inversions also emerge [98, 99]. When this occurs and the ecosystem experiences a net heat loss through latent and sensible heat from the canopy, the heat leaving the ecosystem travels in the opposite direction of the temperature gradient. Thus, in this case, ecosystems perform negative work. Our findings demonstrate how extended periods of time in this last case of work lead to thermodynamic infeasibility for the alpine/Arctic ecosystem counterfactual

vegetation scenarios; i.e., the ecosystems cannot be sustained in these conditions and, hence, they do not occur in nature.

3.3.2 Negative Work

By visualizing the work performed through dissipation of heat for a resultant temperature gradient, we are able to assess the thermodynamic feasibility of the various scenarios for each ecosystem. Figure 3.3 displays the work performed versus the resultant temperature gradient at each half-hourly timestep for all sites and scenarios. First considering the scenarios below the treeline, the subalpine/sub-Arctic forest (*green*) is more thermodynamically advantageous than the simulated understory alone (*black*) for each location. This advantage is demonstrated by greater work performed by the *X-For* scenarios (i.e., IT-For, US-For, and CA-For; see Table 3.1) for unit increases in resultant temperature gradient, indicating that the existing forest vegetation self-organizes its thermal environment such that it more rapidly dissipates heat from the ecosystem. This result is consistent with conclusions from previous work [35] that the co-existence of multiple functional groups in natural forested ecosystems is more thermodynamically advantageous than each of the individual groups comprising the forest vegetation structure.

For the subalpine/sub-Arctic sites, resultant temperature gradients are generally positive, and under all scenarios positive work is performed (i.e the ecosystems exhibit a net heat loss away from the land surface consistent with the temperature gradient; Fig. 3.2a). Thus, there is no indication that either of these vegetation scenarios should be considered infeasible since they do not perform considerable negative work.

However, the alpine/Arctic sites with both counterfactual and existing vegetation structures exhibit both positive and negative temperature gradients (i.e., temperature inversions). When no temperature inversion is present, the same trend is apparent as before in which the simulated forests (*red*) at each site perform more work for the corresponding resultant temperature gradient than the existing shrubs/grasses (*blue*). Considering merely the positive temperature gradient, the simulated forests at the alpine/Arctic sites actually seem more advantageous. However, alpine/Arctic environmental conditions for all three locations

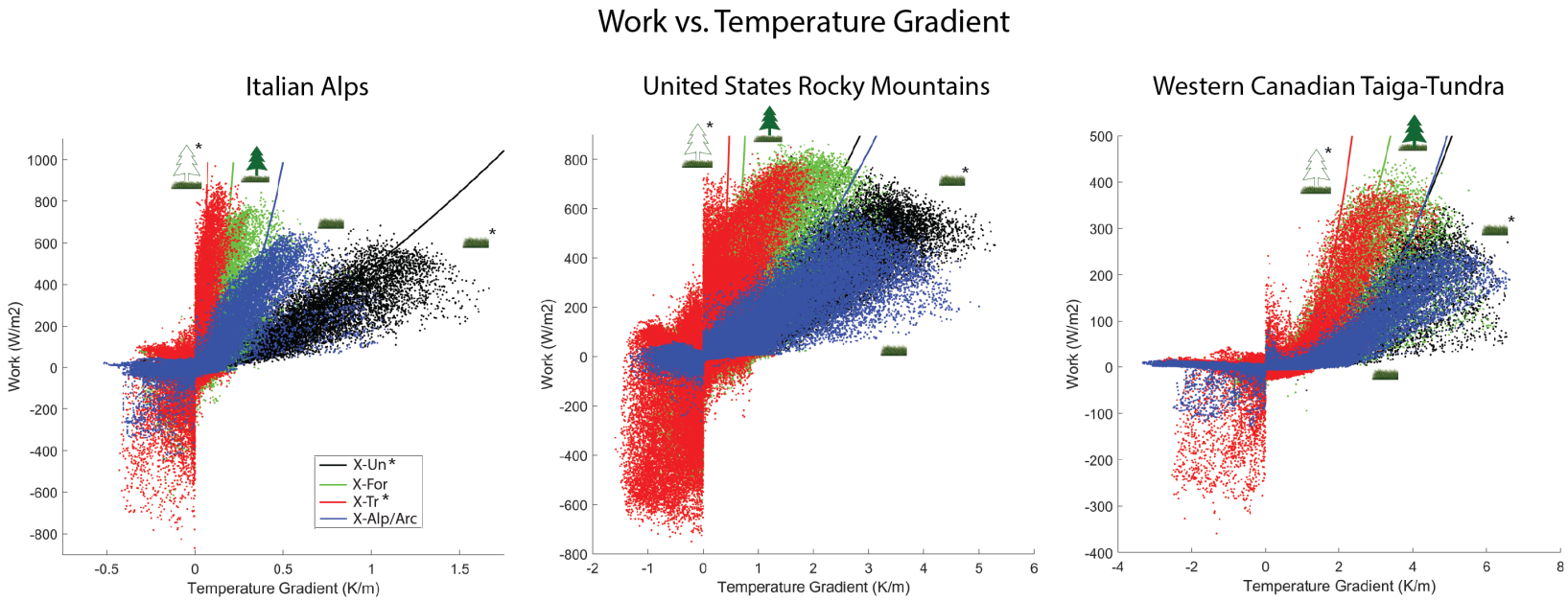

Figure 3.3: The work versus resultant temperature gradient for the three site pairs summarized in Table 3.1. Data points represent half-hourly simulation timesteps over the entire study period (Italy, 2 years; United States, 6 years; Canada, 3 years). The starred vegetation scenarios (*X-Un** & *X-Tr**) indicate counterfactual scenarios. For every region, on the positive x-axis the simulated trees (*X-Tr*) scenario above the treeline performs the most work for the resultant temperature gradient than the other scenarios when the temperature of the earth surface is warmer than that of the air above the canopy. However, when the resultant temperature gradient is negative (*X-Tr* & *X-Alp/Arc*), a temperature inversion occurs (Fig. 3.2), resulting in the vegetation performing negative work – transporting heat in the opposite direction of the temperature gradient.

have considerable time periods that exhibit temperature inversions and large magnitudes of negative work (i.e the ecosystems exhibit a net heat loss upward in the *opposite* direction of the temperature gradient; Fig. 3.2b). This large amount of negative work performed indicates a thermodynamic infeasibility through unsustainable heat loss occurring due to the counterfactual trees modeled at the alpine/Arctic sites.

In the three pairs of sites studied, the majority of temperature inversions occur during snowmelt conditions (see Figs. 3.4 & A.10). Snowmelt temperature inversions occur when the air temperature is warmer than the melting snow surface (Fig. 3.2b). Despite warmer air temperatures, the phase transition associated with snowmelt keeps the surface temperature low. Temperature inversions trap heat within the upper canopy, causing high temperatures in the upper and mid-canopy layers while layers near the earth surface remain cool due to shading. The shrub/grass (*X-Alp/Arc*), the simulated trees (*X-Tr*), and occasionally the subalpine forest (*X-For*) scenarios exhibit inversions during snowmelt. However, excessive shading from added leaf area, measured as leaf area index (LAI; see Fig. A.9), from the simulated trees in the *X-Tr* scenarios extends the snow cover period and causes the snow to take longer to melt and the ecosystem to remain in this inverted state significantly longer, sometimes well into the summer (see Figs. 3.5a and A.11). The result is a net loss of heat upward from the middle and upper layers of the canopy while the lower layers of the control volume at and near the earth surface remain cooler. Thus, heat is lost in the opposite direction of the resultant temperature gradient, corresponding to negative work. Since the LAI of the trees at the sub-Arctic site only reaches around 0.5, the role of tree leaf area on temperature inversions in the CA-Tr scenario is less pronounced, and the duration of temperature inversions is shorter than the US-Tr and IT-Tr scenarios. Alternatively, the existing vegetation scenarios (*X-For*, *X-Un*, and *X-Alp/Arc*) allow for sunlight and heat to penetrate into the lower canopy and warm the melting snow to quickly revert the ecosystem to positive temperature gradients (Fig. 3.2a).

To demonstrate the prevalence of temperature inversions and negative work performed by the alpine counterfactual forest vegetation, Figure 3.4 displays the average daily work for the scenarios in the United States Rocky Mountains. The US-Alp scenario (*blue*) experiences negative work briefly during snowmelt (around day 140). The subalpine forest (*green*; US-

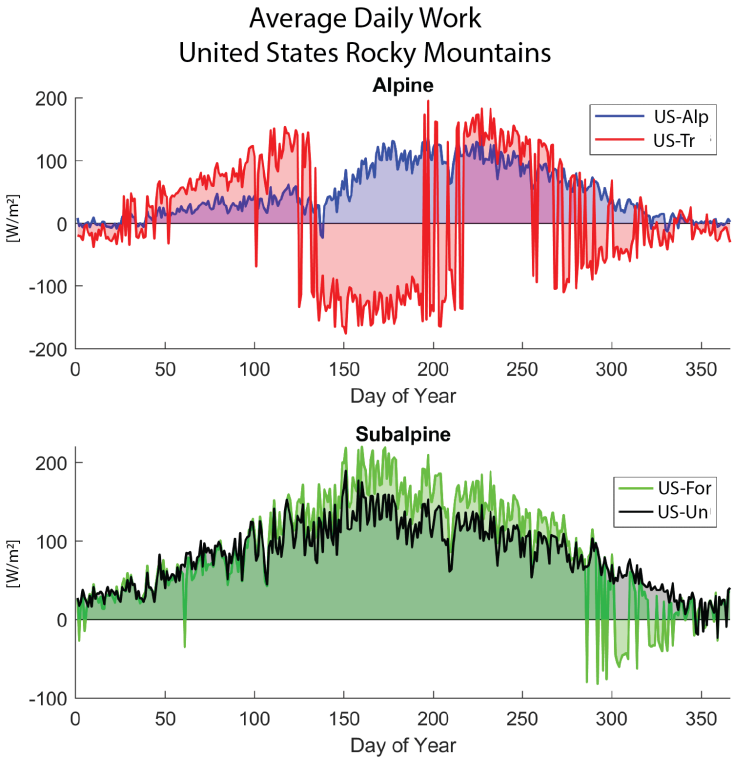

Figure 3.4: Average daily time series of work for the entire study period (2008-2013) for scenarios in the United States Rocky Mountains. The top panel demonstrates the prolonged negative work (i.e., heat transport in the opposite direction of the temperature gradient) associated with snowmelt and winter temperature inversions of the simulated alpine forest (red; US-Tr), indicating that this counterfactual is thermodynamically infeasible. The existing alpine and subalpine vegetation (US-Alp, blue & US-For, green) generally only experience negative work during snowmelt conditions. The subalpine forest (green; US-For) experiences negative work sporadically for short durations during the winter; these instances are a function of snowmelt as well since the snowpack does not persist throughout the winter at this site (see Fig. 3.5a).

For) experiences negative work sporadically for short durations during the winter; these instances are a function of snowmelt as well since the snowpack does not persist throughout the winter at this site (see Fig. 3.5a). Alternatively, the US-Tr scenario (*red*) experiences long durations of negative work during both snowmelt (approximately days 140-210) and winter conditions (around day 300). The IT-Tr and CA-Tr sites experience similar persistence of negative work behavior during snowmelt (see Appendix A.2). The long durations of temperature inversions indicate a thermodynamic infeasibility since ecosystems would not be able to sustain this rate of heat dissipation without energy reaching the lower canopy and soil surface. Based on the analysis of the *X-Tr* scenarios for all three locations, extended periods of unfavorable negative work demonstrates that the existence of trees beyond a treeline would be thermodynamically infeasible.

3.3.3 Net Carbon Loss

In addition to the thermodynamic infeasibility associated with negative work, the extended periods of negative work also lead to another infeasibility. In the alpine counterfactual trees scenarios, these extended periods of negative work lead to excessive net leaf carbon loss at the US-Tr alpine site and a carbon disadvantage at the IT-Tr alpine site. The additional shade created by the greater leaf area of the simulated forest vegetation in the alpine environmental conditions of the these two sites leads to an extended snowmelt season with temperature inversions and negative work performed sometimes well into the summer. To illustrate this behavior, Figure 3.5a displays the snow depth and average daily photosynthetic and above-ground autotrophic respiration rates obtained from model simulations for each United States Rocky Mountains scenario during 2009. The Italian Alps scenarios exhibit similar (though less extreme) behavior (see Fig. A.11 in the *Supplementary Information*). Upon comparing the snow depth trends in the top two panels, the simulated forest ecosystem (US-Tr) accumulates more snow than the alpine fellfield (US-Alp) and has snowpack present well into July, aided by increased shade from the trees. The extended presence of snow in the US-Tr ecosystem prevents photosynthesis from switching on in April or May as it does in the other scenarios [100]. The active photosynthetic period for US-Tr instead begins in July

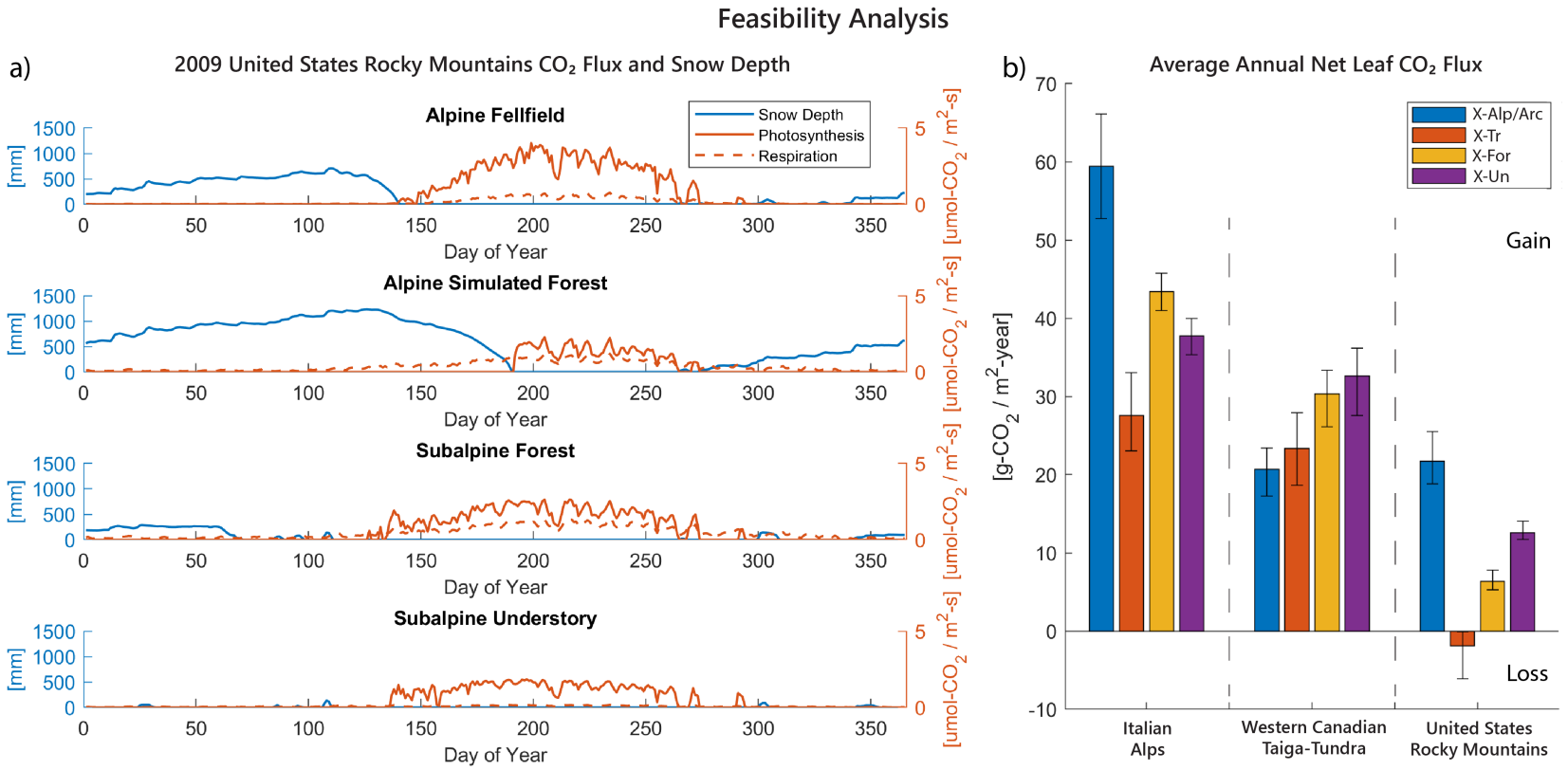

Figure 3.5: easibility analysis demonstrating annual net loss of carbon flux for the United States Rocky Mountains alpine simulated forest counterfactual scenario due to increased snowpack and shortened growing seasons. (a) 2009 daily timeseries of modeled snow depth (*blue*) and leaf CO_2 flux – the averaged daily photosynthetic CO_2 uptake (*orange solid line*) and above-ground autotrophic respiration (*orange dotted line*) – for the United States Rocky Mountains scenarios. For the alpine simulated forest, cooler temperatures near the earth's surface result in faster accumulation of snow and less snowmelt throughout the winter, extending the time needed to melt the snow. Thus, the simulated forest exhibits compounding snow depth and an abbreviated summer season without snowpack, leading to shortened photosynthesis periods compared to the alpine fellfield scenario (*top panel*). (b) Modeled average annual net leaf CO_2 flux over the entire study period (IT, 2 years; CA, 3 years; US, 6 years). Positive flux corresponds to net leaf uptake (i.e., photosynthesis minus above-ground autotrophic respiration). Error bars indicate the range of annual net leaf CO_2 flux for all years of the study period. Simulated forests for the two alpine sites (*orange*; US-Tr & IT-Tr) experience decreases in net CO_2 flux compared to the other scenarios. Further, the US-Tr scenario exhibits overall losses in CO_2 year to year, creating unsustainable mass balance for biomass productivity and indicating that the counterfactual is infeasible.

and ends in October, slightly earlier than the other scenarios as well. In contrast, respiration continues to occur throughout the entirety of the summer for all scenarios [101]. Thus, the shorter photosynthetic period leads to an overall net loss in CO_2 from the vegetation for the simulated forest scenario.

To demonstrate this carbon loss on a yearly basis, Figure 3.5b displays the total modeled annual net leaf CO_2 flux for all scenarios averaged over the years of each location's study period (see *Supplementary Information*, Appendix A.2). The Italian Alps counterfactual trees scenario (IT-Tr; *orange*) exhibits a gain of CO_2 lower than the other scenarios at this location. Although this may not be an infeasibility, the lower net CO_2 gain may not be able to sustain the additional leaf area associated with the trees. Thus, we designate this as a disadvantage for the IT-Tr scenario over the other scenarios in the Italian Alps. Alternatively, the United States Rocky Mountain alpine simulated trees scenario (US-Tr; *orange*) exhibits a net loss of CO_2. This annual net loss of CO_2 indicates that the existence of trees under alpine environmental conditions is not sustainable in the long term. Thus, the existence of the forest vegetation at the alpine site should be considered infeasible. Further, this carbon loss is a result of a feedback loop initiated by the increased leaf area of the simulated trees. The excess shade slows the melting of the snow. By the time the snow fully melts, the delayed start of photosynthetic CO_2 uptake results in a shortened photosynthesis window such that the overall gain of carbon is unable to account for the loss of carbon from respiration. For ecosystems to exist, their leaf carbon exchange (i.e., photosynthetic CO_2 uptake minus above-ground autotrophic respiration) must be positive at minimum. Thus, annual net carbon loss indicates another infeasibility. Although this infeasibility manifests through excessive carbon loss, it is in fact also a consequence of changes in thermodynamic behavior.

3.3.4 Thermodynamic Limits

The analyses described in the previous sections demonstrate how the alpine counterfactual tree scenarios lead to thermodynamic infeasibilites expressed through extensive negative work performed and annual net carbon loss. To better understand the role of additional LAI

resulting from the incorporation of trees in the counterfactual alpine/Arctic scenarios, total LAI is plotted alongside work and resultant temperature gradient (from Fig. 3.3) for the Western Canadian Taiga-Tundra (Fig. 3.6a) and the Italian Alps (Fig. 3.6b). The top-left panel for both locations demonstrates increasing magnitudes of work, both positive and negative, as LAI increases. In the top-right panel, the simulated trees scenarios (red; *X-Tr*) have resultant temperature gradients hovering closer to zero in comparison to the other three scenarios across the entire range of annual LAI, indicating that this vegetation scenario is more effective at dissipating heat throughout the year. The bottom panels show that the marginal work performed for a positive temperature gradient is greatest for Arctic/alpine simulated tree scenarios (red; *X-Tr*). However, the work performed under a negative temperature gradient is largely negative due to the continued loss of heat from the ecosystem (against the temperature gradient) during temperature inversions. The existing Arctic/alpine scenarios (blue; *X-Arc/Alp*) exhibit negative work fluxes as well, but with much lower magnitude. These two plots further demonstrate that as LAI increases, the work versus temperature gradient relationship transitions from lower to higher magnitudes of work, yielding significant negative work performed by the counterfactual forest vegetation structure (*X-Tr*), which demonstrates thermodynamic infeasibility.

We use the Western Canadian Taiga-Tundra and the Italian Alps as examples here to demonstrate that the infeasibility conditions do not need to manifest in terms of net carbon loss for the counterfactual tree scenario (*X-Tr*) to become infeasible. The thermodynamic infeasibility associated with prolonged negative work performance alone is enough to prevent the existence of trees at the Arctic site. For additional context, the sub-Arctic site is located within the forest-tundra ecotone, so the prevalence of trees is less dense than sites further below the treeline. Because of this, the difference in leaf area is not as great between CA-Tr and CA-Arc scenarios as the other sites. Thus, the snowmelt is not excessively prolonged, and the photosynthesis window does not shorten substantially. Thus, the Arctic simulated trees scenario (CA-Tr) does not exhibit the infeasibility or disadvantage from CO_2 loss in comparison with the other two regions. Even so, trees do not exist on the Arctic site, and we attribute this to the thermodynamic infeasibility instituted from the negative work and temperature inversions from the extended snowmelt and snow cover season.

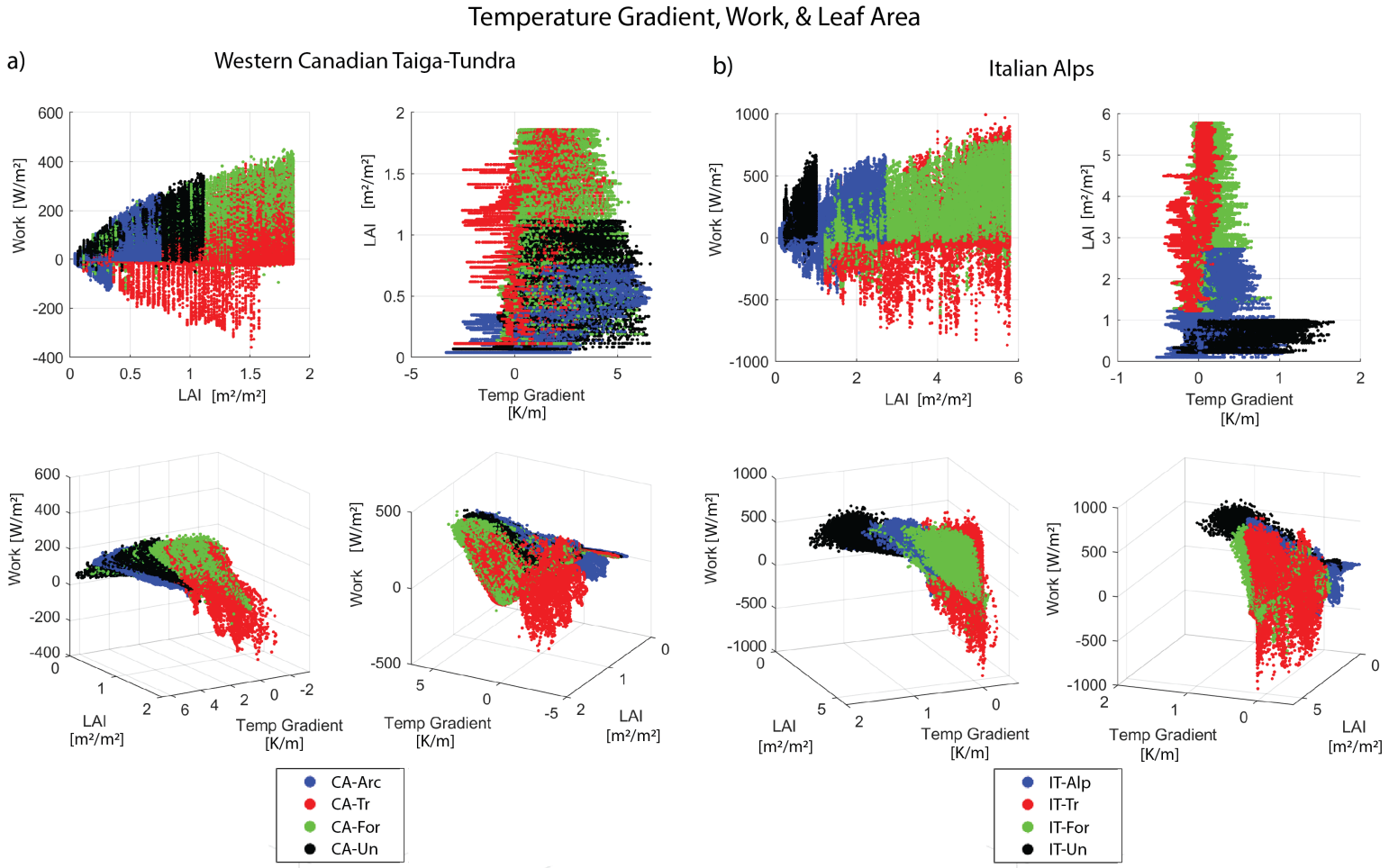

Figure 3.6: Four projected views from the 3-D plot of work, temperature gradient, and total leaf area index (LAI) for the (a) Western Canadian Taiga-Tundra and (b) Italian Alps scenarios. The top panels display that increases in LAI lead to increases in the magnitude of work and smaller resultant temperature gradients. The 3-D views in the bottom panels show the transition from flatter curves to greater magnitudes of work with increases in resultant temperature gradient as more LAI is incorporated for each set of environmental conditions (i.e., alpine, subalpine). The simulated alpine/Arctic forest scenarios (red; *X-Tr*) exhibit considerable negative work performed since the LAI is beyond the supported limit of the local environmental conditions.

Overall, the results highlighted in Figure 3.6 demonstrate that marginal changes in work have a positive relationship with LAI, yielding considerably larger magnitudes of work (both positive and negative) with increases in LAI. Further, the persistence of resultant temperature gradients for the Arctic/alpine counterfactual trees scenarios (X-Tr) around and below zero throughout the year indicates that the greater dissipation of heat by this vegetation structure leads to feedbacks such that the resultant temperature gradient inverts and negative work becomes common. Thus, the vegetation for the X-Tr counterfactual scenarios is too effective at dissipating heat for the given incoming radiation and environmental conditions. This behavior is consistent for all three locations considered in this study (see Fig. A.12 in the *Supplementary Information*, Appendix A.2). Based on these observations, we conclude that the negative work demonstrated during temperature inversions in the simulated forest scenarios (X-Tr) offsets the advantages (greater marginal work increases) exhibited during positive resultant temperature gradients. Thus, for each of the three locations studied, trees modeled beyond the treeline are thermodynamically infeasible.

3.4 Discussion

The counterfactual scenarios of trees simulated at alpine and Arctic sites resulted in thermodynamic conditions of infeasibility at all three locations modeled in this study: the Italian Alps, the United States Rocky Mountains, and the Western Canadian Taiga-Tundra. Further, the results from all three locations demonstrate how the relationship among LAI, work, and temperature gradient reveals that the additional leaf area associated with trees at Arctic/alpine sites leads to higher magnitudes of work throughout the year, forcing a negative resulting temperature gradient. We, therefore, discuss and propose a new framework associated with this phenomenon in terms of the thermodynamic behavior of ecosystems.

As previously mentioned, existence of vegetation is made thermodynamically feasible through the establishment of a temperature gradient from the earth surface to the air above the canopy that supports positive work associated with the net dissipation of heat. Based on the results presented, we propose that the vegetation and associated leaf area present in an ecosystem are directly related to the strength of the incoming radiation and its feedback

with local environmental conditions, which we refer to as a location's *potential dissipation capacity*.

Similar to the concept of potential evapotranspiration or potential net ecosystem production [102], potential dissipation capacity indicates the maximum possible dissipation of heat that is thermodynamically feasible in a given ecosystem. In ecosystems, vegetation structure and temperature gradient self-organize concurrently based on the potential dissipation capacity of a given ecosystem. The resultant temperature gradient is a consequence of the net radiation, air temperature and other environmental conditions, and the dissipation of heat performed by the vegetation itself, or the actual dissipation rate. This process can be represented by either a positive or negative feedback loop (Fig. 3.7). Feasible vegetation structures perform work equivalent to or below their ecosystem's potential dissipation capacity, meaning heat dissipation and positive work lead to lower surface temperatures and weaker resultant temperature gradients, indicating a negative feedback loop. When the leaf area present dissipates heat beyond the potential dissipation capacity of an ecosystem (e.g., simulated trees at an alpine/Arctic site), the resultant temperature gradient becomes negative, leading to prolonged temperature inversions and thermodynamic infeasibility. In this case, a positive feedback loop occurs such that additional heat dissipation further inverts the temperature gradient leading to additional negative work performed. With a lower potential dissipation capacity, less leaf area is needed to dissipate heat throughout the ecosystem on an annual basis, and the ecosystem will self-organize towards a less effective dissipative structure (e.g., shrubs or grasses only) in response. Additional leaf area then becomes less advantageous, or even infeasible. The inherent thermodynamic difference above and below the treeline is the following: the potential dissipation capacity of the ecosystem is greater below the treeline than above, resulting in the need for more effective dissipators, or trees. Trees and their additional leaf area are too productive at performing work for the sites beyond the treeline, and thus, they do not exist.

Figure 3.7 provides a conceptual model representing the thermodynamic behavior of the subalpine/sub-Arctic and alpine/Arctic ecosystems. Both plots present three curves representing different vegetation scenarios for a given ecosystem with set environmental conditions: bare soil (*dotted line*), understory only (*orange, blue*), and forest vegetation including

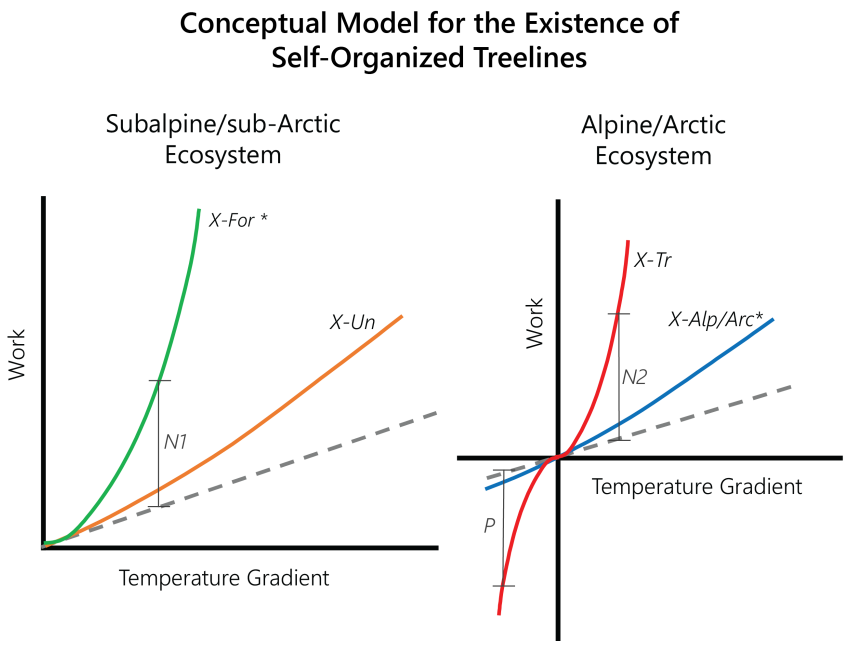

Figure 3.7: Conceptual model for the existence of treelines as a result of self-organization from the balance of positive or negative feedback between the work performed by various vegetation structures and the resulting temperature gradient. The dotted line represents an ecosystem without vegetation (i.e., bare soil). The colored solid lines represent vegetation curves as defined in Table 3.1. Dissipation rates leading to negative (*N1* or *N2*) or positive (*P*) feedback loops between temperature gradient and vegetation structure are shown as the vertical distance from the bare soil curve to the vegetation scenarios. The starred scenario on each plot represents the most advantageous viable vegetation structure for the given ecosystem. The plot on the left represents ecosystems in which both vegetation scenarios (*X-For* & *X-Un*) are viable options, and the *X-For* scenario is most advantageous. The plot on the right represents ecosystems in which one of the vegetation scenarios (*X-Tr*) is infeasible due to positive feedback loops that result in continued dissipation of heat during temperature inversions. Instead, the *X-Alp/Arc* scenario is the most advantageous viable vegetation structure.

understory and overstory trees (*green, red*). The vertical distance from the dotted line to any vegetation scenario curve at a given temperature gradient indicates the rate of work performed as a result of self-organized vegetation structure. When the vegetation curve is above the dotted line, then the vertical distance (*N1* or *N2*) represents the energy dissipation that results in a typical negative feedback loop between the vegetation and the temperature gradient. When the vegetation curve is below the dotted line (*X-Tr*), then the vertical distance (*P*) represents the energy dissipation that results in a positive feedback loop between vegetation and the temperature gradient, meaning that the ecosystem loses heat against the resultant temperature gradient. When strong enough, this positive feedback results in prolonged temperature inversions and thermodynamic infeasibility. The subalpine/sub-Arctic ecosystem diagram on the left represents ecosystems in which all vegetation scenarios are viable options, and the *X-For* scenario is most advantageous. The alpine/Arctic ecosystem diagram on the right represents ecosystems in which one of the vegetation scenarios (*X-Tr*) is infeasible due to a strong positive feedback loop that results in continued dissipation during temperature inversions. As a result, the *X-Alp/Arc* scenario is the most advantageous viable vegetation structure.

N1 and *N2* in Figure 3.7 indicate the additional work performed from dissipative structures (i.e., vegetation) for a given resultant temperature gradient. This represents the improved ability of the ecosystem to export energy from the earth surface to the air above the canopy rapidly and efficiently. However, this chapter demonstrates that more dissipation does not always indicate the optimal or more probable state, such as in the case of trees simulated beyond a treeline. In this case, the trees actually transport energy out of the ecosystem more quickly than warranted by the ecosystem's potential dissipation capacity, resulting in considerable temperature inversions, as demonstrated by *P* in Figure 3.7. The incoming radiation and environmental conditions of the alpine and Arctic sites do not yield a strong enough potential dissipation capacity to warrant the dissipation of heat facilitated by the *X-Tr* vegetation; thus, prolonged temperature inversions occur. Overall, trees cause heat dissipation that is not needed or beneficial to the ecosystem under alpine or Arctic conditions.

This research opens the door for further study defining the naturally-occurring transition

of vegetation structures. We present potential dissipation capacity as a theoretical concept for understanding the maximum dissipation rate for any given ecosystem, dependent on the incoming radiation and environmental conditions at its location. We anticipate that there is a relation among incoming radiation, temperature, and other local properties, such as emissivity and reflectance, that could further define this concept into a measurable quantity. The definition of such a relation would enable scientists to anticipate changes in vegetation structure from human-induced perturbations as well as gradual alterations to environmental conditions.

3.5 Conclusion

Based on the results of this study, we conclude that the trees do not exist beyond a treeline because they would be thermodynamically infeasible due to the considerable negative work demonstrated by the counterfactual scenarios for all Arctic/alpine locations, *X-Tr*. An additional condition of thermodynamic infeasibility limits trees from existing beyond the treeline due to the annual net loss of carbon resulting from compounding accumulation of snowpack and shortened photosynthesis windows exhibited at the United States Rocky Mountains counterfactual alpine scenario, US-Tr. Overall, these two conditions of infeasibility associated with this counterfactual elucidate the thermodynamic requirement for the existence of vegetation structure. The thermodynamic basis for the demarcation of Arctic and alpine treelines is determined by the location beyond which the dissipation rate of trees is greater than what is needed for the ecosystem based on feedback loops among the local environmental conditions and the concurrent self-organization of vegetation structure and temperature gradient, or its potential dissipation capacity.

This research arrives at a thermodynamic theory for the directionality of ecosystem self-organization towards the vegetation structure that most effectively dissipates heat without resulting in a positive feedback loop leading to prolonged temperature inversions. This dissipation rate will correlate to the magnitude of the potential dissipation capacity at a given site. Therefore, greater potential dissipation capacity calls for higher dissipation rates enabled by multiple functional groups and increased LAI. When such vegetation structure with

multiple functional groups produces higher dissipation rates than the ecosystem's potential dissipation capacity – as is the case for forest vegetation with trees beyond a treeline – the vegetation structure is then thermodynamically infeasible and does not exist.

3.6 Additional Information

Supplementary information is available for this chapter in Appendix A.2.

CHAPTER 4

ECOSYSTEM THERMODYNAMIC RESPONSE TO ANTHROPOGENIC ALTERATION OF VEGETATION STRUCTURE

4.1 Introduction

As human activities modify the architecture of Earth's natural systems, researchers are struggling to capture how these systems will respond over the next century [103–106]. As ecosystem vegetation is altered through human activities, responses can impact the function and stability of the entire ecosystem [105]. Furthermore, as plant and ecosystem functions deviate from present conditions, the ecosystem-derived services will also change, creating a feedback from human activities to life-sustaining services – such as those related to clean air, and water and food availability – that last generations [107]. To better predict these changes in services, we need methods to assess the holistic behavior of ecosystems as perturbations increase. This chapter studies the ecosystem impacts of direct human alterations to vegetation structure in the form of logging in the Brazilian Amazon and controlled burns in the United States Great Plains by modeling ecosystems as open thermodynamic systems.

By viewing ecosystems as open thermodynamic systems, maintained far from equilibrium by the spatial imbalance of energy, mass and energy fluxes in and out of the system control volumes can be studied to assess the thermodynamic behavior and self-organization of natural ecosystems. Self-organization describes how ecosystems naturally evolve to develop different structured forms, or stable states, such as vegetation. In response to external forcing, ecosystem vegetation will organize to dissipate heat from higher to lower temperatures along a gradient. Recent work asserts that ecosystem organization is thermodynamically driven by the concurrent self-organization of vegetation structure and temperature gradients based on the strength of an ecosystem's dissipation capacity – determined by the incoming radiation and other site-specific environmental/weather conditions (e.g., wind, soil type, emissivity,

etc.) (Chapter 3). We define vegetation structure as the composition of the number and types of plant functional groups in an ecosystem. A plant functional group corresponds to a set of species that perform the same ecosystem functions [6]. Due to the one-dimensional functionality of the physics-based ecosystem model used, we assume a homogeneous spatial organization at a given location. In previous chapters, the organization of vegetation structure for natural ecosystems has been characterized by both thermodynamic feasibility and thermodynamic advantage, stating that ecosystems will evolve to the state with the greatest thermodynamic advantage – defined by larger entropy fluxes, more work performed, and higher work efficiency – which is thermodynamically feasible (Chapters 2 & 3) [35]. This work developed a framework for understanding the self-organization and natural structure of ecosystems. However, little has been done to study ecosystem thermodynamic behavior in response to human-induced perturbations [22].

Similar to natural ecosystems, anthropogenically-altered ecosystems are driven by changes in environmental forcing; yet, they also have an additional driver of change: human activities. Human activities can alter ecosystem structure and function both indirectly, by causing changes to environmental forcing entering and/or leaving an ecosystem, and directly, by altering the vegetation structure itself. In this chapter, we focus on the latter case in that environmental conditions are relatively unchanged, but human activities directly alter vegetation structure. In looking at this type of manupulation, we seek to understand the impact of these alterations on ecosystem thermodynamic behavior, which drives the overall stability and organization of vegetation structure.

Former studies modeling the thermodynamic behavior of natural ecosystems assume a quasi-stable state, meaning these ecosystems have maintained the same vegetation structure over decades of observation (Chapters 2 & 3). Those ecosystems are assumed to have already undergone self-organization such that they exist in a quasi-stable state with regard to vegetation structure (multiple functional groups or one functional group, grasses or shrubs, etc.). However, when human activities alter vegetation structure, the ecosystem no longer exists in a quasi-stable state. We consider these ecosystems as experiencing a phase transition.

Phase transitions are a conduit between varying levels of order and disorder which "imply the change in internal symmetry of the components" [108]. In ecosystems, phase transitions

correspond to changes in levels of order between vegetation structures, both spatially and temporally. For this chapter, we study the latter to identify how human activities that alter vegetation structure lead to changes in thermodynamic behavior. Following such an event, the ecosystem incoming radiation and local environmental conditions remain relatively unchanged (see *potential dissipation capacity* in Section 4.2.3), but the vegetation structure undergoes self-organization to return to an optimal, quasi-stable vegetation structure. By considering a perturbed ecosystem as undergoing a phase transition, we can diagnose changes in the internal order of an ecosystem by observing ecosystem-level thermodynamics. In particular, we ask the following question: *How does the act and frequency of vegetation structural alteration from human activities affect ecosystem thermodynamic behavior?* To address this question, we compare the thermodynamic behavior of forest ecosystems due to logging in the Brazilian Amazon and tallgrass prairie ecosystems due to controlled burns in the Kansas Konza Prairie. This work allows us to better understand ecosystem response to human activities such that we can identify the degree to which thermodynamic advantage is linked to ecosystem stability. *We hypothesize that ecosystems experiencing alterations to vegetation structure from human activities will be held in a sub-optimal and, therefore, thermodynamically disadvantageous state.*

4.2 Materials and Methods

In this study, we characterize two different types of ecosystems experiencing direct alterations to vegetation structure, each modeled based on data from two sites with varying frequency or levels of disturbance.

First, we study and model two sites located in the Brazilian Amazon. The Santarem Logged Forest (Sa3) experiences selective logging every two years on average. This site is compared with the Santarem Primary Forest (Sa1; *TAP in Chapter 2*), which does not experience logging and is considered for this study as the undisturbed site. These two sites are modeled and compared over the duration of data availability for a common period (2002). This analysis demonstrates the variation in thermodynamic behavior between logged and undisturbed sites in the year following a logging event.

Second, we compare two sites in the Konza Prairie Long-Term Ecological Research (LTER) Program (`http://lter.konza.ksu.edu/`): KON, which is burned every year and consists almost entirely of native tallgrass, and KFB, which is burned every four years and consists of patches of dogwood and native tallgrass based on the burn cycle [109, 110]. The percent landcover occupied by the dogwood is dependent on the time expired since a burn event, with larger percentages prior to a burn and lower percentages directly following one (see Fig. 4.1a). The first site is identified as KON by the AmeriFlux Network and 1D or KNZ by the Konza Prairie LTER. The second site is identified as KFB by the AmeriFlux Network and 4B or K4B by the Konza Prairie LTER. We model these sites over the duration of data availability for a common period: mid-2016 through the end of 2018. We then compare the two sites to determine how varying burn frequencies impact thermodynamic behavior. Further, we compare the KON tallgrass site and the KFB site with transient behavior between grass and dogwood with a counterfactual 100% dogwood vegetation scenario. For this scenario, we use the environmental forcing and vegetation parameters of the KFB site, assuming that it is 100% covered by dogwood. This allows us to compare the three different vegetation structure scenarios on the Konza prairie: 100% shrubcover, 100% tallgrass, and a transient vegetation structure between shrubs and grasses imposed by the burn frequency.

We model all four sites using a one-dimensional physics-based model that encompasses the canopy, soil and root subsystem. The following sections provide in-depth model (Section 4.2.2) and site (Section 4.2.1) descriptions as well as definitions of important thermodynamic properties (Section 4.2.3).

4.2.1 Site Descriptions

Brazilian Amazon

The study sites used to model behavior with respect to logging events are the Santarem Km 83 Logged Forest (Sa3; 3.0180°S, 54.9714°W) and the Santarem Km 67 Primary Forest (Sa1; 2.8567°S, 54.9589°W) sites in the FLUXNET2015 network located 16 km apart in the Tapajos National Forest in Pará, Brazil [59, 111]. This evergreen broadleaf forest in

Amazonian Brazil has a tropical monsoon climate with vegetation consisting of dozens of known tree species and lianas [7, 55]. Domingues et al. [7] demonstrated the importance of modeling ecosystems based on functional groups to balance model performance with accuracy. For this high biodiversity ecosystem in Amazonia, the vegetation is represented by four groups within the MLCan model: understory tree (UN), mid-canopy tree (MT), upper-canopy tree (OT), and upper-canopy liana (L) according to Domingues et al. [7] and Quijano and Kumar [55].

The Sa3 logged site was selectively logged for tree diameters greater than 50cm in September 2001 and September through December 2003 [111–113]. On the other hand, the Sa1 site has not experienced logging. The Sa3 logged site is compared with the neighboring Sa1 undisturbed site to the identify the differences in thermodynamic behavior for the year following a logging event (2002).

Kansas Prairie

Two proximally located (less than one mile apart) native tallgrass prairie sites in the Konza LTER in Kansas were used to study the thermodynamic impact of controlled burns on a grassland (native tallgrass prairie) in a humid subtropical climate [109, 110]. The KON site (39.0824°N, 96.5603°W) experienced controlled burns every year [109]. The KFB site (39.0745°N, 96.5951°W) experienced burns every four years [110]. Both sites are dominated by perennial C4 grasses, including switchgrass (*Panicum virgatum*), indiangrass (*Sorghastrum nutans*), and species of bluestem (*Andropogon gerardii*, *Schizachyrium scoparium*). However, there has been recent rapid encroachment of dogwood (*Cornus drummondii*) overtaking the prairie grass at the KFB site [114–116].

At the 4-year burned KFB site, woody vegetation has been encroaching into tallgrass prairie in the form of shrub islands. These shrub islands are patches of land where shrubs organize close together, and once large enough can protect the interior of the islands to fires, allowing further growth and expansion of woody species [115, 116]. Since these shrub islands take up distinct land area from the C4 grasses of the tallgrass prairie, we model the KFB site as the aggregation of two separate vertical columns, creating a weighted average of the two

with a linear increase in shrubcover after a burn event from 10% to 95% shrubcover based on conversations with the site manager (Fig. 4.1a). Periods without burn events are necessary for the establishment of woody species encroachment, such as dogwood [116]. Therefore, this only occurs at the KFB and not the KON site.

Eddy covariance data from the US-KON and US-KFB sites in the AmeriFlux network were used as model input [109, 110]. We analyze both sites for the extent of the available data for running the model. For KON, the model was run for ten years (2009-2018). There were significant gaps in relative humidity in 2015 and 2016 and air pressure and wind speed in 2016. These data gaps were filled with a mean of the historical data for the date and time for each timestep to create a consecutive 10-year run, but are excluded from analysis. For KFB, the model was run for three years (2016-2018) due to limitation of data availability. This time period allows us to analyze the behavior of the ecosystem for a year prior to the burn in April 2017 and almost two years following. 2016 through 2018 are used for comparison purposes directly between the KFB and KON sites.

4.2.2 Model Description

A multi-layer canopy-root-soil model (MLCan) [27, 28, 52, 53] summarized in Section 1.5 is used to calculate the energy and entropy fluxes and temperatures for each of the ecosystem layers. Eddy covariance and additional weather forcing data at a half-hourly timescale for KON, KFB, and Sa3 and an hourly timescale for Sa1 were downloaded from the AmeriFlux and FLUXNET2015 networks, including air temperature, air pressure, global radiation, precipitation, wind speed, friction velocity, and relative humidity [59, 109–111]. The simulation period for each site was chosen based on data availability, and direct comparisons between sites were utilized only for time periods with data availability at both sites (see Section 4.2.1). The initial soil moisture and temperature profiles were produced from a spin-up of the model prior to the first year of simulation. Preparation of model input for leaf area index (LAI) half-hourly forcing data for each functional group are described below. Additional model input parameters can be found in Table 4.1.

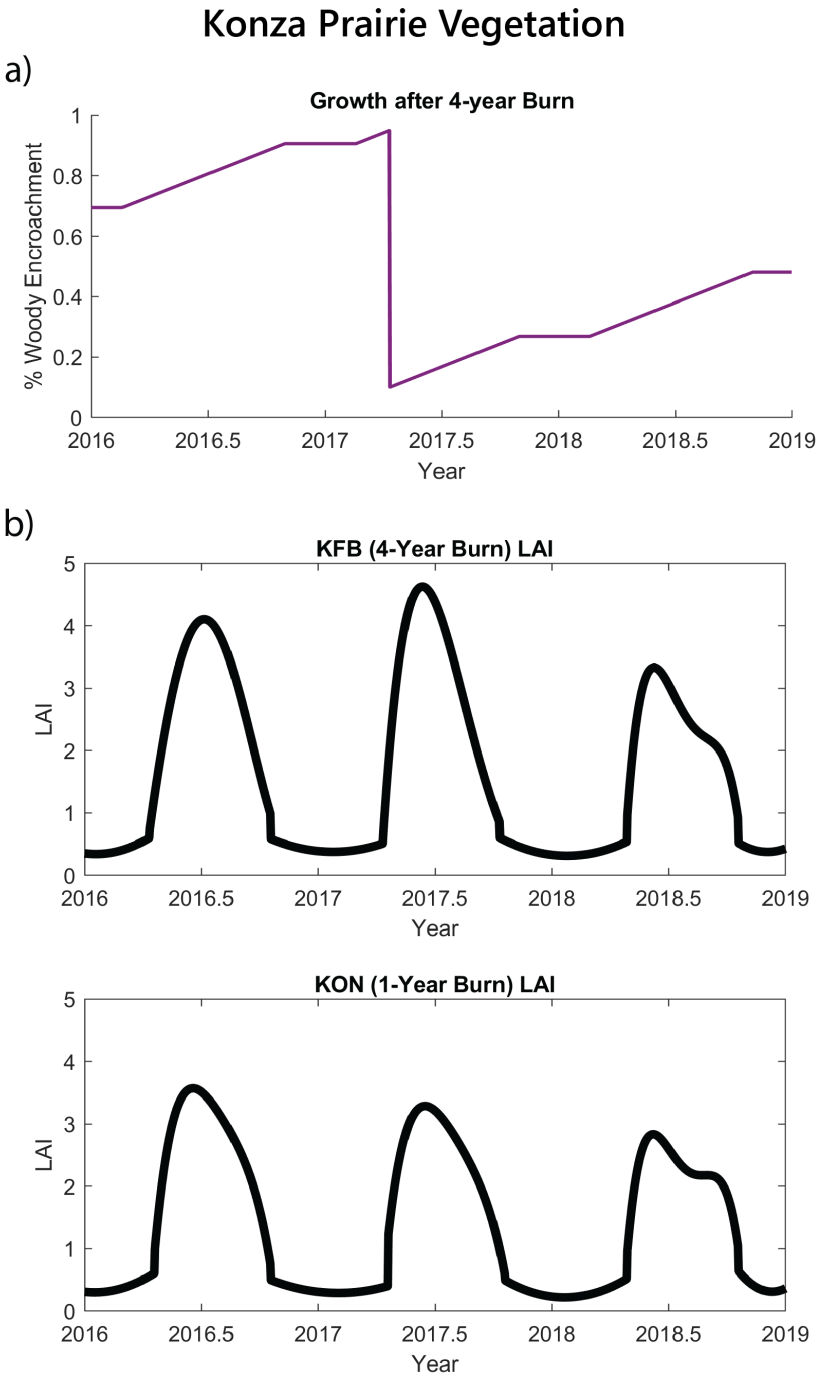

Figure 4.1: (a) Growth of woody vegetation by percent land area. The 4-year burn event occurs in April 2017. (b) Leaf area index for the Konza Prairie.

Table 4.1: List of Model Parameters

Ecosystem	**Tapajos**				**Konza**		
Site	**Sa1 & Sa3**				**KON**	**KFB**	
Functional Group	UN	MT	OT	L	UN	UN	OT
Site Information							
Percent Sand[a]	10				5[f]	7[f]	
Percent Clay[a]	80				50[f]	40[f]	
Canopy Height[a] (m)	38				1.4[g]	2.8[j]	
Ecosystem Height (m)	38				2.8	2.8	
Fluxtower Height[a] (m)	64				3[g]	3[g]	
Leaf Properties							
Vc_{max} (μmol/m^{2}s)	31.6[b]	57.5[b]	81[b]	59.7[b]	40[h]	40[h]	35[i]
J_{max} (μmol/m^{2}s)	37.9[b]	81[b]	112[b]	87.5[b]	110[h]	110[h]	140[i]
Respiration $Q10$ (mol/m^{2}s)	2[c]				2.02[e]	1.59[e]	
Root Properties							
Root Depth (m)	1	4	12	12	0.5[l]	0.5[l]	1.5[k]
z_{50} [d]	0.07	0.24	0.65	0.65	0.12[k,l]	0.12[k,l]	0.25[k]
z_{95} [d]	0.4	1.5	4	4	0.25[k,l]	0.25[k,l]	0.75[k]

[a] FLUXNET2015 Network [59, 111]
[b] Domingues et al. [7]
[c] Melton et al. [117]
[d] Schenk and Jackson [118]
[e] Zhou et al. [119]
[f] Wehmueller [120]
[g] Brunsell et al. [115]
[h] Nippert [121]
[i] Msanne et al. [122]
[j] Briggs et al. [116]
[k] Ratajczak et al. [123]
[l] Logan and Brunsell [114]

Leaf Area

LAI for the undisturbed primary forest (Km 67; Sa1) was taken from the MODIS network [124, 125] and prepared in the same way as TAP in Chapter 2 (see Appendix A.1.2; Fig. 4.2). Total LAI for the logged study site (Km 83; Sa3) was interpolated from MODIS data [124, 126] and scaled and partitioned as described above to Sa1 (Fig. 4.2). However, there is not partitioning data after logging. Further, LAI interpolated from MODIS data indicates that there is surprisingly not much difference in total LAI between the sites [124–126] (*Multi-group* in Fig. 4.2). Thus, to simulate logging we alter the partitioning of LAI among the functional groups. During logging, we assume the LAI of the overstory trees (OT) is decreased to half of its natural LAI fraction while the understory shrubs and trees (UN) increase their LAI fraction as they receive more sunlight. After logging, a growth function based on data from

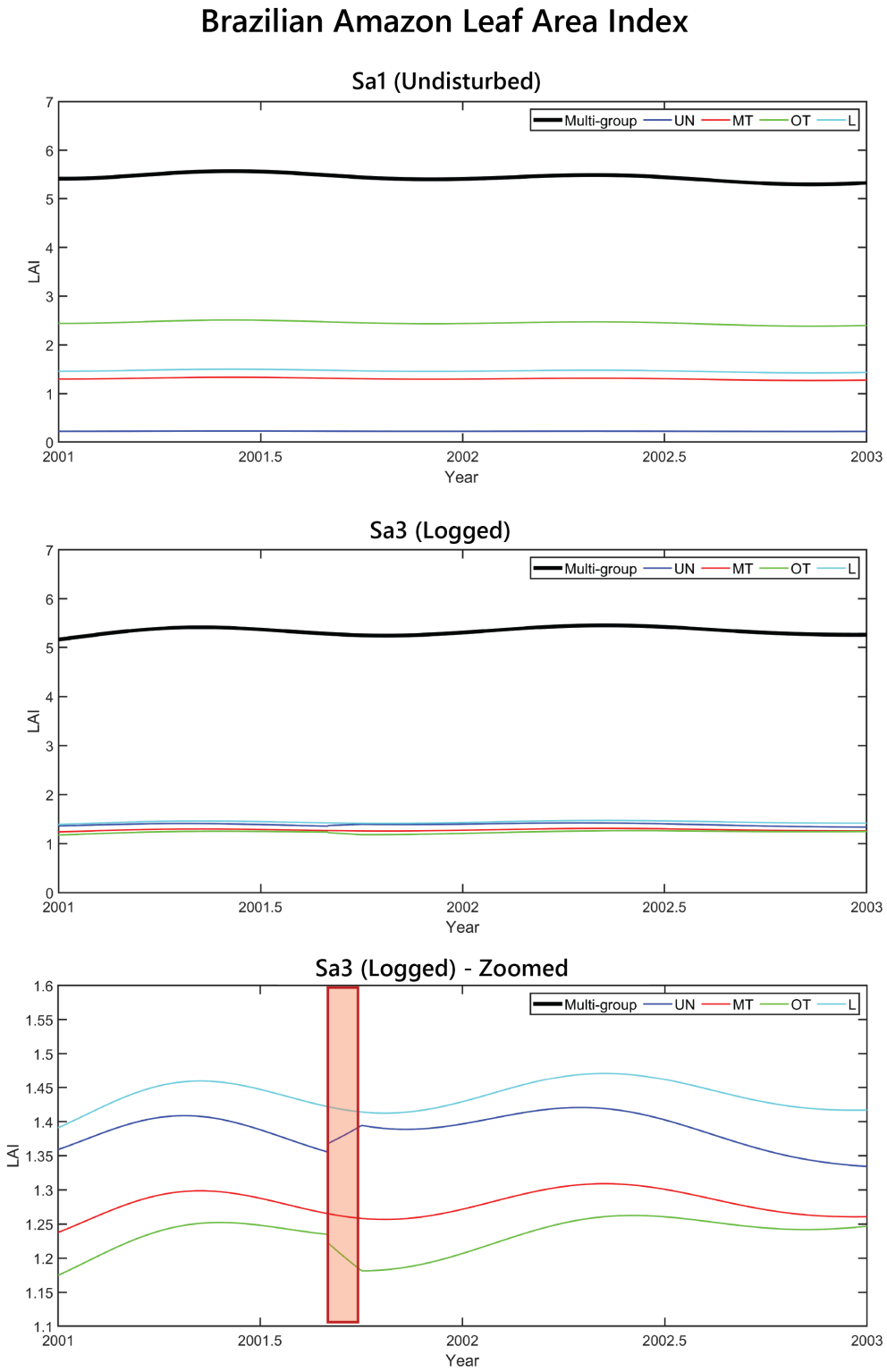

Figure 4.2: Leaf area index for the Brazilian Amazon. The shaded red area in the zoomed view of the Sa3 logged site indicates the period of selective logging.

Silva et al. [127] and Baker et al. [128] is implemented for the OT functional group.

LAI for the Konza Prairie (Fig. 4.1b) was prepared from the MODIS dataset at each site [124, 129, 130]. The LAI at both sites were modeled using two separate polynomial functions per year – a second-degree polynomial for the winter and a fourth-degree polynomial for the growing season. For KON, the MODIS LAI was scaled to include peaks to match observations in 2009 from Nippert et al. [131]. KFB is scaled by the same factor as KON for a consistent comparison.

4.2.3 Thermodynamic Properties

Entropy flux can serve as a reflection of the internal order of an ecosystem. Entropy enters into an ecosystem, is further generated by the ecosystem, and is consequently expelled to the environment. In this process, self-organization occurs within the ecosystem in the form of vegetation. This self-organization leads to reduction in entropy inside the system, but the overall outgoing entropy generally increases, consistent with the second law of thermodynamics. Changes in entropy flux leaving the ecosystem can, therefore, help us deduce alterations in the internal order of the ecosystem associated with phase transitions of vegetation structure. Larger entropy fluxes correspond to greater internal order within the ecosystem, while lower entropy fluxes indicate that an ecosystem is more homogeneous in structure (e.g., grasses) [18, 35]. Thus, we anticipate presence of human perturbations will correspond to fewer functional groups or decreases in leaf area, leading to decreases in total ecosystem entropy flux.

Entropy is calculated from an ecosystem's outgoing energy fluxes and the temperature of their source location within the ecosystem (or for shortwave radiation, the sun) [35]. Fluxes considered are shortwave radiation (SW), longwave radiation (LW), latent heat (LE), and sensible heat (H). Since all analyses are performed on a yearly basis, ground heat is assumed as net zero over the time periods studied, and is thus ignored. In its simplest form, entropy flux (in W/m^2-K) is estimated as:

$$J = \frac{E}{T} \tag{4.1}$$

in which E is the energy flux in W/m^2, and T is the temperature of the energy flux's source in K. Additional information on entropy calculations can be found in Quijano [18] and Richardson and Kumar [35] (see Chapter 2, Section 2.2.3).

Within the context of ecosystems, work is a measure of an ecosystem's ability to dissipate heat and overcome the vertical imbalance of energy with the ecosystem. Work is an indicator of the feedback of the vegetation structure with the incoming radiation and temperature profile of the ecosystem. More work performed through heat dissipation from higher to lower temperatures upwards out of the ecosystem results in a weaker resultant temperature gradient between the earth surface and the air above the canopy. Work is thus defined for ecosystems as heat transport along the temperature gradient:

$$Work = (LE + H) \times sign(\Delta T) \tag{4.2}$$

in which work, LE, and H are in units of W/m^2, and $\Delta T = T_{surf} - T_{air}$ (Chapter 3), where T_{surf} is the temperature of the soil surface, T_{air} is the temperature of the air observed above the canopy.

Work efficiency represents the ability of the ecosystem to perform work relative to the incoming energy [35]. Work efficiency is thus calculated as:

$$WE = \frac{Work}{E_{SWin} + E_{LWin}} = \frac{Work}{E_{in}} \tag{4.3}$$

in which E_{SWin} and E_{LWin} are the energy flux of incoming shortwave and longwave radiation, respectively, that consist of the total incoming energy, E_{in}, in W/m^2 (Chapter 2) [35]. Work efficiency is useful for comparing ecosystems at separate sites to determine if an ecosystem is performing more work because the vegetation is more productive at dissipating the incoming energy or if it is performing more work because it merely has more incoming energy that is available to convert into heat.

Each of the above thermodynamic properties are calculated from model output from each layer (20 canopy layers and one layer at the soil surface) and aggregated at the ecosystem level, resulting in an ecosystem's net entropy flux, work performed, or work efficiency for

each half-hourly or hourly timestep. Due to the different frequency of measurements (and hence model calculations), all analyses are performed on at least an average daily level.

The temperature gradient within an ecosystem is a self-organized outcome with the vegetation structure based on the incoming radiation and local environmental conditions. Temperature gradient is calculated at each timestep based on the modeled temperature of the soil surface and the observed temperature of the air above the canopy, both in Kelvin:

$$\frac{\Delta T}{\Delta z} = \frac{T_{surf} - T_{air}}{h_e} \tag{4.4}$$

where h_e is average the ecosystem height (Table 4.1) (Chapters 2 & 3) [35].

Lastly, we introduce the concepts of potential dissipation capacity and dissipation deficit. *Potential dissipation capacity* is the maximum possible heat dissipation rate supported by the thermodynamic environment of an ecosystem, determined by its incoming radiation and other local environmental conditions (introduced in Section 3.4). A formulation for potential dissipation capacity has not yet been developed. Yet, it is widely accepted among ecologists that nature (if unperturbed) will self-organize to exist in a form that represents its optimal state [11, 20, 22–25]. If we consider a natural ecosystem an indicator of the maximum dissipation supported by the local environment, we can estimate the potential dissipation capacity from its dissipation rate. In the context of this study, the undisturbed forest site, Sa1, is assumed to exist in a quasi-stable self-organized vegetation structure that dissipates heat that matches the potential dissipation capacity of the ecosystem (D_p), such that D_p is estimated as the actual dissipation rate (D_a) of the Sa1 ecosystem. D_a is similar to work performed, except it is not dependent on the sign of the temperature gradient. Thus, $D_a = LE+H$. For the sites studied using this analysis (Sa1 & Sa3), the temperature gradient rarely drops below zero, so actual dissipation rates and work performed are assumed to be the same.

When human activities directly alter vegetation structure, an ecosystem's D_a can be adversely impacted. Here, we introduce *dissipation deficit* to measure the degree to which such an ecosystem is impacted. A dissipation deficit occurs when the actual dissipation rate of an ecosystem or vegetation structure is less than the potential dissipation capacity of the

ecosystem. Thus, dissipation deficit is defined as:

$$D_d = D_p - D_a \tag{4.5}$$

in which D_p is estimated as the actual dissipation rate of an undisturbed site, and D_a is the actual dissipation rate of the site under consideration. For an undisturbed site, it is assumed that $D_p = D_a$ and $D_d = 0$. Dissipation deficit is calculated only for the selective logging analysis since the controlled burn study does not include an undisturbed ecosystem for estimation of D_p.

4.3 Results

For the Brazilian Amazon, we compare a logged site with an undisturbed site nearby to compare the transient state of the disturbed site with the undisturbed site for a year following a logging event. For the Konza prairie, we compare the behavior over the entire study period of two sites with consistent controlled burns of different frequencies. By analyzing both of these sites, we can document the thermodynamic impact of a transient state vs. a stable state (Amazon) and the impacts of varying frequency of disturbance events (Konza).

4.3.1 Logged Forest

For our first analysis, we compare the selectively logged Sa3 site with the undisturbed Sa1 site over the entire year following the 2001 logging event at Sa3. Figure 4.3a displays the average daily entropy flux, work performed, and work efficiency distributions for each site over the year. To prove statistical significance, these distributions are compared using the two-sample Kolmogorov-Smirnov (KS) test, which measures the maximum absolute difference between two empirical cumulative distribution functions [69–71]. For each scenario, we test the null hypotheses, H_0, that the entropy flux, work performed, and work efficiency values from the logged site are from the same continuous distribution as those from the undisturbed site. The alternate hypothesis, H_{A1}, states that the entropy flux, work performed, and work

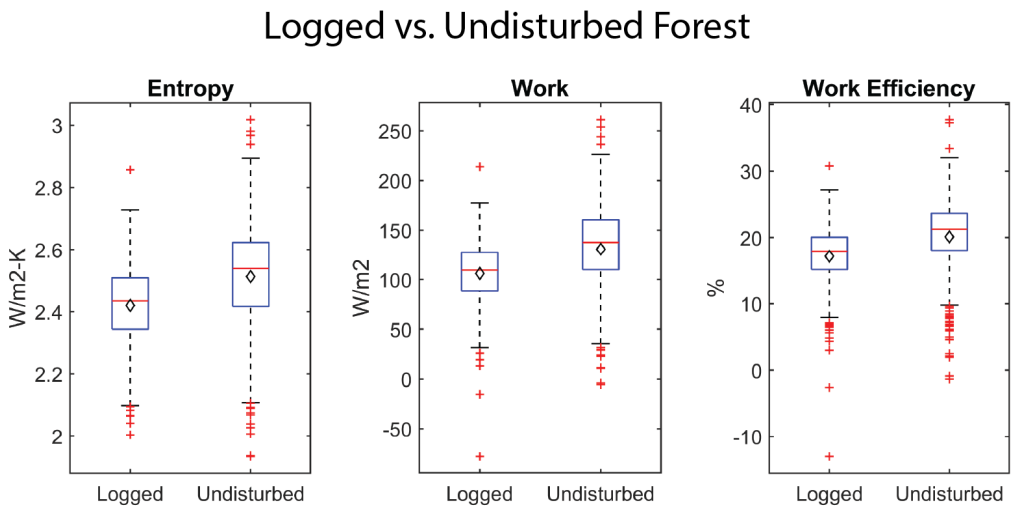

Figure 4.3: Average daily entropy flux, work, and work efficiency distributions for the logged (Sa3) and undisturbed (Sa1) forests in the Brazilian Amazon in 2002. The mean of each distribution is indicated by a black diamond. The undisturbed forest yields larger distributions for all properties; statistical significance is indicated in Table 4.2.

efficiency values for the logged site come from distributions with larger empirical cumulative distribution functions (with smaller values) than those from the undisturbed site. The results from these tests, shown in Table 4.2, indicate that H_0 is rejected in favor of H_{A1} at the 5% significance level for all three properties. This demonstrates that the thermodynamic fluxes at the logged site are statistically lower than the fluxes at the undisturbed site, indicating that the logged site is held in a sub-optimal state than the undisturbed site after a selective logging event. This state is characterized by lower internal organization (smaller entropy fluxes), lower heat dissipation rates (less total work performed), as well as less work performed for the incoming energy into the ecosystem (lower work efficiencies).

4.3.2 Prairie Controlled Burns

For the controlled burn scenarios, two variations in frequency are compared. Figure 4.4a displays the distributions of entropy flux and work efficiency for the KON and KFB sites. After comparison using the KS test (Table 4.2), we find that over the study period, the two sites do not yield significantly different values of entropy flux, work, or work efficiency (Fig. 4.4a). However, we do find that the KFB site has a weaker temperature gradient, and

Table 4.2: Two-Sample Kolmogorov-Smirnov Test

Disturb.	Alternate	Entropy		Work		WE	
Scenario	Hypothesis	p-value	Result	p-value	Result	p-value	Result
Logging	H_{A1}	1.36e-20	Reject H_0	3.55e-25	Reject H_0	1.42e-26	Reject H_0
Burns	H_{A2}	0.059	Accept H_0	0.338	Accept H_0	0.439	Accept H_0

H_{A1}: The empirical distributions of entropy flux, work performed, and work efficiency (WE) for the logged site have larger cumulative distribution functions (with smaller values) than the empirical distributions of entropy flux, work performed, and work efficiency for the undisturbed site.
H_{A2}: The empirical distributions of entropy flux, work performed, and work efficiency (WE) for the KON (1-year burn) site have larger cumulative distribution functions (with smaller values) than the empirical distributions of entropy flux, work performed, and work efficiency values for the KFB (4-year burn) site.
H_0 is rejected if $p < 0.05$ at the 5% significance level.

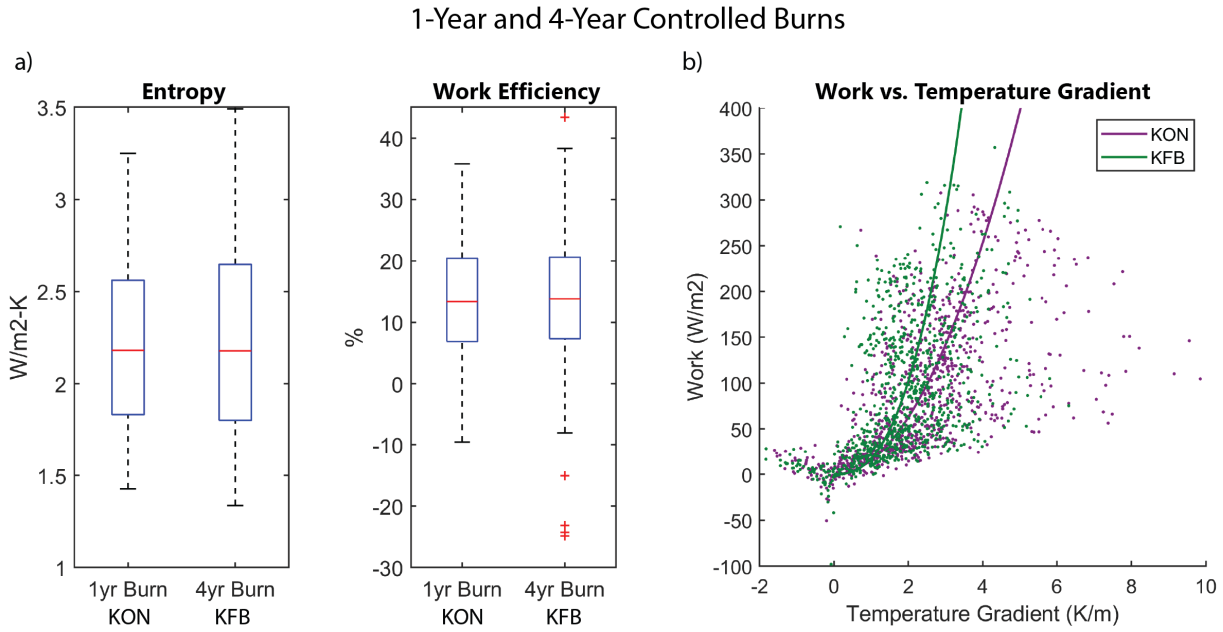

Figure 4.4: The (a) entropy flux and work efficiency distributions and (b) work versus temperature gradient plot for the prairie sites with 1-year (KON) and 4-year (KFB) burns over the entire study period. Distributions of entropy flux and work efficiency are not significantly different in (a). However, when work is set alongside temperature gradient, the difference in thermodynamic behavior is evident. (b) demonstrates that the KFB (4-year burn) vegetation structure results in a weaker temperature gradient, meaning that the presence of KFB vegetation leads to lesser vertical imbalance of energy throughout the ecosystem despite performing similar amounts of work throughout the year.

the work performed for each value of temperature gradient is greater (Fig. 4.4b). This means that although the two sites perform similar magnitudes of work, the heat dissipation at the site with the four-year burn cycle has a stronger negative feedback loop with the temperature gradient, resulting in lower surface temperatures and a weaker resultant temperature gradient. This is not surprising as the KFB site has a considerable amount of dogwood present, which could provide additional shade to the surface and strengthen the negative feedback loop.

Further, we study whether a counterfactual ecosystem with 100% shrubcover would be advantageous over either the 1-year burn cycle with 100% grasses or the 4-yr burn cycle with transient vegetation between shrubs and grasses. Figure 4.5a (similar to Fig. 4.4b) displays the work versus temperature gradient for each ecosystem. Additionally, Figure 4.5b displays temperature gradient plotted against the energy entering into the control volume. In both plots, we find that the 100% shrubcover scenario does not perform considerably differently than the KFB 4-year burn scenario with transient vegetation. At the KFB site, there is a spring-up of grasses when the dogwood has been diminished to 10% of land cover following a controlled burn. We interpret the similarities between the actual KFB site and the 100% shrubcover KFB scenario to indicate that this spring-up of grasses performs enough work and provides enough shading benefit to result in a weaker temperature gradient (i.e., cooler surface temperature) to make up for the loss of the dogwood.

Upon comparing the KFB and KON real vegetation scenarios in Figure 4.5, the KON scenario has larger temperature gradients than KFB for the same magnitudes of incoming energy as well as work performed. This indicates that tallgrass prairie vegetation has a weaker feedback with temperature gradient even though it performs similar work. Both ecosystems yield similar work performed for the energy entering into the ecosystem, but the additional shade provided by the dogwood leads to a slight thermodynamic advantage for the KFB site.

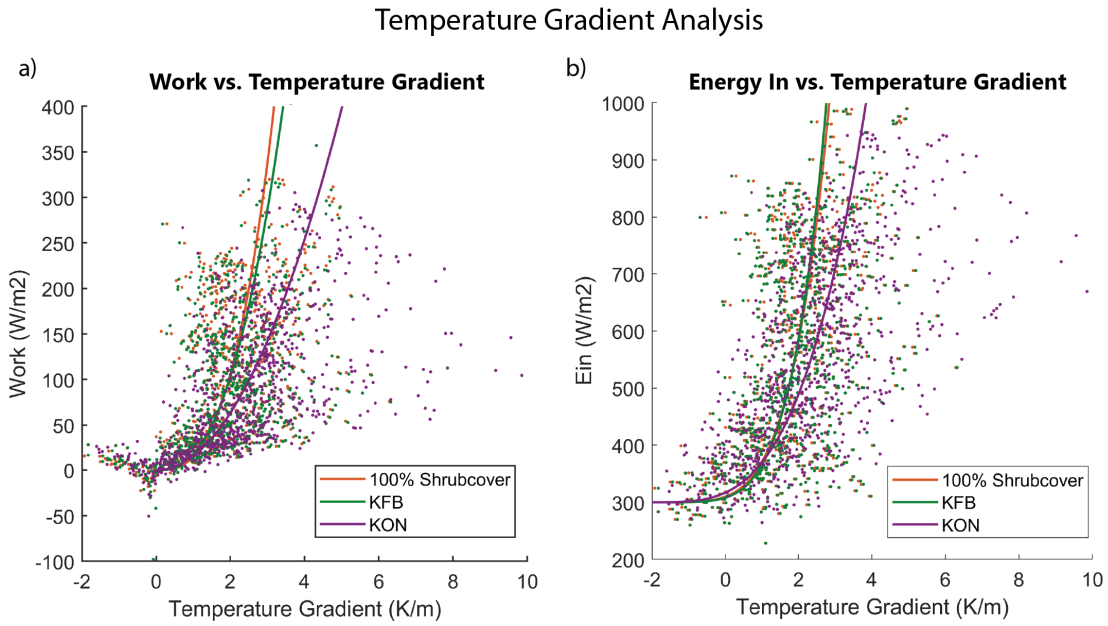

Figure 4.5: The prairie sites with 1-year (KON) and 4-year (KFB) burns are compared with a counterfactual 100% shrubcover scenario modeled at the KFB site over the entire study period. (a) Work versus temperature gradient. (b) Total incoming energy (E_{in} from Equation 4.3) versus temperature gradient. For both graphs, the 100% shrubcover scenario performs similarly to the KFB transient vegetation structure scenario. The KON site has larger resultant temperature gradients than the KFB existing and 100% shrubcover scenarios for the same E_{in} as well as work performed.

4.4 Discussion

After a logging or controlled burn disturbance event, ecosystems immediately have a different structure with a new dissipation rate than before. However, the potential dissipation capacity of the ecosystem is the same before and after the disturbance event, meaning that there is not a sudden change to ecosystem inputs, or environmental conditions, after the direct structural alteration occurs. Because the potential dissipation capacity, D_p, is the same, but the dissipation rate of the vegetation has changed, the ecosystem is performing at a dissipation deficit (Equation 4.5).

Based on these analyses, we find that the logged ecosystem is held to a dissipation deficit relative to the undisturbed forest ecosystem (Table 4.3), meaning that it is unable to dissipate heat at its optimal rate, D_p. During dissipation deficits, spikes in work efficiency will occur as ecosystems attempt through all means available to utilize this deficit. Schneider and Kay

Table 4.3: Logged Ecosystem Dissipation Deficit

Disturbance Scenario	**Avg Dissipation Rate** (W/m^2)	**Dissipation Deficit** (MJ/m^2-day)
Logged (Sa3)	106.1	2.14
Undisturbed (Sa1)	130.9	–

[11] anticipated this behavior by theorizing that dissipative structures (e.g., vegetation) will respond to changes from the external environment to remain near their quasi-stable states. To do this, when ecosystem leaf area is reduced by a disturbance event to an extent that shade to the soil surface is diminished, understory grasses and similar vegetation will spring up quickly. Trees and other woody species take longer to respond inherently since they take longer to grow and mature. Because of this, forested ecosystems are more susceptible to alterations if their species cannot regrow on timescales equivalent to or shorter than those on which they are altered. For example, trees do not grow greater than 50cm in diameter over the two-year period at which selective logging occurs. As a result, consistently selectively logged forests will be held to a sub-optimal state in the long term, resulting in a dissipation deficit, despite fluctuations in work efficiency and entropy fluxes in the short term in response to structural alterations.

This point is further demonstrated by the fact that the burned ecosystems do not experience dissipation deficits relative to each other or the 100% dogwood counterfactual scenario. Instead, the ecosystems with two different burn frequencies perform statistically similar magnitudes of work. Since the vegetation in the burned ecosystems are able to respond and mature on scales similar to the burn cycles, they are not held in a sub-optimal state. Historically, the prairie is expected to have experienced wildfires every three to four years on average prior to European settlement [116]. Thus, the viability of the vegetation structure present at the sites experiencing the four-year burn cycle, in addition to the one-year burn cycle that perpetuates the existence of the tallgrass species, is not surprising.

Since neither of these ecosystems on the Konza Prairie (with current environmental conditions) has a clear thermodynamic advantage in terms of entropy and work efficiency, we presume that either the one-year burn cycle with one functional group associated with the traditional tallgrass prairie vegetation or the four-year burn cycle with multiple functional

groups could be viable and advantageous based on the frequency of burn experienced. In current environmental conditions, the yearly burn events at the KON site provide a self-reinforcing feedback to the single functional group vegetation structure. Alternatively, the four-year burns at the KFB site do not provide the reinforcing feedback needed for the tall-grass vegetation under current environmental conditions. The extended duration of time between burns at the KFB site does not provide the ecosystem with the yearly spring-up of grasses that the KON site experiences after a burn. Instead, dogwood encroachment occurs, resulting in a stronger negative feedback between the vegetation and the temperature gradient leading to a weaker resultant temperature gradient (Fig. 4.5) and a slight advantage when fires are kept at bay.

Since available data only cover one disturbance event for the logged and 4-year burn sites, study of the changes in thermodynamic behavior directly before and after a disturbance event are limited. Access to longer continuous datasets for site pairs experiencing disturbance events will be necessary for further conclusions to be drawn as to the direct impact of human activities on the thermodynamic stability of ecosystems.

4.5 Conclusions

In this work, we compare two cases in which vegetation structure is manually perturbed. These two cases are opposite in terms of how they impact the thermodynamic stability of their respective vegetation structures. The selective logging holds the logged ecosystem at a sub-optimal state relative to the undisturbed site since the vegetation is unable to return back to its original fully-developed forest vegetation structure on scales equivalent to the frequency of disturbance (every two years on average). Alternatively, the controlled burns on the Konza Prairie actually provide a reinforcing feedback such that the ecosystems with both burn frequencies perform similar work throughout the course of the study period. The yearly burns experienced at the KON site reinforce the single functional group vegetation structure through rapid spring-up of grasses. The four-year burn cycle provides the benefit of grass spring-up every four years, but the additional time between burns allows the additional shading of the earth surface provided by the dogwood to benefit the ecosystem with lower

temperature gradients until the burn. Both sites perform similar work, but the temperature gradient of the KFB site is weaker, resulting in a slight advantage exhibited through the 4-year burn cycle.

Overall, our findings demonstrate that disturbance events from human activities can negatively impact thermodynamic behavior as well as reinforce ecosystem vegetation structure. The difference lies in the nature of the two disturbances. The logging in the Brazilian Amazon is not similar to any naturally-occurring phenomenon. Instead, human activities manually alter the organization of the forest by selectively choosing the largest trees to remove. On the other hand, the Konza Prairie has a long history of wildfires with an estimated recurrence of four years. Since the controlled burns mimic the naturally-occurring wildfires, the vegetation responds similarly, resulting in feedback between the disturbance and the vegetation structure itself.

CHAPTER 5

CONCLUSIONS

This thesis develops a thermodynamic framework for the self-organization of an ecosystem towards a vegetation structure demonstrating both thermodynamic advantage and thermodynamic feasibility. Additional methods are introduced to study ecosystems experiencing direct alterations to vegetation structure through human activities. These methods capture the thermodynamic response of such ecosystems, providing insight into the reinforcing feedback mechanisms of ecosystem processes and disturbance events and their associated timescales at the site-specific level.

5.1 Thermodynamic Advantage and Thermodynamic Feasibility

Thermodynamic advantage is defined as a vegetation structure that produces larger fluxes of entropy, performs more work, and yields higher work efficiency. Entropy is an indicator of the internal order within an ecosystem, with larger fluxes indicating more complex internal organization, typically associated with greater leaf area and multiple functional groups. However, as demonstrated in Chapter 2, entropy cannot be the sole determinant of optimal vegetation structure due to its weight given to longwave radiation. Longwave radiation is a high producer of entropy; yet, it does not directly contribute to useful work for the ecosystem. Since the outgoing longwave radiation and ground heat flux are passive loss of heat and not contributors to work performed by the ecosystem, the concepts of work and work efficiency are utilized to account for work-driven dissipation of incident energy involved in self-organization. Work demonstrates the ability of an ecosystem's vegetation structure to weaken the resulting temperature gradient by dissipating heat rapidly out of the ecosystem. This heat dissipation is an important mechanism characterizing the feedback of vegetation

structure with its local environment and the ecosystem's vertical imbalance of energy.

Thermodynamic advantage indicates that a given vegetation structure undergoes self-organizing feedbacks such that it experiences a more favorable thermal environment than another vegetation structure at a given location. Chapter 2 demonstrates that ecosystems will naturally self-organize to a vegetation structure with multiple functional groups when local availability of energy, water, and nutrients are not limiting. Through this analysis, we identify a framework that explains the prevalence of this vegetation structure due to its thermodynamic advantage over the existence of the individual functional groups that it comprises.

However, a multiple functional group vegetation structure is not always feasible. Thermodynamic feasibility, illustrated in Chapter 3, demonstrates why multiple functional groups do not exist at all locations in nature. This infeasibility arises when the actual (modeled) dissipation rate of an ecosystem is greater than the dissipation capacity of an ecosystem, i.e., $D_a > D_p$. This excess dissipation leads to positive feedback loops between the work performed by the vegetation structure and the vertical temperature gradient from the earth surface to the air above the canopy, leading to negative temperature gradients (temperature inversions) and unsustainable periods of negative work performed (i.e., heat is dissipated out of the ecosystem in the opposite direction of the temperature gradient). Sustained periods of negative work demonstrate the infeasibility associated with vegetation structures with dissipation rates exceeding the potential dissipation rates supported by the ecosystem's thermal environment. In the case of trees modeled beyond a treeline, this thermodynamic infeasibility manifests through physical indicators as well, including extended periods of snowmelt and annual net losses in leaf carbon.

This work provides a novel framework for characterizing the self-organization of natural ecosystems driven by thermodynamic advantage and thermodynamic feasibility. To incorporate the strong feedback of vegetation with climate and resource availability, we conclude that the vegetation structure to which an ecosystem will self-organize must: first, be thermodynamically feasible; second, have adequate resource availability, such as water and nutrients; and third, demonstrate a thermodynamic advantage.

5.2 Ecosystem Response to Human Perturbations

In addition to developing a framework for the self-organization of natural ecosystem vegetation structure, this thesis characterizes the ecosystem-level thermodynamic response of two types of human activities that directly alter ecosystem vegetation structure. Following a disturbance event an ecosystem is given new initial conditions of vegetation structure imposed by human activities and begins self-organization towards a feasible thermodynamically advantageous state. The study and comparison of a logged forest with an undisturbed forest demonstrates how a disturbed ecosystem could be held at a thermodynamically disadvantageous state, the degree to which is estimated as its dissipation deficit. Since forest ecosystems take decades to mature, logging events occurring at frequencies shorter than the time required for regrowth will not allow the ecosystem to self-organize to its most thermodynamically advantageous state, and thus, the ecosystem will be held at a sub-optimal vegetation structure. On the other hand, the frequency of controlled burns results in self-organization towards two different vegetation structures depending on the frequency of the burn events. When longer time periods exist between burn events, the ecosystem is able to self-organize into a more complex state with multiple functional groups. However, when the time period between burns is shorter, the vegetation structure actually benefits from the burn events, indicating a reinforcing feedback between the vegetation structure and the controlled burn.

In disturbed ecosystems, vegetation structure is greatly determined by the recurrence of the disturbance event and the feedback loops between the thermal environment, the disturbance event, and the vegetation structure itself. Self-organization must then occur within the confines of the disturbance events, the thermodynamically feasible vegetation structures, thermodynamic advantage, and the effect of the disturbance on local resource availability.

5.3 Avenues for Future Research

This thesis develops a framework for characterizing the self-organization of the vegetation structure of natural ecosystems and the response of vegetation structure to human activities from a thermodynamic perspective. The framework presented opens up new opportunities for future study, such as the following:

- Development of a mathematical estimation for potential dissipation capacity as a function of incoming radiation, temperature, and other local properties, such as emissivity and reflectance, as discussed in Section 3.4. Rather than the current estimation based on an undisturbed ecosystem, a direct estimation will enable more precise comparisons of vegetation structure and enable better understanding of possible shifts in ecosystem behavior as thermal environments change over time.

- An analysis of ecosystem thermodynamic behavior in response to additional types of human-induced perturbations, such as agricultural cultivation, which forces an ecosystem to sustain a specific vegetation structure, or long-term changes in environmental forcing that may lead to emergent climate scenarios.

- Research into the site-specific thermodynamic behavior of ecosystems leading up to and following a catastrophic shift in vegetation structure, or a regime shift, as a result of both human activities and natural disasters.

The value of this work is demonstrated by the array of research opportunities enabled by the framework proposed. As human activities increasingly affect ecosystems throughout the world, it is important to understand the potential impacts to ecosystem structure and associated function from human-induced as well as natural disturbance events. The site-specific calculations and experimental design presented in this research enable analysis of impacts of perturbations to local-scale vegetation structure, which can have important implications for land-owners and decision-makers in addition to scientific researchers. This thesis provides a foundation for deriving new insight with respect to self-organization of vegetation structure in current and future climate and disturbance regimes.

REFERENCES

[1] Mikhail Ivanovich Budyko. *Evaporation under natural conditions*. Israel Program for Scientific Translations; [available from the Office of Technical Services, US Dept. of Commerce, Washington], 1963.

[2] Mikhail Ivanovich Budyko. *Climate and life*. International Geophysics Series. Academic Press, 1974.

[3] Dan Li, Ming Pan, Zhentao Cong, Lu Zhang, and Eric Wood. Vegetation control on water and energy balance within the budyko framework. *Water Resources Research*, 49(2):969–976, 2013. doi: 10.1002/wrcr.20107.

[4] Pierre Gentine, Paolo D'Odorico, Benjamin R Lintner, Gajan Sivandran, and Guido Salvucci. Interdependence of climate, soil, and vegetation as constrained by the budyko curve. *Geophysical Research Letters*, 39(19), 2012. doi: 10.1029/2012GL053492.

[5] R. J. Donohue, M. L. Roderick, and T. R. Mcvicar. On the importance of including vegetation dynamics in Budyko's hydrological model. *Hydrology and Earth System Sciences Discussions*, 3(4):1517–1551, July 2006.

[6] Sandra Lavorel, Sue McIntyre, Jill Landsberg, and TDA Forbes. Plant functional classifications: from general groups to specific groups based on response to disturbance. *Trends in Ecology & Evolution*, 12(12):474–478, 1997. doi: 10.1016/S0169-5347(97)01219-6.

[7] Tomas F. Domingues, Luiz A. Martinelli, and James R. Ehleringer. Ecophysiological traits of plant functional groups in forest and pasture ecosystems from eastern Amazonia, Brazil. *Plant Ecology*, 193(1):101–112, 2007. doi: 10.1007/s11258-006-9251-z.

[8] Gordon B. Bonan, Samuel Levis, Laurent Kergoat, and Keith W. Oleson. Landscapes as patches of plant functional types: An integrating concept for climate and ecosystem models. *Global Biogeochemical Cycles*, 16(2):5–1, 2002. doi: 10.1029/2000GB001360.

[9] Stan D. Wullschleger, Howard E. Epstein, Elgene O. Box, Eugénie S. Euskirchen, Santonu Goswami, Colleen M. Iversen, Jens Kattge, Richard J. Norby, Peter M. van

Bodegom, and Xiaofeng Xu. Plant functional types in earth system models: past experiences and future directions for application of dynamic vegetation models in high-latitude ecosystems. *Annals of botany*, 114(1):1–16, 2014. doi: 10.1093/aob/mcu077.

[10] Susan L. Ustin and John A. Gamon. Remote sensing of plant functional types. *New Phytologist*, 186(4):795–816, 2010. doi: 10.1111/j.1469-8137.2010.03284.x.

[11] Eric D. Schneider and James J Kay. Life as a manifestation of the second law of thermodynamics. *Mathematical and Computer Modelling*, 19(6-8):25–48, 1994. doi: 10.1016/0895-7177(94)90188-0.

[12] Dilip Kondepudi and Ilya Prigogine. *Modern thermodynamics: from heat engines to dissipative structures*. John Wiley & Sons, 2014.

[13] Max Planck. *The theory of heat radiation*. Courier Corporation, 2013.

[14] Wei Wu and Yangang Liu. Radiation entropy flux and entropy production of the Earth system. *Reviews of Geophysics*, 48(2), 2010. doi: 10.1029/2008RG000275.

[15] P. T. Landsberg and G. Tonge. Thermodynamics of the conversion of diluted radiation. *Journal of Physics A: Mathematical and General*, 12(4):551, 1979. doi: 10.1088/0305-4470/12/4/015.

[16] S.E. Wright, D.S. Scott, J.B. Haddow, and M.A. Rosen. On the entropy of radiative heat transfer in engineering thermodynamics. *International Journal of Engineering Science*, 39(15):1691–1706, 2001. doi: 10.1016/S0020-7225(01)00024-6.

[17] Ichiro Aoki. Radiation entropies in diffuse reflection and scattering and application to solar radiation. *Journal of the Physical Society of Japan*, 51(12):4003–4010, 1982. doi: 10.1143/JPSJ.51.4003.

[18] Juan C. Quijano. *Coupled dynamics of above- and below-ground interactions in the critical zone*. Ph.D. University of Illinois at Urbana-Champaign, 2013. URL `http://hdl.handle.net/2142/44473`.

[19] Sven Erik Jørgensen, Søren Nors Nielsen, and Henning Mejer. Emergy, environ, exergy and ecological modelling. *Ecological Modelling*, 77(2-3):99–109, 1995. doi: 10.1016/0304-3800(93)E0080-M.

[20] Sven Erik Jorgensen and Yuri M Svirezhev. *Towards a thermodynamic theory for ecological systems*. Elsevier, 2004. doi: 10.1016/B978-0-08-044166-5.X5000-9.

[21] Sven Erik Jørgensen. *Eco-exergy as sustainability*, volume 16. Wit Press, 2006.

[22] Søren Nors Nielsen, Felix Müller, Joao Carlos Marques, Simone Bastianoni, and Sven Erik Jørgensen. Thermodynamics in ecology—an introductory review. *Entropy*, 22(8):820, 2020. doi: 10.3390/e22080820.

[23] Alfred J. Lotka. Contribution to the energetics of evolution. *Proceedings of the National academy of Sciences of the United States of America*, 8(6):147, 1922. doi: 10.1073/pnas.8.6.147.

[24] Alfred J. Lotka. Natural selection as a physical principle. *Proceedings of the National Academy of Sciences of the United States of America*, 8(6):151, 1922. doi: 10.1073/pnas.8.6.151.

[25] Eric D. Schneider and James J Kay. Complexity and thermodynamics: towards a new ecology. *Futures*, 26(6):626–647, 1994. doi: 10.1016/0016-3287(94)90034-5.

[26] D. T. Drewry, P. Kumar, S. Long, C. Bernacchi, X. Z. Liang, and M. Sivapalan. Ecohydrological responses of dense canopies to environmental variability: 2. Role of acclimation under elevated CO2. *Journal of Geophysical Research: Biogeosciences*, 115(G4), 2010. doi: 10.1029/2010JG001341.

[27] Phong V. V. Le, Praveen Kumar, Darren T. Drewry, and Juan C. Quijano. A graphical user interface for numerical modeling of acclimation responses of vegetation to climate change. *Computers & Geosciences*, 49:91–101, 2012. doi: 10.1016/j.cageo.2012.07.007.

[28] Juan C. Quijano, Praveen Kumar, Darren T. Drewry, Allen Goldstein, and Laurent Misson. Competitive and mutualistic dependencies in multispecies vegetation dynamics enabled by hydraulic redistribution. *Water Resources Research*, 48(5), 2012. doi: 10.1029/2011WR011416.

[29] Ying Zhao, Bingcheng Si, Zhenhua Zhang, Min Li, Hailong He, and Robert Lee Hill. A new thermal conductivity model for sandy and peat soils. *Agricultural and Forest Meteorology*, 274:95–105, 2019. doi: 10.1016/j.agrformet.2019.04.004.

[30] Yuanqiao Wu, Diana L. Verseghy, and Joe R. Melton. Integrating peatlands into the coupled Canadian Land Surface Scheme (CLASS) v3. 6 and the Canadian Terrestrial Ecosystem Model (CTEM) v2.0. *Geoscientific Model Development*, 9(8), 2016. doi: 10.5194/gmd-9-2639-2016.

[31] Sebastian A. Krogh, John W. Pomeroy, and Philip Marsh. Diagnosis of the hydrology of a small arctic basin at the tundra-taiga transition using a physically based hydrological model. *Journal of Hydrology*, 550:685–703, 2017. doi: 10.1016/j.jhydrol.2017.05.042.

[32] Sanna Sevanto, Tanja Suni, Jukka Pumpanen, Tiia Grönholm, Pasi Kolari, Eero Nikinmaa, Pertti Hari, and Timo Vesala. Wintertime photosynthesis and water uptake in a boreal forest. *Tree Physiology*, 26(6):749–757, 2006. doi: 10.1093/treephys/26.6.749.

[33] David R. Bowling, Barry A. Logan, Koen Hufkens, Donald M. Aubrecht, Andrew D. Richardson, Sean P. Burns, William R.L. Anderegg, Peter D. Blanken, and David P.

Eiriksson. Limitations to winter and spring photosynthesis of a rocky mountain subalpine forest. *Agricultural and Forest Meteorology*, 252:241–255, 2018. doi: 10.1016/j.agrformet.2018.01.025.

[34] Johan Bergh, Ross E. McMurtrie, and Sune Linder. Climatic factors controlling the productivity of norway spruce: a model-based analysis. *Forest ecology and management*, 110(1-3):127–139, 1998. doi: 10.1016/S0378-1127(98)00280-1.

[35] Meredith Richardson and Praveen Kumar. Discerning the thermodynamic feasibility of the spontaneous coexistence of multiple functional vegetation groups. *Scientific reports*, 10(1):1–13, 2020. doi: 10.1038/s41598-020-75050-4.

[36] Ilya Prigogine and Jean-Marie Wiame. Biologie et thermodynamique des phénomènes irréversibles. *Experientia*, 2(11):451–453, 1946. doi: 10.1007/BF02153597.

[37] Ilya Prigogine. *Étude thermodynamique des phénomènes irréversibles*. Ph.D. Brussels University, 1947.

[38] Ludwig Von Bertalanffy, Joseph Henry Woodger, et al. *Modern Theories of Development.* Humphrey Milford., 1938.

[39] Ludwig Von Bertalanffy. The theory of open systems in physics and biology. *Science*, 111(2872):23–29, 1950. doi: 10.2307/1676073.

[40] Ilya Prigogine, Ilya Prigogine, Chimiste Physicien, Ilya Prigogine, Chemist Physicist, and Ilya Prigogine. *Introduction to thermodynamics of irreversible processes*, volume 7. Interscience Publishers New York, 1961.

[41] Eric D. Schneider and James J. Kay. Order from disorder: the thermodynamics of complexity in biology. *What is life? The next fifty years: Speculations on the future of biology*, pages 161–172, 1995. doi: 10.1017/CBO9780511623295.013.

[42] Jerry S. Olson. Energy storage and the balance of producers and decomposers in ecological systems. *Ecology*, 44(2):322–331, 1963. doi: 10.2307/1932179.

[43] Crawford S. Holling. Resilience and stability of ecological systems. *Annual review of ecology and systematics*, 4(1):1–23, 1973. doi: 10.1146/annurev.es.04.110173.000245.

[44] Garth W. Paltridge. Climate and thermodynamic systems of maximum dissipation. *Nature*, 279(5714):630, 1979. doi: 10.1038/279630a0.

[45] Axel Kleidon. *Thermodynamic foundations of the Earth system*. Cambridge University Press, 2016. doi: 10.1017/CBO9781139342742.005.

[46] Eugene P. Odum. Energy flow in ecosystems: a historical review. *American Zoologist*, 8(1):11–18, 1968. doi: 10.1093/icb/8.1.11.

[47] Eugene P. Odum. Energy, ecosystem development and environmental risk. *The Journal of Risk and Insurance*, 43(1):1–16, 1976. doi: 10.2307/251605.

[48] Lionel Johnson. The thermodynamics of ecosystems. In *The Natural Environment and the Biogeochemical Cycles*, pages 1–47. Springer, 1990.

[49] G. Bendoricchio and S.E. Jørgensen. Exergy as goal function of ecosystems dynamic. *Ecological modelling*, 102(1):5–15, 1997. doi: 10.1016/S0304-3800(97)00091-4.

[50] Yuri M. Svirezhev. Thermodynamics and ecology. *Ecological Modelling*, 132(1-2): 11–22, 2000. doi: 10.1016/S0304-3800(00)00301-X.

[51] Sven E Jørgensen and Brian D Fath. Application of thermodynamic principles in ecology. *Ecological complexity*, 1(4):267–280, 2004. doi: 10.1016/j.ecocom.2004.07.001.

[52] Darren T. Drewry, Praveen Kumar, Stephen Long, Carl Bernacchi, X. Z. Liang, and Murugesu Sivapalan. Ecohydrological responses of dense canopies to environmental variability: 1. Interplay between vertical structure and photosynthetic pathway. *Journal of Geophysical Research: Biogeosciences*, 115(G4), 2010. doi: 10.1029/2010JG001340.

[53] Phong V. V. Le, Praveen Kumar, and Darren T. Drewry. Implications for the hydrologic cycle under climate change due to the expansion of bioenergy crops in the Midwestern United States. *Proceedings of the National Academy of Sciences*, 108 (37):15085–15090, 2011. doi: 10.1073/pnas.1107177108.

[54] Juan C. Quijano, Praveen Kumar, and Darren T. Drewry. Passive regulation of soil biogeochemical cycling by root water transport. *Water Resources Research*, 49(6): 3729–3746, 2013. doi: 10.1002/wrcr.20310.

[55] Juan C. Quijano and Praveen Kumar. Numerical simulations of hydraulic redistribution across climates: The role of the root hydraulic conductivities. *Water Resources Research*, 51(10):8529–8550, 2015. doi: 10.1002/2014WR016509.

[56] Gilberto Pastorello et al. The FLUXNET2015 dataset and the ONEFlux processing pipeline for eddy covariance data. *Scientific Data*, 7(1):225, July 2020. ISSN 2052-4463. doi: 10.1038/s41597-020-0534-3.

[57] Russell Scott. FLUXNET2015 US-SRM Santa Rita Mesquite. 2004-2014. doi: 10.18140/FLX/1440090.

[58] Ankur Desai. FLUXNET2015 US-WCr Willow Creek, 1999-2014.

[59] Scott Saleska. FLUXNET2015 BR-Sa1 Santarem-Km67-Primary Forest. 2002-2011. doi: 10.18140/FLX/1440032.

[60] Megan E. McGroddy, Whendee L. Silver, and Raimundo Cosme de Oliveira. The effect of phosphorus availability on decomposition dynamics in a seasonal lowland amazonian forest. *Ecosystems*, 7(2):172–179, 2004. doi: 10.1007/s10021-003-0208-y.

[61] ORNL DAAC 2018. MODIS and VIIRS Land Products Global Subsetting and Visualization Tool. ORNL DAAC, Oak Ridge, Tennessee, USA. Accessed April, 2019. Subset obtained for MOD15A2H product at -3.01803, -54.9714400, time period: 2000 to 2018, and subset size: 0.5 x 0.5 km. 2018. doi: 10.3334/ORNLDAAC/1379.

[62] Esther Lee, Praveen Kumar, Greg A. Barron-Gafford, Sean M. Hendryx, Enrique P. Sanchez-Cañete, Rebecca L. Minor, Tony Colella, and Russell L. Scott. Impact of hydraulic redistribution on multispecies vegetation water use in a semiarid savanna ecosystem: An experimental and modeling synthesis. *Water Resources Research*, 54 (6):4009–4027, 2018. doi: 10.1029/2017WR021006.

[63] Russell L. Scott, G. Darrel Jenerette, Daniel L. Potts, and Travis E. Huxman. Effects of seasonal drought on net carbon dioxide exchange from a woody-plant-encroached semiarid grassland. *Journal of Geophysical Research: Biogeosciences*, 114(G4), 2009. doi: 10.1029/2008JG000900.

[64] Peter S. Curtis, P. J. Hanson, Paul Bolstad, Carol Barford, J. C. Randolph, H. P. Schmid, and Kell B. Wilson. Biometric and eddy-covariance based estimates of annual carbon storage in five eastern North American deciduous forests. *Agricultural and Forest Meteorology*, 113(1):3–19, 2002. doi: 10.1016/S0168-1923(02)00099-0.

[65] Bruce D. Cook, Kenneth J. Davis, Weiguo Wang, Ankur Desai, Bradford W. Berger, Ron M. Teclaw, Jonathan G. Martin, Paul V. Bolstad, Peter S. Bakwin, Chuixiang Yi, et al. Carbon exchange and venting anomalies in an upland deciduous forest in northern Wisconsin, USA. *Agricultural and Forest Meteorology*, 126(3-4):271–295, 2004. doi: 10.1016/j.agrformet.2004.06.008.

[66] B.E. Ewers, D.S. Mackay, J. Tang, P.V. Bolstad, and S. Samanta. Intercomparison of sugar maple (Acer saccharum Marsh.) stand transpiration responses to environmental conditions from the Western Great Lakes Region of the United States. *Agricultural and Forest Meteorology*, 148(2):231–246, 2008. doi: 10.1016/j.agrformet.2007.08.003.

[67] Myles Hollander, Douglas A. Wolfe, and Eric Chicken. The two-sample dispersion problem and other two-sample problems. *Nonparametric Statistical Methods*, pages 151–201, 2015. doi: 10.1002/9781119196037.ch5.

[68] Rupert G. Miller. Jackknifing variances. *The Annals of Mathematical Statistics*, 39 (2):567–582, 1968. doi: 10.1214/aoms/1177698418.

[69] Donald A. Darling. The Kolmogorov-Smirnov, Cramer-von Mises Tests. *The Annals of Mathematical Statistics*, 28(4):823–838, 1957. doi: 10.2307/2237048.

[70] Ian T. Young. Proof without prejudice: use of the Kolmogorov-Smirnov test for the analysis of histograms from flow systems and other sources. *Journal of Histochemistry & Cytochemistry*, 25(7):935–941, 1977. doi: 10.1177/25.7.894009.

[71] J.D. Gibbons and S. Chakraborti. *Nonparametric Statistical Inference, Fifth Edition*. Taylor & Francis, 2010. ISBN 9781420077612.

[72] P. L. Silveston. Warmedurchange in horizontalen flassigkeitschichtem. *Heat Changes in Horizontal Silicon Oil, PhD thesis, Techn. Hochsch. Muenchen, Germany*, 1957.

[73] Andrew D. Richardson and Andrew J. Friedland. A review of the theories to explain arctic and alpine treelines around the world. *Journal of Sustainable Forestry*, 28(1-2): 218–242, 2009. doi: 10.1080/10549810802626456.

[74] Terry V. Callaghan, Ben R. Werkman, and Robert M.M. Crawford. The tundra-taiga interface and its dynamics: Concepts and applications. *Ambio*, pages 6–14, 2002.

[75] Friedrich-Karl Holtmeier and Gabriele Broll. Treeline research—from the roots of the past to present time. a review. *Forests*, 11(1):38, 2020. doi: 10.3390/f11010038.

[76] Peter Wardle. An explanation for alpine timberline. *New Zealand journal of botany*, 9(3):371–402, 1971. doi: 10.1080/0028825X.1971.10430192.

[77] Peili Shi, Christian Körner, and Günter Hoch. A test of the growth-limitation theory for alpine tree line formation in evergreen and deciduous taxa of the eastern himalayas. *Functional Ecology*, 22(2):213–220, 2008. doi: 10.1111/j.1365-2435.2007.01370.x.

[78] Stuart A. Kauffman et al. *The origins of order: Self-organization and selection in evolution*. Oxford University Press, USA, 1993.

[79] Scott Camazine, Jean-Louis Deneubourg, Nigel R Franks, James Sneyd, Eric Bonabeau, and Guy Theraula. *Self-organization in biological systems*. Princeton university press, 2003.

[80] Henning Mejer and Sven Erik Jørgensen. Exergy and ecological buffer capacity. In *State-of-the-art in Ecological Modelling*, pages 829–846. Elsevier, 1979. doi: 10.1016/B978-0-08-023443-4.50042-7.

[81] Damiano Gianelle, Roberto Zampedri, Mauro Cavagna, and Matteo Sottocornola. FLUXNET2015 IT-Lav Lavarone, Dataset. 2003-2014. doi: 10.18140/FLX/1440169.

[82] Damiano Gianelle, Mauro Cavagna, Roberto Zampedri, and Barbara Marcolla. FLUXNET2015 IT-MBo Monte Bondone. 2016. doi: 10.18140/FLX/1440170.

[83] Barbara Marcolla, A. Pitacco, and A. Cescatti. Canopy architecture and turbulence structure in a coniferous forest. *Boundary-layer meteorology*, 108(1):39–59, 2003.

[84] Dario Papale, Mirco Migliavacca, Edoardo Cremonese, Alessandro Cescatti, Giorgio Alberti, Manuela Balzarolo, Luca Belelli Marchesini, Eleonora Canfora, Raffaele Casa, Pierpaolo Duce, Osvaldo Facini, Marta Galvagno, Lorenzo Genesio, Damiano Gianelle, Vincenzo Magliulo, Giorgio Matteucci, Leonardo Montagnani, Fabio Petrella, Andrea Pitacco, Guenther Seufert, Donatella Spano, Paolo Stefani, Francesco P. Vaccari, and Riccardo Valentini. *Carbon, Water and Energy Fluxes of Terrestrial Ecosystems in Italy*, pages 11–45. Springer Berlin Heidelberg, Berlin, Heidelberg, 2015. ISBN 978-3-642-32424-6. doi: 10.1007/978-3-642-32424-6_2.

[85] M. Tudoroiu, E. Eccel, B. Gioli, D. Gianelle, H. Schume, L. Genesio, and F. Miglietta. Negative elevation-dependent warming trend in the eastern alps. *Environmental Research Letters*, 11(4):044021, 2016.

[86] Peter D. Blanken, Russel K. Monson, Sean P. Burns, David R. Bowling, and Andrew A. Turnipseed. AmeriFlux US-NR1 Niwot Ridge Forest (LTER NWT1), Dataset. 1998-. doi: 10.17190/AMF/1246088.

[87] John F. Knowles, Peter D. Blanken, Mark W. Williams, and Kurt M. Chowanski. Energy and surface moisture seasonally limit evaporation and sublimation from snow-free alpine tundra. *Agricultural and Forest Meteorology*, 157:106–115, 2012. doi: 10.1016/j.agrformet.2012.01.017.

[88] J. Knowles. Infilled climate and heat flux data for Tvan towers data loggers (CR3000), 2008 - ongoing. ver 1. Environmental Data Initiative. 2018. doi: 10.6073/pasta/10fb65e51cd04631bb80c82288b5c51a.

[89] S.P. Burns, P.D. Blanken, A.A. Turnipseed, J. Hu, and R.K. Monson. The influence of warm-season precipitation on the diel cycle of the surface energy balance and carbon dioxide at a colorado subalpine forest site. *Biogeosciences*, 12(23):7349–7377, 2015. doi: 10.5194/bg-12-7349-2015.

[90] A.A. Turnipseed, P.D. Blanken, D.E. Anderson, and Russell K. Monson. Energy budget above a high-elevation subalpine forest in complex topography. *Agricultural and Forest Meteorology*, 110(3):177–201, 2002. doi: 10.1016/S0168-1923(01)00290-8.

[91] Peter D. Blanken, Mark W. Williams, Sean P. Burns, Russell K. Monson, John Knowles, Kurt Chowanski, and Todd Ackerman. A comparison of water and carbon dioxide exchange at a windy alpine tundra and subalpine forest site near niwot ridge, colorado. *Biogeochemistry*, 95(1):61–76, 2009. doi: 10.1007/s10533-009-9325-9.

[92] O. Sonnentag and P. Marsh. AmeriFlux CA-HPC Havikpak Creek, Ver. 1-5, AmeriFlux AMP, (Dataset). 2021. doi: 10.17190/AMF/1773392.

[93] O. Sonnentag and P. Marsh. AmeriFlux CA-TVC Trail Valley Creek, Ver. 1-5, AmeriFlux AMP, (Dataset). 2021. doi: 10.17190/AMF/1767831.

[94] M. Helbig, K. Wischnewski, G.H. Gosselin, S.C. Biraud, I. Bogoev, W.S. Chan, E.S. Euskirchen, A.J. Glenn, P.M. Marsh, W.L. Quinton, et al. Addressing a systematic bias in carbon dioxide flux measurements with the ec150 and the irgason open-path gas analyzers. *Agricultural and Forest Meteorology*, 228:349–359, 2016. doi: 10.1016/j.agrformet.2016.07.018.

[95] Andrea K. Eaton, Wayne R. Rouse, Peter M. Lafleur, Philip Marsh, and Peter D. Blanken. Surface energy balance of the western and central canadian subarctic: Variations in the energy balance among five major terrain types. *Journal of Climate*, 14(17):3692–3703, 2001. doi: 10.1175/1520-0442(2001)014⟨3692:SEBOTW⟩2.0.CO;2.

[96] Evan J. Wilcox, Dawn Keim, Tyler de Jong, Branden Walker, Oliver Sonnentag, Anastasia E Sniderhan, Philip Mann, and Philip Marsh. Tundra shrub expansion may amplify permafrost thaw by advancing snowmelt timing. *Arctic Science*, 5(4): 202–217, 2019. doi: 10.1139/as-2018-0028.

[97] Cory A. Wallace and Jennifer L. Baltzer. Tall shrubs mediate abiotic conditions and plant communities at the taiga–tundra ecotone. *Ecosystems*, 23(4):828–841, 2020. doi: 10.1007/s10021-019-00435-0.

[98] C. David Whiteman. *Mountain meteorology: fundamentals and applications*. Oxford University Press, 2000.

[99] Jonathan D. Kahl, Mark C. Serreze, and Russell C. Schnell. Tropospheric low-level temperature inversions in the canadian arctic. *Atmosphere-Ocean*, 30(4):511–529, 1992. doi: 10.1080/07055900.1992.9649453.

[100] John F. Knowles, Sean P. Burns, Peter D. Blanken, and Russell K. Monson. Fluxes of energy, water, and carbon dioxide from mountain ecosystems at niwot ridge, colorado. *Plant Ecology & Diversity*, 8(5-6):663–676, 2015. doi: 10.1080/17550874.2014.904950.

[101] Paul Grogan. Cold season respiration across a low arctic landscape: the influence of vegetation type, snow depth, and interannual climatic variation. *Arctic, antarctic, and alpine research*, 44(4):446–456, 2012. doi: 10.1657/1938-4246-44.4.446.

[102] Matthias Peichl, Oliver Sonnentag, Georg Wohlfahrt, Lawrence B. Flanagan, Dennis D. Baldocchi, Gerard Kiely, Marta Galvagno, Damiano Gianelle, Barbara Marcolla, Casimiro Pio, et al. Convergence of potential net ecosystem production among contrasting c3 grasslands. *Ecology letters*, 16(4):502–512, 2013. doi: 10.1111/ele.12075.

[103] Paul J. Crutzen. The "anthropocene". In *Earth system science in the anthropocene*, pages 13–18. Springer, 2006.

[104] Johan Rockström, Will Steffen, Kevin Noone, Åsa Persson, F Stuart Chapin III, Eric F Lambin, Timothy M Lenton, Marten Scheffer, Carl Folke, Hans Joachim Schellnhuber, et al. A safe operating space for humanity. *Nature*, 461(7263):472, 2009. doi: 10.1038/461472a.

[105] Will Steffen, Katherine Richardson, Johan Rockström, Sarah E. Cornell, Ingo Fetzer, Elena M. Bennett, Reinette Biggs, Stephen R. Carpenter, Wim De Vries, Cynthia A. De Wit, et al. Planetary boundaries: Guiding human development on a changing planet. *Science*, 347(6223):1259855, 2015. doi: 10.1126/science.1259855.

[106] Will Steffen, Johan Rockström, Katherine Richardson, Timothy M. Lenton, Carl Folke, Diana Liverman, Colin P. Summerhayes, Anthony D. Barnosky, Sarah E. Cornell, Michel Crucifix, et al. Trajectories of the Earth System in the

Anthropocene. *Proceedings of the National Academy of Sciences*, 115(33):8252–8259, 2018. doi: 10.1073/pnas.1810141115.

[107] Meredith Richardson and Praveen Kumar. Critical zone services as environmental assessment criteria in intensively managed landscapes. *Earth's Future*, 5(6):617–632, 2017. doi: 10.1002/2016EF000517.

[108] Ricard Solé. *Phase Transitions*. Princeton University Press, 2011.

[109] Nathaniel Brunsell. AmeriFlux US-Kon Konza Prairie LTER (KNZ), Ver. 5-5, AmeriFlux AMP, (Dataset). 2020. doi: 10.17190/AMF/1246068.

[110] Nathaniel Brunsell. AmeriFlux US-KFB Konza Prairie LTER (4B), (Dataset). 2019.

[111] Mike Goulden. AmeriFlux BR-Sa3 Santarem-Km83-Logged Forest. 2000-2004. doi: 10.17190/AMF/1245995.

[112] Michael L. Goulden and Humberto R. Miller, Scott D .and Da Rocha. Nocturnal cold air drainage and pooling in a tropical forest. *Journal of Geophysical Research: Atmospheres*, 111(D8), 2006. doi: 10.1029/2005JD006037.

[113] C.C. Vinson, M. Kanashiro, S.A. Harris, and D.H. Boshier. Impacts of selective logging on inbreeding and gene flow in two amazonian timber species with contrasting ecological and reproductive characteristics. *Molecular Ecology*, 24(1): 38–53, 2015. doi: 10.1111/mec.13002.

[114] K.E. Logan and N.A. Brunsell. Influence of drought on growing season carbon and water cycling with changing land cover. *Agricultural and Forest Meteorology*, 213: 217–225, 2015.

[115] Nathaniel A. Brunsell, Erik S. Van Vleck, M. Nosshi, Z. Ratajczak, and Jesse B. Nippert. Assessing the roles of fire frequency and precipitation in determining woody plant expansion in central us grasslands. *Journal of Geophysical Research: Biogeosciences*, 122(10):2683–2698, 2017.

[116] John M. Briggs, Alan K. Knapp, John M. Blair, Jana L. Heisler, Greg A. Hoch, Michelle S. Lett, and James K. McCarron. An ecosystem in transition: causes and consequences of the conversion of mesic grassland to shrubland. *BioScience*, 55(3): 243–254, 2005.

[117] J. R. Melton, R. K. Shrestha, and V. K. Arora. The influence of soils on heterotrophic respiration exerts a strong control on net ecosystem productivity in seasonally dry Amazonian forests. *Biogeosciences*, 12(4):1151–1168, 2015. doi: 10.5194/bg-12-1151-2015.

[118] H. Jochen Schenk and Robert B. Jackson. The global biogeography of roots. *Ecological monographs*, 72(3):311–328, 2002. doi: 10.1890/0012-9615(2002)072[0311:TGBOR]2.0.CO;2.

[119] Tao Zhou, Peijun Shi, Dafeng Hui, and Yiqi Luo. Global pattern of temperature sensitivity of soil heterotrophic respiration (q10) and its implications for carbon-climate feedback. *Journal of Geophysical Research: Biogeosciences*, 114(G2), 2009.

[120] William A. Wehmueller. Genesis and morphology of soils on the konza prairie research natural area, riley and geary counties, kansas. Master's thesis, Kansas State University, 1996.

[121] Jesse Brian Nippert. *Life by the drop: Water as a physiological driver of the tallgrass prairie plant community*. Colorado State University, 2006.

[122] Joseph Msanne, Tala Awada, NM Bryan, W. Schacht, R. Drijber, Y. Li, X. Zhou, J Okalebo, D. Wedin, J. Brandle, et al. Ecophysiological responses of native invasive woody juniperus virginiana l. to resource availability and stand characteristics in the semiarid grasslands of the nebraska sandhills. *Photosynthetica*, 55(2):219–230, 2017.

[123] Zak Ratajczak, Jesse B. Nippert, Jeffrey C. Hartman, and Troy W. Ocheltree. Positive feedbacks amplify rates of woody encroachment in mesic tallgrass prairie. *Ecosphere*, 2(11):1–14, 2011.

[124] R. Myneni, Y. Knyazikhin, and T. Park. MCD15A2H MODIS/Terra+Aqua Leaf Area Index/FPAR 8-Day L4 Global 500m SIN Grid V006. *NASA EOSDIS Land Processes DAAC*, 2015. doi: 10.5067/MODIS/MCD15A2H.006.

[125] ORNL DAAC. Fixed sites subsetting and visualization tool, 2018. ORNL DAAC, Oak Ridge, Tennessee, USA. Subset obtained for MCD15A2H product at site id 'br_para_santarem_km67_primary_forest'.

[126] ORNL DAAC. Fixed sites subsetting and visualization tool, 2018. ORNL DAAC, Oak Ridge, Tennessee, USA. Subset obtained for MCD15A2H product at site id 'br_para_santarem_km83_logged_forest'.

[127] José Natalino Macedo Silva, J.O.P. de de Carvalho, J. do Ca Lopes, B.F. De Almeida, D.H.M. Costa, L.C. de de Oliveira, Jerome K. Vanclay, and J.P. Skovsgaard. Growth and yield of a tropical rain forest in the brazilian amazon 13 years after logging. *Forest Ecology and Management*, 71(3):267–274, 1995. doi: 10.1016/0378-1127(94)06106-S.

[128] Timothy R. Baker, Oliver L. Phillips, Yadvinder Malhi, Samuel Almeida, Luzmila Arroyo, Anthony Di Fiore, Terry Erwin, Timothy J. Killeen, Susan G. Laurance, William F. Laurance, et al. Variation in wood density determines spatial patterns inamazonian forest biomass. *Global Change Biology*, 10(5):545–562, 2004. doi: 10.1111/j.1365-2486.2004.00751.x.

[129] ORNL DAAC. Fixed sites subsetting and visualization tool, 2018. ORNL DAAC, Oak Ridge, Tennessee, USA. Subset obtained for MCD15A2H product at site id 'us_kansas_konza_prairie_lter_knz'.

[130] ORNL DAAC. Fixed sites subsetting and visualization tool, 2018. ORNL DAAC, Oak Ridge, Tennessee, USA. Subset obtained for MCD15A2H product at site id 'us_kansas_konza_prairie_lter_4b'.

[131] Jesse B. Nippert, Troy W. Ocheltree, Adam M. Skibbe, Laura C. Kangas, Jay M. Ham, Kira B. Shonkwiler Arnold, and Nathaniel A. Brunsell. Linking plant growth responses across topographic gradients in tallgrass prairie. *Oecologia*, 166(4): 1131–1142, 2011.

[132] Thomas Wutzler, Antje Lucas-Moffat, Mirco Migliavacca, Jürgen Knauer, Kerstin Sickel, Ladislav Šigut, Olaf Menzer, and Markus Reichstein. Basic and extensible post-processing of eddy covariance flux data with reddyproc. *Biogeosciences Discussions*, 15(16):5015–5030, 2018. doi: 10.5194/bg-15-5015-2018.

[133] Ankur R. Desai, Asko Noormets, Paul V. Bolstad, Jiquan Chen, Bruce D. Cook, Kenneth J. Davis, Eugenie S. Euskirchen, Christopher Gough, Jonathan G. Martin, Daniel M Ricciuto, et al. Influence of vegetation and seasonal forcing on carbon dioxide fluxes across the Upper Midwest, USA: Implications for regional scaling. *agricultural and forest meteorology*, 148(2):288–308, 2008. doi: 10.1016/j.agrformet.2007.08.001.

[134] A. Noormets, A. R. Desai, B. D. Cook, E. S. Euskirchen, D. M. Ricciuto, K. J. Davis, P. V. Bolstad, H. P. Schmid, C. V. Vogel, E V Carey, et al. Moisture sensitivity of ecosystem respiration: comparison of 14 forest ecosystems in the Upper Great Lakes Region, USA. *Agricultural and Forest Meteorology*, 148(2):216–230, 2008. doi: {10.1016/j.agrformet.2007.08.002}.

[135] Ankur R. Desai. Climatic and phenological controls on coherent regional interannual variability of carbon dioxide flux in a heterogeneous landscape. *Journal of Geophysical Research: Biogeosciences*, 115(G3), 2010. doi: 10.1029/2010JG001423.

[136] Nikolay V. Shabanov, Dong Huang, Wenze Yang, Bin Tan, Yuri Knyazikhin, Ranga B. Myneni, Douglas E. Ahl, Stith T. Gower, Alfredo R. Huete, Luiz Eduardo OC Aragão, et al. Analysis and optimization of the modis leaf area index algorithm retrievals over broadleaf forests. *IEEE Transactions on Geoscience and Remote Sensing*, 43(8):1855–1865, 2005. doi: 10.1109/TGRS.2005.852477.

[137] Ranga B. Myneni, Wenze Yang, Ramakrishna R. Nemani, Alfredo R. Huete, Robert E. Dickinson, Yuri Knyazikhin, Kamel Didan, Rong Fu, Robinson I. Negrón Juárez, Sasan S. Saatchi, et al. Large seasonal swings in leaf area of Amazon rainforests. *Proceedings of the National Academy of Sciences*, 104(12):4820–4823, 2007. doi: 10.1073/pnas.0611338104.

[138] E. Joetzjer, C. Delire, Herve Douville, Philippe Ciais, B. Decharme, Rosemary Fisher, B. Christoffersen, J.C. Calvet, Antonio Carlos Lola da Costa, L.V. Ferreira, et al. Predicting the response of the amazon rainforest to persistent drought conditions under current and future climates: a major challenge for global land

surface models. *Geoscientific Model Development*, 7(6):2933–2950, 2014. doi: 10.5194/gmd-7-2933-2014.

[139] Paulo M. Brando, Daniel C. Nepstad, Eric A. Davidson, Susan E. Trumbore, David Ray, and Plínio Camargo. Drought effects on litterfall, wood production and belowground carbon cycling in an Amazon forest: results of a throughfall reduction experiment. *Philosophical Transactions of the Royal Society of London B: Biological Sciences*, 363(1498):1839–1848, 2008. doi: 10.1098/rstb.2007.0031.

[140] Philip J. Radtke and Paul V. Bolstad. Laser point-quadrat sampling for estimating foliage-height profiles in broad-leaved forests. *Canadian Journal of Forest Research*, 31(3):410–418, 2001. doi: 10.1139/x00-182.

[141] Waloddi Weibull. A statistical distribution function of wide applicability. *Journal of applied mechanics*, 103(730):293–297, 1951.

[142] Vaida Bartkute and Leonidas Sakalauskas. The method of three-parameter weibull distribution estimation. *Acta et commentationes Universitatis Tartuensis de mathematica*, 12:65–78, 2008.

[143] Scott C. Stark, Veronika Leitold, Jin L. Wu, Maria O. Hunter, Carolina V. de Castilho, Flávia R.C. Costa, Sean M. McMahon, Geoffrey G. Parker, Mônica Takako Shimabukuro, Michael A. Lefsky, et al. Amazon forest carbon dynamics predicted by profiles of canopy leaf area and light environment. *Ecology Letters*, 15(12):1406–1414, 2012. doi: 10.1111/j.1461-0248.2012.01864.x.

[144] M. Elizabeth Rodríguez-Ronderos, Gil Bohrer, Arturo Sanchez-Azofeifa, Jennifer S. Powers, and Stefan A. Schnitzer. Contribution of lianas to plant area index and canopy structure in a Panamanian forest. *Ecology*, 97(12):3271–3277, 2016. doi: 10.1002/ecy.1597.

[145] Robert J. Hijmans, Susan E. Cameron, Juan L. Parra, Peter G. Jones, and Andy Jarvis. Very high resolution interpolated climate surfaces for global land areas. *International Journal of Climatology: A Journal of the Royal Meteorological Society*, 25(15):1965–1978, 2005. doi: 10.1002/joc.1276.

[146] Keisuke Nishida and Yuko T. Hanba. Photosynthetic response of four fern species from different habitats to drought stress: relationship between morpho-anatomical and physiological traits. *Photosynthetica*, 55(4):689–697, 2017. doi: 10.1007/s11099-017-0694-3.

[147] Brett Raczka, Michael C. Dietze, Shawn P. Serbin, and Kenneth J. Davis. What limits predictive certainty of long-term carbon uptake? *Journal of Geophysical Research: Biogeosciences*, 123(12):3570–3588, 2018. doi: 10.1029/2018JG004504.

[148] Mark E. Kubiske, Donald R. Zak, Kurt S. Pregitzer, and Yu Takeuchi. Photosynthetic acclimation of overstory Populus tremuloides and understory Acer

saccharum to elevated atmospheric CO2 concentration: interactions with shade and soil nitrogen. *Tree Physiology*, 22(5):321–329, 2002. doi: 10.1093/treephys/22.5.321.

[149] Paul V. Bolstad, Kenneth J. Davis, Jonathan Martin, B.D. Cook, and W. Wang. Component and whole-system respiration fluxes in northern deciduous forests. *Tree physiology*, 24(5):493–504, 2004. doi: 10.1093/treephys/24.5.493.

[150] M. Saito, S. Maksyutov, R. Hirata, and A. D. Richardson. An empirical model simulating diurnal and seasonal CO2 flux for diverse vegetation types and climate conditions. *Biogeosciences*, 6(4):585–599, 2009. doi: 10.5194/bg-6-585-2009.

[151] Christoph Ritschel, Uwe Ulbrich, Peter Névir, and Henning W Rust. Precipitation extremes on multiple timescales–bartlett–lewis rectangular pulse model and intensity–duration–frequency curves. *Hydrology and Earth System Sciences*, 21(12): 6501, 2017. doi: 10.5194/hess-21-6501-2017.

[152] K. Jennings, T. Kittel, and N. Molotch. Infilled climate data for C1, Saddle, and D1, 1990 - 2013, hourly. ver 1. Environmental Data Initiative. 2019. doi: 10.6073/pasta/1538ccf520d89c7a11c2c489d973b232.

[153] ORNL DAAC. Fixed sites subsetting and visualization tool, 2018. ORNL DAAC, Oak Ridge, Tennessee, USA. Accessed August 03, 2020. Subset obtained for MCD15A2H product at site id 'it_trentino_altoadige_lavarone'.

[154] ORNL DAAC. Fixed sites subsetting and visualization tool, 2018. ORNL DAAC, Oak Ridge, Tennessee, USA. Accessed August 03, 2020. Subset obtained for MCD15A2H product at site id 'it_trentino_altoadige_monte_bondone'.

[155] ORNL DAAC. Fixed sites subsetting and visualization tool, 2018. ORNL DAAC, Oak Ridge, Tennessee, USA. Accessed August 03, 2020. Subset obtained for MCD15A2H product at site id 'ca_northwestterritories_havikpak_creek'.

[156] ORNL DAAC. Fixed sites subsetting and visualization tool, 2018. ORNL DAAC, Oak Ridge, Tennessee, USA. Accessed August 03, 2020. Subset obtained for MCD15A2H product at site id 'us_alaska_trail_valley_creek'.

[157] ORNL DAAC. Fixed sites subsetting and visualization tool, 2018. ORNL DAAC, Oak Ridge, Tennessee, USA. Accessed August 03, 2020. Subset obtained for MCD15A2H product at site id 'us_colorado_niwot_ridge'.

[158] ORNL DAAC. Fixed sites subsetting and visualization tool, 2018. ORNL DAAC, Oak Ridge, Tennessee, USA. Accessed August 03, 2020. Subset obtained for MCD15A2H product at site id 'us_colorado_niwot_ridge_mountain_research_station'.

[159] Damien Lemoine, Hervé Cochard, and André Granier. Within crown variation in hydraulic architecture in beech (fagus sylvatica l): evidence for a stomatal control of xylem embolism. *Annals of forest science*, 59(1):19–27, 2002.

[160] Damiano Gianelle, Loris Vescovo, Barbara Marcolla, G. Manca, and A. Cescatti. Ecosystem carbon fluxes and canopy spectral reflectance of a mountain meadow. *International Journal of Remote Sensing*, 30(2):435–449, 2009.

[161] Youngryel Ryu, Tiit Nilson, Hideki Kobayashi, Oliver Sonnentag, Beverly E. Law, and Dennis D. Baldocchi. On the correct estimation of effective leaf area index: Does it reveal information on clumping effects? *Agricultural and Forest Meteorology*, 150 (3):463–472, 2010. doi: 10.1016/j.agrformet.2010.01.009.

[162] O. Sonnentag, J.M. Chen, D.A. Roberts, J. Talbot, K.Q. Halligan, and A. Govind. Mapping tree and shrub leaf area indices in an ombrotrophic peatland through multiple endmember spectral unmixing. *Remote Sensing of Environment*, 109(3): 342–360, 2007. doi: 0.1016/j.rse.2007.01.010.

[163] O. Sonnentag, J. Talbot, J.M. Chen, and N.T. Roulet. Using direct and indirect measurements of leaf area index to characterize the shrub canopy in an ombrotrophic peatland. *Agricultural and Forest Meteorology*, 144(3-4):200–212, 2007. doi: 10.1016/j.agrformet.2007.03.001.

[164] Daniela Cava and Gabriel G. Katul. Spectral short-circuiting and wake production within the canopy trunk space of an alpine hardwood forest. *Boundary-layer meteorology*, 126(3):415–431, 2008.

[165] Martin E. Alexander and Northern Forestry Centre (Canada). *Characterizing the jack pine-black spruce fuel complex of the International Crown Fire Modelling Experiment (ICFME)*. Canadian Forest Service, Northern Forestry Centre, 2004.

[166] Kirsikka Heinilä, Miia Salminen, Sari Metsämäki, Petri Pellikka, Sampsa Koponen, and Jouni Pulliainen. Reflectance variation in boreal landscape during the snow melting period using airborne imaging spectroscopy. *International Journal of Applied Earth Observation and Geoinformation*, 76:66–76, 2019. doi: 10.1016/j.jag.2018.10.017.

[167] B. Henderson-Sellers. A new formula for latent heat of vaporization of water as a function of temperature. *Quarterly Journal of the Royal Meteorological Society*, 110 (466):1186–1190, 1984. doi: 10.1002/qj.49711046626.

[168] Juan Miguel Ramírez-Cuesta, Daniela Vanella, Simona Consoli, Antonio Motisi, and Mario Minacapilli. A satellite stand-alone procedure for deriving net radiation by using seviri and modis products. *International journal of applied earth observation and geoinformation*, 73:786–799, 2018.

[169] M. Groenendijk. *Boxing Nature: Global generalities in terrestrial ecosystem photosynthesis and transpiration*. PhD thesis, Vrije Universiteit Amsterdam, 2012. Naam instelling promotie: VU Vrije Universiteit Naam instelling onderzoek: VU Vrije Universiteit.

[170] P. Marsh, P. Bartlett, M. MacKay, S. Pohl, and T. Lantz. Snowmelt energetics at a shrub tundra site in the western canadian arctic. *Hydrological Processes*, 24(25): 3603–3620, 2010. doi: 10.1002/hyp.7786.

[171] Sean P. Burns, Sean C. Swenson, William R. Wieder, David M. Lawrence, Gordon B. Bonan, John F. Knowles, and Peter D. Blanken. A comparison of the diel cycle of modeled and measured latent heat flux during the warm season in a colorado subalpine forest. *Journal of Advances in Modeling Earth Systems*, 10(3):617–651, 2018. doi: 10.1002/2017MS001248.

[172] T.R. Seastedt and Gina A. Adams. Effects of mobile tree islands on alpine tundra soils. *Ecology*, 82(1):8–17, 2001. doi: doi.org/10.1890/0012-9658(2001)082[0008:EOMTIO]2.0.CO;2.

[173] Hua Chen and Han-Qin Tian. Does a general temperature-dependent q10 model of soil respiration exist at biome and global scale? *Journal of integrative plant biology*, 47(11):1288–1302, 2005. doi: 10.1111/j.1744-7909.2005.00211.x.

[174] O. Urban, A. Ač, J. Kalina, T. Priwitzer, M. Šprtová, V. Špunda, and M.V. Marek. Temperature dependences of carbon assimilation processes in four dominant species from mountain grassland ecosystem. *Photosynthetica*, 45(3):392–399, 2007.

[175] William J. Sacks, David S. Schimel, and Russell K. Monson. Coupling between carbon cycling and climate in a high-elevation, subalpine forest: a model-data fusion analysis. *Oecologia*, 151(1):54–68, 2007. doi: 10.1007/s00442-006-0565-2.

[176] Mark G. Tjoelker, Jacek Oleksyn, and Peter B. Reich. Modelling respiration of vegetation: evidence for a general temperature-dependent Q10. *Global Change Biology*, 7(2):223–230, 2001. doi: 10.1046/j.1365-2486.2001.00397.x.

[177] A Cescatti and B Marcolla. Drag coefficient and turbulence intensity in conifer canopies. *Agricultural and forest meteorology*, 121(3-4):197–206, 2004.

[178] Barbara Marcolla and Alessandro Cescatti. Experimental analysis of flux footprint for varying stability conditions in an alpine meadow. *Agricultural and Forest Meteorology*, 135(1-4):291–301, 2005.

[179] F.M. Kelliher, R. Leuning, and Ernst Detlef Schulze. Evaporation and canopy characteristics of coniferous forests and grasslands. *Oecologia*, 95(2):153–163, 1993. doi: 10.1007/BF00323485.

[180] Jason Beringer, F. Stuart Chapin III, Catharine C. Thompson, and A. David McGuire. Surface energy exchanges along a tundra-forest transition and feedbacks to climate. *Agricultural and Forest Meteorology*, 131(3-4):143–161, 2005. doi: 10.1016/j.agrformet.2005.05.006.

[181] M.I. Litaor, M. Williams, and T.R. Seastedt. Topographic controls on snow distribution, soil moisture, and species diversity of herbaceous alpine vegetation, niwot ridge, colorado. *Journal of Geophysical Research: Biogeosciences*, 113(G2), 2008. doi: 10.1029/2007JG000419.

[182] Ed Dlugokencky and Pieter Tans. NOAA/GML (www.esrl.noaa.gov/gmd/ccgg/trends/). 2020.

[183] Katherine F Wentz, Jason C Neff, and Katharine N Suding. Leaf temperatures mediate alpine plant communities' response to a simulated extended summer. *Ecology and evolution*, 9(3):1227–1243, 2019. doi: 10.1002/ece3.4816.

[184] Rodolphe Liozon, Franz-Werner Badeck, Bernard Genty, Sylvie Meyer, and Bernard Saugier. Leaf photosynthetic characteristics of beech (fagus sylvatica) saplings during three years of exposure to elevated co2 concentration. *Tree Physiology*, 20(4): 239–247, 2000.

[185] Piotr Robakowski, Pierre Montpied, and Erwin Dreyer. Responses to temperature and shade in abies alba seedlings from diverse provenances. *Scandinavian journal of forest research*, 20(6):459–470, 2005.

[186] G. Wohlfahrt, M. Bahn, E. Haubner, I. Horak, W. Michaeler, K. Rottmar, U. Tappeiner, and A. Cernusca. Inter-specific variation of the biochemical limitation to photosynthesis and related leaf traits of 30 species from mountain grassland ecosystems under different land use. *Plant, Cell & Environment*, 22(10):1281–1296, 1999.

[187] Jill L. Bubier, Rose Smith, Sari Juutinen, Tim R. Moore, Rakesh Minocha, Stephanie Long, and Subhash Minocha. Effects of nutrient addition on leaf chemistry, morphology, and photosynthetic capacity of three bog shrubs. *Oecologia*, 167(2):355–368, 2011. doi: 10.1007/S00442-011-1998-9.

[188] Danielle A. Way and Rowan F. Sage. Elevated growth temperatures reduce the carbon gain of black spruce [picea mariana (mill.) bsp]. *Global Change Biology*, 14 (3):624–636, 2008. doi: 10.1111/j.1365-2486.2007.01513.x.

[189] Stan D. Wullschleger. Biochemical limitations to carbon assimilation in c3 plants—a retrospective analysis of the a/ci curves from 109 species. *Journal of Experimental Botany*, 44(5):907–920, 1993. doi: 10.1093/jxb/44.5.907.

[190] Timothy Tomaszewski and Herman Sievering. Canopy uptake of atmospheric n deposition at a conifer forest: Part ii-response of chlorophyll fluorescence and gas exchange parameters. *Tellus B: Chemical and Physical Meteorology*, 59(3):493–501, 2007. doi: 10.1111/j.1600-0889.2007.00265.x.

[191] N. Cannone, A. Augusti, F. Malfasi, E. Pallozzi, C. Calfapietra, and E. Brugnoli. The interaction of biotic and abiotic factors at multiple spatial scales affects the

variability of co 2 fluxes in polar environments. *Polar Biology*, 39(9):1581–1596, 2016. doi: 10.1007/s00300-015-1883-9.

[192] Yuzhi Fan, Zhiming Zhong, and Xianzhou Zhang. Determination of photosynthetic parameters vcmax and jmax for a c3 plant (spring hulless barley) at two altitudes on the tibetan plateau. *Agricultural and Forest Meteorology*, 151(12):1481–1487, 2011. doi: 10.1016/j.agrformet.2011.06.004.

[193] Robert Keiner, Marie-Cécile Gruselle, Beate Michalzik, Jürgen Popp, and Torsten Frosch. Raman spectroscopic investigation of 13 co 2 labeling and leaf dark respiration of fagus sylvatica l.(european beech). *Analytical and bioanalytical chemistry*, 407(7):1813–1817, 2015. doi: 10.1007/s00216-014-8446-8.

[194] Edward M. Smith and Elmer B. Hadley. Photosynthetic and respiratory acclimation to temperature in ledum groenlandicum populations. *Arctic and Alpine Research*, 6 (1):13–27, 1974. doi: 10.1080/00040851.1974.12003756.

[195] Michael L. Goulden, Bruce C. Daube, Song-Miao Fan, Douglas J. Sutton, Ammar Bazzaz, J. William Munger, and Steven C. Wofsy. Physiological responses of a black spruce forest to weather. *Journal of Geophysical Research: Atmospheres*, 102(D24): 28987–28996, 1997. doi: 10.1029/97JD01111.

[196] Peter B. Reich, Michael B. Walters, David S. Ellsworth, James M. Vose, John C. Volin, Charles Gresham, and William D. Bowman. Relationships of leaf dark respiration to leaf nitrogen, specific leaf area and leaf life-span: a test across biomes and functional groups. *Oecologia*, 114(4):471–482, 1998. doi: 10.1007/s004420050471.

[197] Masahito Ueyama, Narumi Tahara, Hirohiko Nagano, Naoki Makita, Hiroki Iwata, and Yoshinobu Harazono. Leaf-and ecosystem-scale photosynthetic parameters for the overstory and understory of boreal forests in interior alaska. *Journal of Agricultural Meteorology*, 74(2):79–86, 2018. doi: 10.2480/agrmet.D-17-00031.

[198] Eric R. Stoner, M.F. Baumgardner, L.L. Biehl, and B.F. Robinson. *Atlas of soil reflectance properties*. Purdue University West Lafayette, 1980.

[199] Asahi Hashimoto, Hendrik Segah, Nina Yulianti, Nobuyasu Naruse, and Yukihiro Takahashi. A new indicator of forest fire risk for indonesia based on peat soil reflectance spectra measurements. *International Journal of Remote Sensing*, 42(5): 1917–1927, 2021.

[200] Georg Wohlfahrt, Michael Bahn, Ingrid Horak, Ulrike Tappeiner, and Alexander Cernusca. A nitrogen sensitive model of leaf carbon dioxide and water vapour gas exchange: application to 13 key species from differently managed mountain grassland ecosystems. *Ecological Modelling*, 113(1-3):179–199, 1998.

[201] Cristina Martinez, Giorgio Alberti, M. Francesca Cotrufo, Federico Magnani, Damiano Zanotelli, Federica Camin, Damiano Gianelle, Alessandro Cescatti, and

Mirco Rodeghiero. Belowground carbon allocation patterns as determined by the in-growth soil core 13c technique across different ecosystem types. *Geoderma*, 263: 140–150, 2016.

[202] François Hébert and Nelson Thiffault. The biology of canadian weeds. 146. rhododendron groenlandicum (oeder) kron and judd. *Canadian Journal of Plant Science*, 91(4):725–738, 2011. doi: 10.4141/cjps2010-012.

[203] V.J. Lieffers and R.L. Rothwell. Effects of depth of water table and substrate temperature on root and top growth of picea mariana and larix lancina seedlings. *Canadian Journal of Forest Research*, 16(6):1201–1206, 1986. doi: 10.1139/x86-214.

[204] P.W. Flanagan and K. Van Cleve. Microbial biomass, respiration and nutrient cycling in a black spruce taiga ecosystem. *Ecological Bulletins*, pages 261–273, 1977.

APPENDIX A

SUPPLEMENTARY INFORMATION

A.1 Supplementary Information for Chapter 2

Figure A.1 provides a conceptual diagram of the ecosystem control volume and fluxes modeled in this study. Figure A.2 shows the locations overlaid upon the mean annual precipitation of the study sites considered. Table A.1 outlines the abbreviations for the vegetation considered within each of the functional groups for each site.

A.1.1 Further Results

The Two-sample Kolmogorov-Smirnov test measures the maximum absolute vertical distance between two cumulative distribution functions (CDF) [69–71]. Figure A.3 displays the work efficiency CDF's for all functional group scenarios at each site. This figure demonstrates that the multiple-functional-group (MG) scenario at each site has the largest values (aside from WCR-OT; see Table 2.2 in the main text) due to the smaller CDF's indicated by a significantly large vertical distance between MG and the other functional groups.

A.1.2 Additional Parameters and Calculations

All variables except friction velocity and relative humidity were already gap-filled in the available Fluxnet2015 dataset [57–59]. In order to fill gaps in the relative humidity, variables were run through REddyProc online tool [132]. The interpolation scheme fills gaps based on other variables available at the same timestep. The vapor pressure deficit was then calculated from relative humidity (RH) and air temperature (T_a) at each timestep.

Additional input parameters for MLCan are displayed in Table A.2.

The leaf area index (LAI) data for all sites are taken from MODIS [61] and calibrated and partitioned based on site documentation (Fig. A.4). The LAI for each site is also interpolated for the appropriate timescale based on data fitted to one or composite polynomial functions depending on the shape. Before fitting, outliers past two standard deviations were removed.

The LAI for Santa Rita mesquite (SRM) was calibrated to the site and partitioned based on Lee et al. [62] for two years.

LAI for Willow Creek (WCR) is taken from the MODIS network and compared with field measurements. The understory LAI was taken from a local shrubland near the WCR site, given as 0.2 [133, 134]. This site, also located in the Chequamegon-Nicolett National Forest, has been frequently used to compare vegetation responses with WCR and several other local sites in the forest [133, 134]. This LAI of 0.2 is assumed as the maximum understory value for the year, and the overstory LAI was extrapolated from the difference in the interpolated total LAI curve from MODIS and this understory LAI value. Field measurements for total LAI for 2000 to 2006 in WCR ranges from 0.0 to 5.3 [65, 135], similar to the MODIS range of 0.1 to 5.8. Thus, the curves were fitted to the original MODIS data. The LAI curve for WCR was created from a composite of five different polynomial functions. The winters (low LAI) are characterized by second degree curves, and the summers (high LAI) are characterized by fourth degree curves.

LAI for Tapajos National Forest (TAP) is obtained from MODIS data and compared with and partitioned based on Domingues et al. [7]. Quality issues with MODIS pixels existed over this site due to the denser cloud cover in the wet season. Shabanov et al. [136] and Myneni et al. [137] compare field measurements with MODIS algorithm performance; the range of values observed at these field sites was 5.4 to 7.0. Alternatively, field studies by Joetzjer et al. [138] and Brando et al. [139] indicate that the range of acceptable LAI for 2004 is from 4.7 to 5.7 and up to around 6.3 for 2005. The resulting LAI we use for TAP is based on an interpolated scheme for the MODIS data scaled to the range of values that satisfy a compilation of the field studies (4.7-6.3). A curve was fitted to the original MODIS data and scaled up to fit within this published range. The resulting curve is a fifth-order polynomial function over the entire two year period.

Leaf area density (LAD) (i.e., the normalized vertical distribution of LAI) was solved for

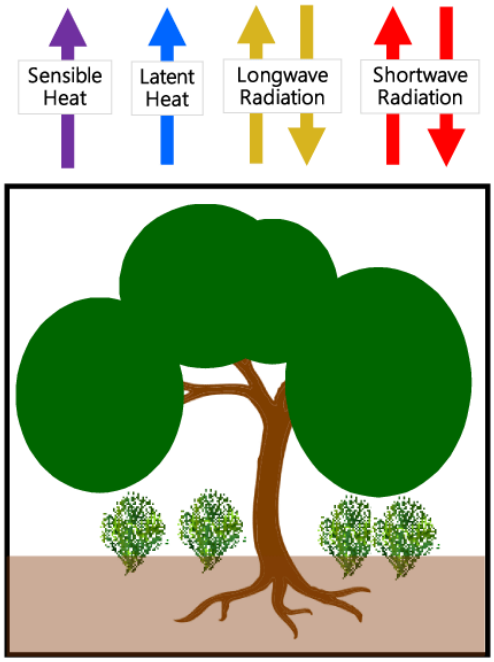

Figure A.1: Schematic diagram of ecosystem control volume and energy fluxes considered for a situation with two functional groups. The lower boundary corresponds to a constant temperature with zero thermal gradient.

each functional group by different techniques based on data availability. LAD for WCR was taken from Radtke and Bolstad [140], and Weibull distributions were fitted to this data for each functional group [141, 142]. The same process was repeated for TAP, where the LAD was taken from Stark et al. [143]. Understory was assumed to be 10% of the total LAD distribution up to its maximum height, 2m. Lianas take up a smaller distribution of the LAI than overstory and mid-canopy trees [144]; thus, the remaining LAD distribution was then partitioned at each layer 2-parts MT, 2-parts OT, and 1-part up to the mean maximum heights of each functional group described in Domingues et al. [7]. LAD for SRM was taken from Lee et al. [62].

MLCan has been previously validated for each of these sites [55, 62]. For the present study, model validation for latent heat is shown in Fig. A.5.

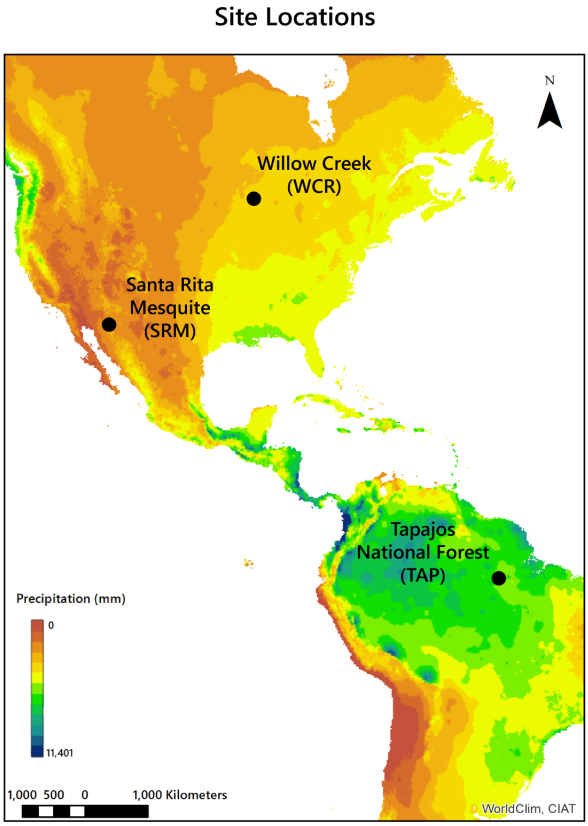

Figure A.2: Map of site locations existing in Wisconsin and Arizona, United States, and Pará, Brazil. Background map displaying mean annual precipitation was adapted from Hijmans et al. [145].

Table A.1: Functional Group Abbreviations for All Sites

Abbrev.	WCR	SRM	TAP
UN	understory shrubs	understory shrubs	understory trees
MT	–	–	mid-canopy trees
OT	overstory trees	overstory trees	upper-canopy trees
L	–	–	lianas
MG	UN & OT	UN & OT	UN, MT, OT, & L

Sites: Willow Creek (WCR), Santa Rita Mesquite (SRM), and Tapajos National Forest (TAP). Multi-group scenarios (MG) include simulations for species interactions of all identified functional groups.

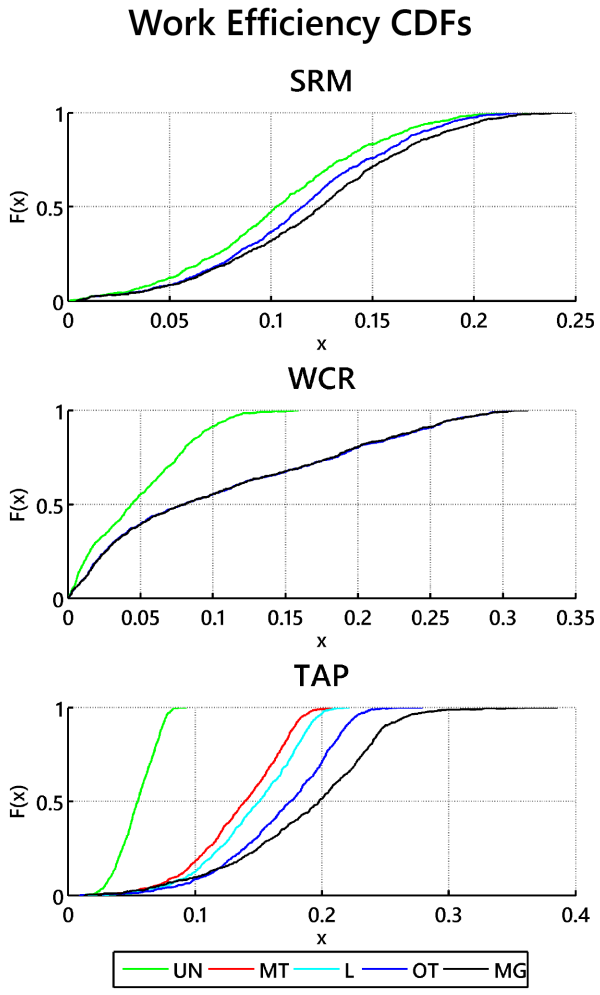

Figure A.3: The cumulative distribution functions of work efficiency associated with each functional group and coexisting multi-functional vegetation groups (see Table A.1).

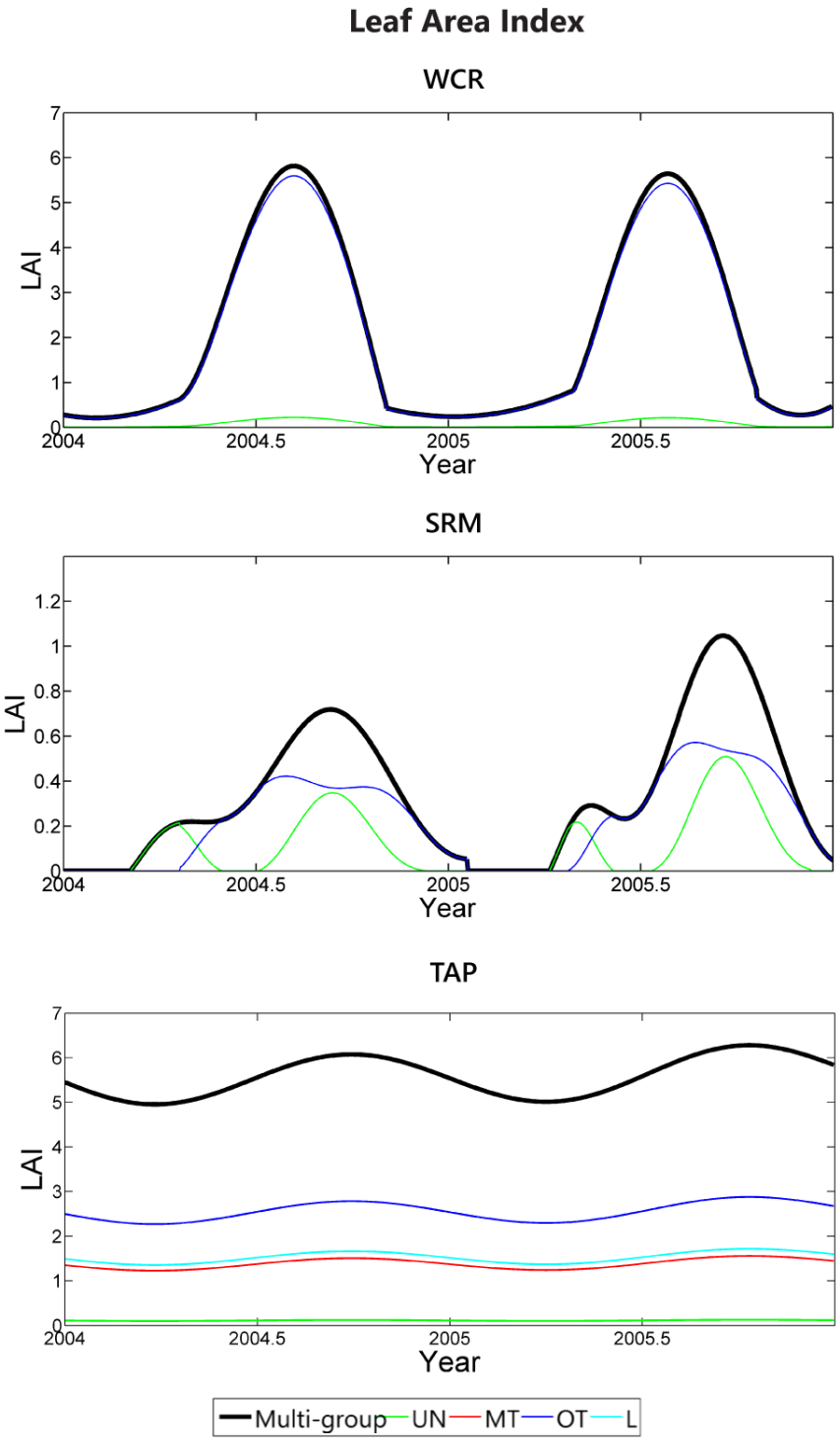

Figure A.4: Leaf area index for all Chapter 2 sites.

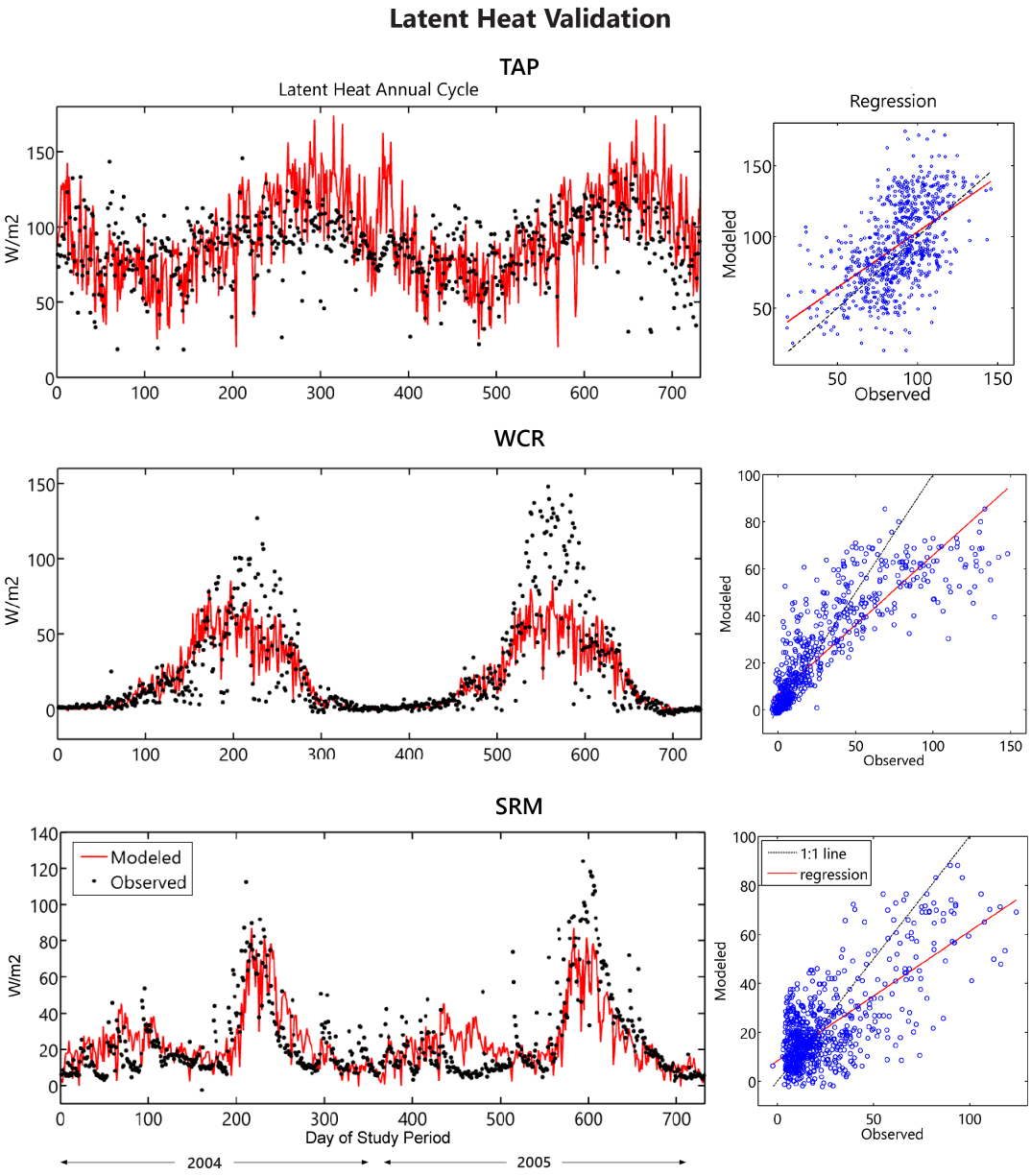

Figure A.5: Latent heat validation for all Chapter 2 sites.

Table A.2: Chapter 2 Model Parameters

Site	WCR		SRM		TAP			
Functional Group	UN	OT	UN	OT	UN	MT	OT	L
Site Information								
Percent Sand[a]	63		75		10			
Percent Clay[a]	13		10		80			
Ecosystem Height[b] (m)	24		2.4375		32			
Flux Tower Observation Height[a] (m)	30		7.82		64			
Leaf Properties								
Vc_{max} (μmol/m^{2}s)	26.9[c]	44.8[d]	39[e]	17.62[e]	31.6[f]	57.5[f]	81[f]	59.7[f]
J_{max} (μmol/m^{2}s)	47.[c]	100[g]		13.55[e]	37.9[f]	81[f]	112[f]	87.5[f]
Respiration $Q10$ (mol/m^{2}s)	2.98[h]		3.36[m]		2[n]			
Root Properties								
Root Depth (m)	2.5	3	2.5	2.5	1	4	12	12
z_{50} [p]	0.19	0.2	0.24	0.28	0.07	0.24	0.65	0.65
z_{95} [p]	1.71	1	0.65	1.5	0.4	1.5	4	4

[a] FLUXNET2015 Network [57–59]
[b] Modified from Fluxnet2015 Network [57–59] canopy heights based on leaf area density
[c] Nishida and Hanba [146]
[d] Racza et al. [147]
[e] Lee et al. [62]
[f] Domingues et al. [7]
[g] Inferred from Kubiske et al. [148]
[h] Bolstad et al. [149]
[m] Saito et al. [150]
[n] Melton et al. [117]
[p] Schenk and Jackson [118]

A.2 Supplementary Information for Chapter 3

A.2.1 Model Inputs & Pre-processing

The multi-layer canopy model, MLCan, models the mass and energy fluxes occurring within the canopy, roots, and soil system to resolve the energy and entropy fluxes, and associated work efficiencies for each ecosystem [27, 28, 35, 52, 53]. Environmental meteorological data (e.g. wind speed, air temperature, global radiation, precipitation, friction velocity, air pressure, and relative humidity) from various sources [81, 82, 86, 87, 92, 93] were used as forcing for the model. Site-specific meteorological data sources and pre-processing methods are described by location below. Table A.3 documents additional input parameters for MLCan for all sites. Model outputs include soil and canopy layer temperatures, snow depth, photosynthesis and respiration rates, and energy and entropy fluxes at each timestep. All sites were run on a half-hourly time scale. The study period for each pair of sites was chosen as the longest consecutive time series of available data for both sites: 2012-2013 for the Italian Alps, 2008-2013 for the United States Rocky Mountains, and 2016-2018 for the Western Canadian Taiga-Tundra.

Italian Alps

Data for the Italian Alps sites were taken from the FLUXNET2015 Lavarone (Lav) and Monte Bondone (MBo) sites [81, 82] and gap-filled using the REddyProc online tool [132]. Validation for the Lav and MBo sites is illustrated in Figure A.6.

Western Canadian Taiga-Tundra

The Western Canadian Taiga-Tundra site pair was composed of the Havikpak Creek (HPC) and Trail Valley Creek (TVC) AmeriFlux sites [92, 93]. Precipitation data was available at the daily timescale. This was disaggregated to a half-hourly timestep for model simulation using the Bartlett-Lewis rectangular pulse method [151]. There were many gaps in incoming shortwave radiation for the HPC site. These gaps were filled by linear regression

with no intercept based on available observed data pairs with the TVC site. Validation for the HPC and TVC sites is illustrated in Figure A.7.

United States Rocky Mountains

For the United States Rocky Mountains in Colorado, the alpine data is taken as the T-Van site from Knowles et al. [87], and the subalpine data is taken from the Niwot Ridge (NR1) site in the AmeriFlux network [86, 88]. Incoming shortwave radiation was taken from the Subnivean lab site 500m from the T-Van site. The precipitation data is hourly data from the the nearby Saddle site [152] that was disaggregated from hourly to evenly-distributed half-hourly data. The NR1 site has subalpine firs (*Abies lasiocarpa* var. *bifolia*) and Englemann spruce (*Picea engelmannii*) west of the tower, and lodgepole pine (*Pinus contorta*) east of the tower [33, 89, 90]. We use the species located west of the tower as the dominant vegetation in our simulations due to the direction of the prevailing winds [89]. Validation for NR1 and T-Van is illustrated in Figure A.8.

Leaf Area

Time-series of leaf area index (LAI) for all sites (Fig. A.4) were interpolated from MODIS [124, 153–158] and calibrated and partitioned as in Richardson and Kumar [35] based on site documentation: Lav − Marcolla and Cescatti, 2003 [83] and Lemoine et al, 2002 [159], MBo − Gianelle et al, 2009 [160], NR1 − Turnipseed et al, 2002 [90] and Knowles et al, 2015 [100], T-Van − Knowles et al, 2012 [87] and Blanken et al, 2009 [91], HPC & TVC − Krogh et al, 2017 [31] and site measurements. HPC and TVC curves were scaled to fit in-situ observations. LAI (LAI-2200 Plant Canopy Analyser, Li-COR Biosciences, Lincoln, NE) at HPC and TVC were estimated using methods outlined in Ryu et al, 2010 [161] and Sonnentag et al, 2007a and 2007b [162, 163]. For the HPC site on September 3, 2018, tree LAI was measured at 0.34 ± 0.16 (n = 39) and shrub LAI was 0.51 ± 0.19 (n=39). We assumed a constant partitioning percentage between trees and shrubs within HPC based on the observed scale. For the TVC site on September 1, 2018, LAI was measured as 0.38 ± 0.26 (n = 27). Fifth degree polynomials were fitted to all forest LAI and scaled to include the

peaks. All alpine/tundra sites were fitted with fifth degree (MBo & TVC) or fourth degree (T-Van) curves during the time periods with vegetation present. During winter, minimum LAI is assumed to be 0.1 − the minimum detectable LAI in MODIS. Data gaps in the winter for the Western Canadian Taiga-Tundra sites were also assumed to be 0.1. Leaf area density profiles were taken from literature [83, 164, 165] and fitted to Weibull distributions [141, 142].

A.2.2 MLCan Model Updates

MLCan has been validated for numerous sites across the Western Hemisphere [27, 28, 35, 52–55, 62]. To apply MLCan to the harsh winter conditions of Arctic and alpine ecosystems, we included new parameterizations for peat soils and switches to start and stop photosynthesis to simulate dormancy during winter. Cold temperatures, freezing soils, the hibernation behavior of vegetation to not perform photosynthesis in the winter, and the varying behavior of soils with permafrost conditions required updates to model formulation in order to apply MLCan to this new region. The updates to MLCan are validated for all sites in Figures A.6 – A.8.

Soil

Soil properties, such as sand, clay, and organic material content and hydraulic and thermal conductivity are parameterized and held constant throughout the model simulations. Due to the presence of peat soils in the Arctic, we implemented formulations for the thermal conductivity of arctic peat soils instead of basing them entirely off of sand/clay percentages. The thermal conductivity model was based on equations from Zhao et al [29], and parameterizations for thermal and hydraulic conductivity were based on Wu et al [30] and Krogh et al [31]. To further take into account the behavior of Arctic permafrost, the model was altered to turn off plant-soil uptake when a given soil layer was frozen, specifically when the soil temperature within the layer of the subsurface was determined to be below -1°C.

Canopy

We created dynamic switches to stop photosynthetic activity during winter when the mean air temperature in the canopy over the previous 24 hours drops below a certain threshold (-7°C) and restart when it returns above a certain threshold (3°C) [32]. Based on site-specific literature, different photosynthesis stop (-3°C) and start (5°C) thresholds were used for NR1 vegetation [33]. Additional constraints preventing photosynthesis from occurring when the top layer of the soil is frozen or the snow depth is greater than the canopy height are also included [34]. We do not close the stomata or change the respiration routine since literature indicates that respiration can occur during winter, even when photosynthesis is not occurring [101]. The periods of time when photosynthesis was active were validated based on site-specific literature when available.

Further, due to the extended periods of snowpack in the regions studied, new parameters were created to demonstrate the change in canopy reflectance with snow [166]. These *new snow reflection coefficients* vary based on the surface (i.e., canopy, peat soil, sandy soil) and the type of radiation (i.e., PAR, NIR) and are summarized in Table A.3.

Ecosystem-wide

Due to the sensitivity of latent heat of vaporization (Lv) in colder regions, we implemented dynamic Lv based on air temperature [167] rather than keeping it as a static parameter.

We implemented a bi-directional formulation for estimating temperature and vapor pressure values from observed fluxtower measurements. Since counterfactuals were constructed at the alpine/Arctic sites, fluxtower measurements above alpine/Arctic shrubs were located below the height of the simulated trees and, consequently, the ecosystem height (see Table A.3). This ecosystem height was used as the upper bound of the control volume for each site pair such that shorter canopy and flux tower heights (i.e., alpine/Arctic tundra or meadow) could be compared directly with taller ecosystems (i.e., subalpine/subArctic forest). Since fluxtower measurements were collected below the ecosystem height for the alpine/Arctic sites and above the ecosystem height for the subalpine/sub-Arctic sites, the new formulation calculates the estimated temperature and vapor pressure deficit at the

ecosystem height from the observed values from either above or below using similarity theory.

A.2.3 Additional Figures

The main text presents several figures (Figs. 3.4 – 3.6) with data or results from only one or two of the locations studied. The data for the remaining sites are presented in Figs. A.10 – A.12.

Table A.3: Chapter 3 Model Parameters

Location	**Italian Alps**			**Western Canadian Taiga-Tundra**			**United States Rocky Mountains**		
Site	**Lav**		**MBo**	**HPC**		**TVC**	**NR1**		**T-Van**
Functional Group	UN	OT	UN	UN	OT	UN	UN	OT	UN
Site Information									
Latitude	45.9562°N[a]		46.0147°N[a]	68.3203°N[b]		68.7462°N[b]	40.0329°N[c]		40.053°N[d]
Longitude	11.2813°E[a]		11.0458°E[a]	133.519°W[b]		133.502°W[b]	105.546°W[c]		105.586°W[d]
Elevation (m)	1349[a]		1553[a]	80[b]		85[b]	3050[c]		3503[d]
Fluxtower Height (m)	36[e]		2.5[f]	15		4[g]	21.5[c]		3[d]
Canopy Height (m)	4[e]	36[e]	0.3[a]	1.4[h]	8[h]	0.3[h]	0.15[j]	12[j]	0.05[d]
Ecosystem Height[k] (m)	36		36	8		8	12		12
Percent Sand	29.5[e]		37[l]	35[m]		35[m]	72[n]		55.9[o]
Percent Clay	26.5[e]		21[l]	40[m]		40[m]	1[n]		16.3[o]
Respiration $Q10$ (mol/m^{2}s)	2.9[p,q]		4[p]	3.2[p]		9[p]	2.6[p,r]		3.1[s]
Surface Roughness Length (m)	10.8[t]		0.125[u]	1.1[v]		0.08[w]	1.79[j]		0.1[x]
Ambient CO_2[y] (ppm)	393		393	405		405	405[z]		405[z]
Leaf Properties									
Vc_{max} (μmol/m^{2}s)	42[aa]	45[bb]	37.93[cc]	78.1[dd]	44.6[ee]	78.1[aa]	43[ff]	11[gg]	67.81[hh]
J_{max} (μmol/m^{2}s)	78[aa]	100[bb]	84[q]	119.4[dd]	43.7[ee]	119.4[aa]	91[ff]	51.7[cc]	149.86[ii]
Rd_{25} (μmol/m^{2}s)	1[jj]	2.142[bb]	1.4[q]	1.47[kk]	2.32[ll]	2.94[kk]	0.6[mm]	0.9[mm]	1.4[q]
Ball-Berry Slope[nn]	15.6	5.7	15.6	15.6	5.7	15.6	15.6	5.7	9[z]
Ball-Berry Intercept[nn] (mol/m^{2}s)	0.02	0.02	0.02	0.02	0.02	0.02	0.02	0.02	0.002[z]
Reflectance									
PAR reflection coefficient[oo]	0.05		0.1	0.05		0.05	0.05		0.05
NIR reflection coefficient[oo]	0.2		0.35	0.4		0.2	0.2		0.3
Soil reflection coefficient[oo,pp]	0.15		0.3	0.17[qq]		0.3	0.17		0.2
New Snow PAR reflection coefficient[oo]	0.1		0.15	0.1		0.2	0.07		0.1
New Snow NIR reflection coefficient[oo]	0.1		0.3	0.4		0.25	0.1		0.2
New Snow Soil reflection coefficient[oo,rr]	0.6		0.8	0.6		0.8	0.3		0.6
Root Properties									
Root Depth (m)	0.3[tt]	0.5[tt]	0.3[tt]	0.5[i,uu]	0.25[i,vv]	0.5[i,uu]	0.3	0.5[ww]	0.4
z_{50} [ss]	0.03[tt]	0.15[tt]	0.03[tt]	0.1[i,uu]	0.1[i,vv]	0.1[i,uu]	0.03	0.15[ww]	0.03
z_{95} [ss]	0.2[tt]	0.3[tt]	0.2[tt]	0.4[i,uu]	0.19[i,vv]	0.4[i,uu]	0.2	0.3[ww]	0.2

UN refers to the understory, and OT refers to the overstory trees.

[a] Tudoroiu et al, 2016 [85]
[b] AmeriFlux Network: CA-HPC & CA-TVC.
[c] Bowling et al, 2018 [33]
[d] Knowles et al, 2012 [87]
[e] Marcolla et al, 2003 [83]
[f] Ramírez-Cuesta et al, 2018 [168]
[g] Helbig et al, 2016 [94]
[h] Krogh et al, 2017 [31]
[j] Turnipseed et al, 2002 [90]
[k] Taken as maximum canopy height for each region site pair
[l] Groenendij, 2012 [169]
[m] Marsh et al, 2010 [170]. Arctic peat was modeled differently; see *Soil* section in *MLCan Model Updates*.
[n] Burns et al, 2018 [171]
[o] Seastedt & Adams, 2001 [172]
[p] Chen & Tian, 2005 [173]
[q] Urban et al, 2007 [174]
[r] Sacks et al, 2007 [175]
[s] Tjoelker et al, 2001 [176]
[t] Cescatti & Marcolla, 2004 [177]
[u] Marcolla & Cescatti, 2005 [178]
[v] Kelliher et al, 1993 [179]
[w] Beringer et al, 2005 [180]
[x] Litaor et al, 2008 [181]
[y] All ecosystems (aside from the US sites) use the median global average ambient CO_2 of all years modeled for each region [182]
[z] Wentz et al, 2019 [183]
[aa] Liozon et al, 2000 [184]
[bb] Robakowski et al, 2005 [185]
[cc] Wohlfahrt et al, 1999 [186]
[dd] Bubier et al, 2011 [187]
[ee] Way & Sage, 2008 [188]
[ff] Wullschleger, 1993 [189]
[gg] Tomaszewski & Sievering, 2007 [190]
[hh] Cannone et al, 2016 [191]
[ii] Inferred from Fan et al, 2011 [192]
[jj] Keiner et al, 2015 [193]
[kk] Calculated from Smith & Hadley, 1974 [194] & Marsh et al, 2010 [170]
[ll] Goulden et al, 1997 [195]
[mm] Reich et al, 1998 [196]
[nn] Ueyama et al, 2018 [197]
[oo] Inferred from Heinilä et al, 2019 [166]
[pp] Stoner et al, 1980 [198]
[qq] Hashimoto et al, 2021 [199]
[rr] Wiscomb & Warren, 1980 [198]
[ss] Schenk & Jackson [118]
[tt] Wohlfahrt et al, 1998 [200], Martinez et al [201], & Tudoroiu et al, 2016 [85]
[uu] Hébert & Thiffault, 2011 [202]
[vv] Lieffers & Rothwell, 1986 [203]; Flanagan & Van Cleve, 1977 [204]
[ww] Burns et al, 2015 [89]

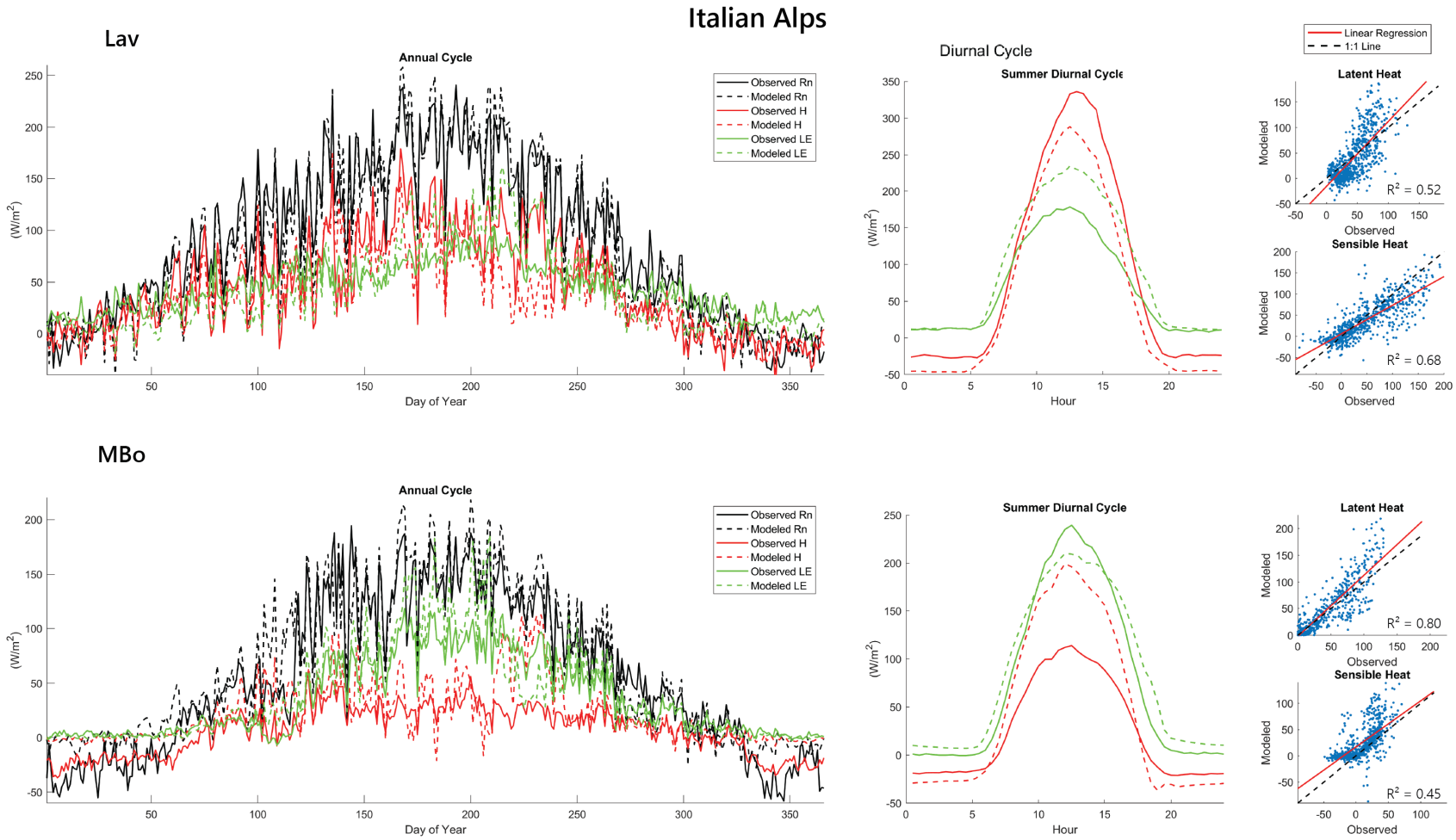

Figure A.6: Model validation for the Italian Alps sites: Lav (subalpine forest) and MBo (alpine meadow). Graphs include average annual cycle, average diurnal cycle during summer, and the 1:1 plot of all shared days within the study period, 2012-2013.

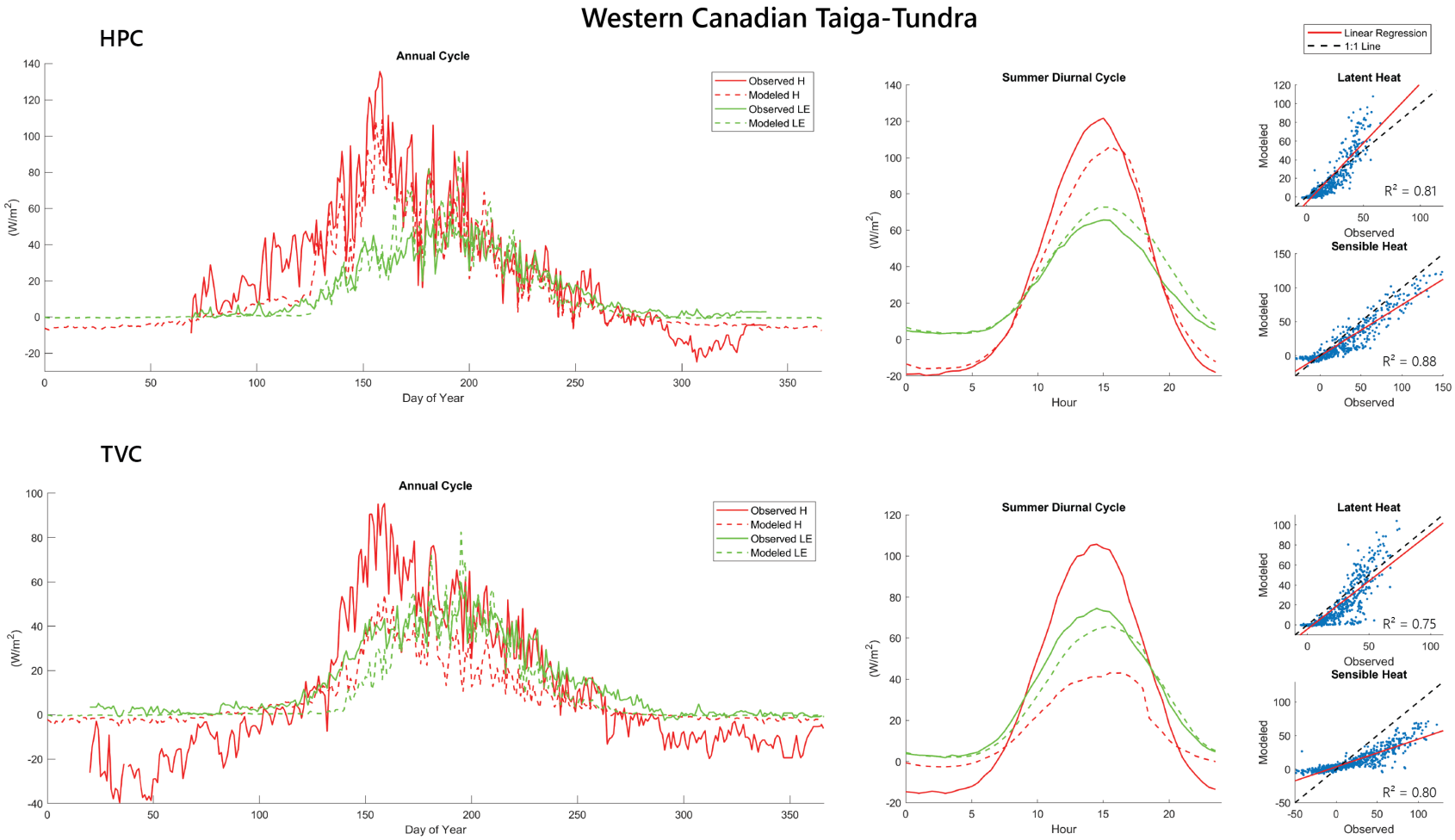

Figure A.7: Model validation for the Western Canadian Taiga-Tundra sites: HPC (sub-Arctic forest) and TVC (Arctic tundra). Graphs include average annual cycle, average diurnal cycle during summer, and the 1:1 plot of all shared days within the study period, 2016-2018.

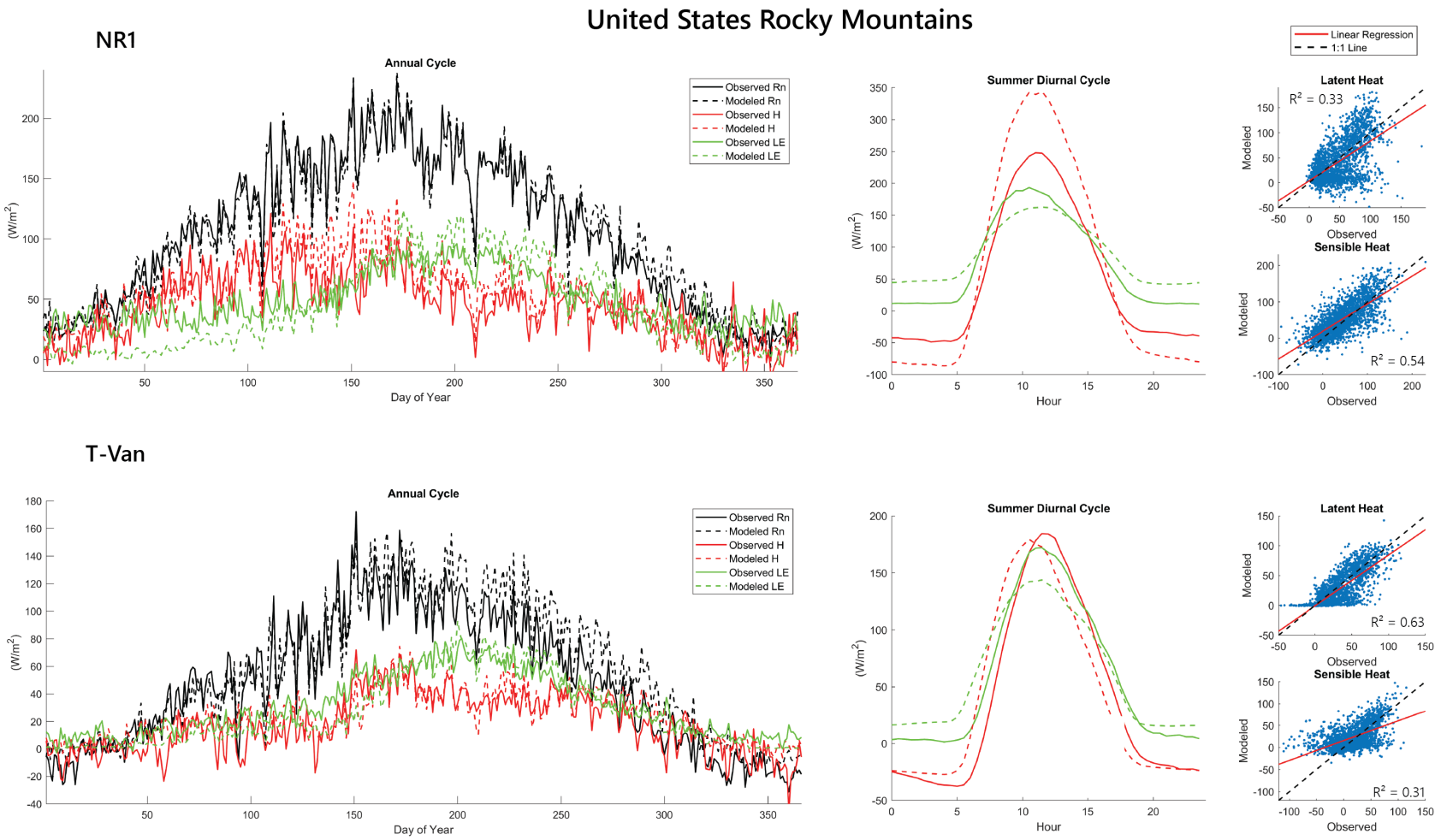

Figure A.8: Model validation for the two United States Rocky Mountains sites: NR1 (subalpine forest) and TVan (alpine fellfield). Graphs include average annual cycle, average diurnal cycle during summer, and the 1:1 plot of all shared days within the study period, 2008-2013.

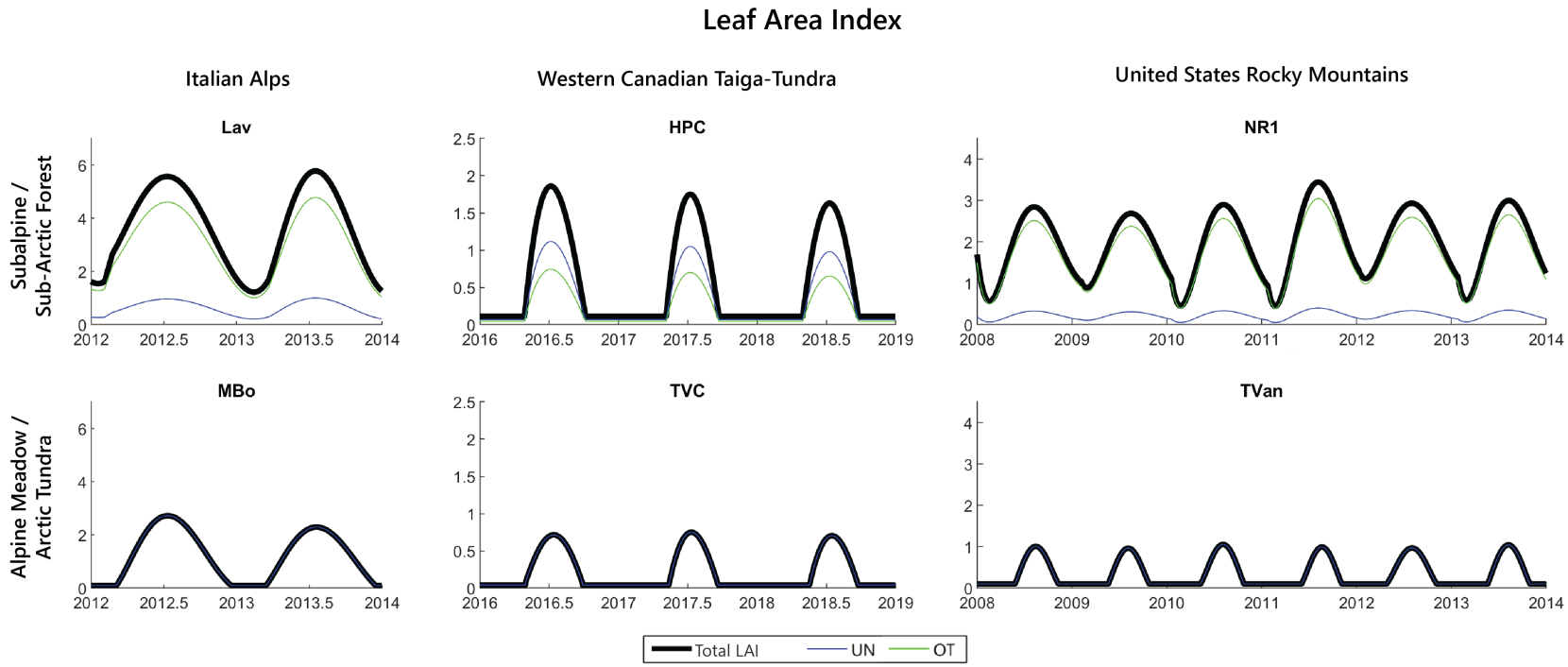

Figure A.9: Leaf area index (LAI) for all sites interpolated from MODIS [124, 153–158] and calibrated and partitioned based on site documentation. UN refers to the understory, and OT refers to the overstory trees.

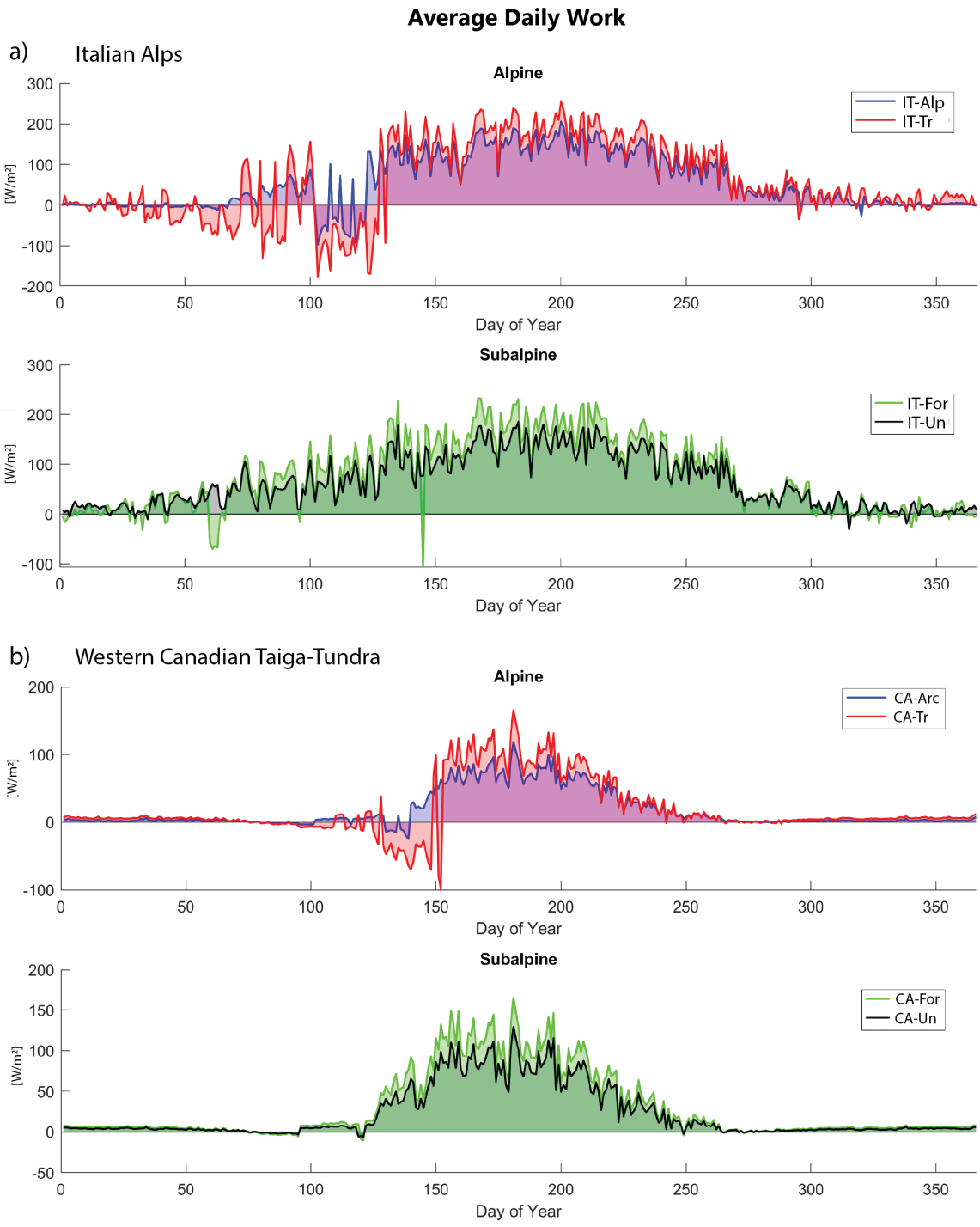

Figure A.10: Annual time series of work, averaged daily, for the entire study period for scenarios in the (a) Italian Alps (2012-2013) and (b) Western Canadian Taiga-Tundra (2016-2018). Refer to Figure 3.4 of the main text for information on the United States Rocky Mountains scenarios.

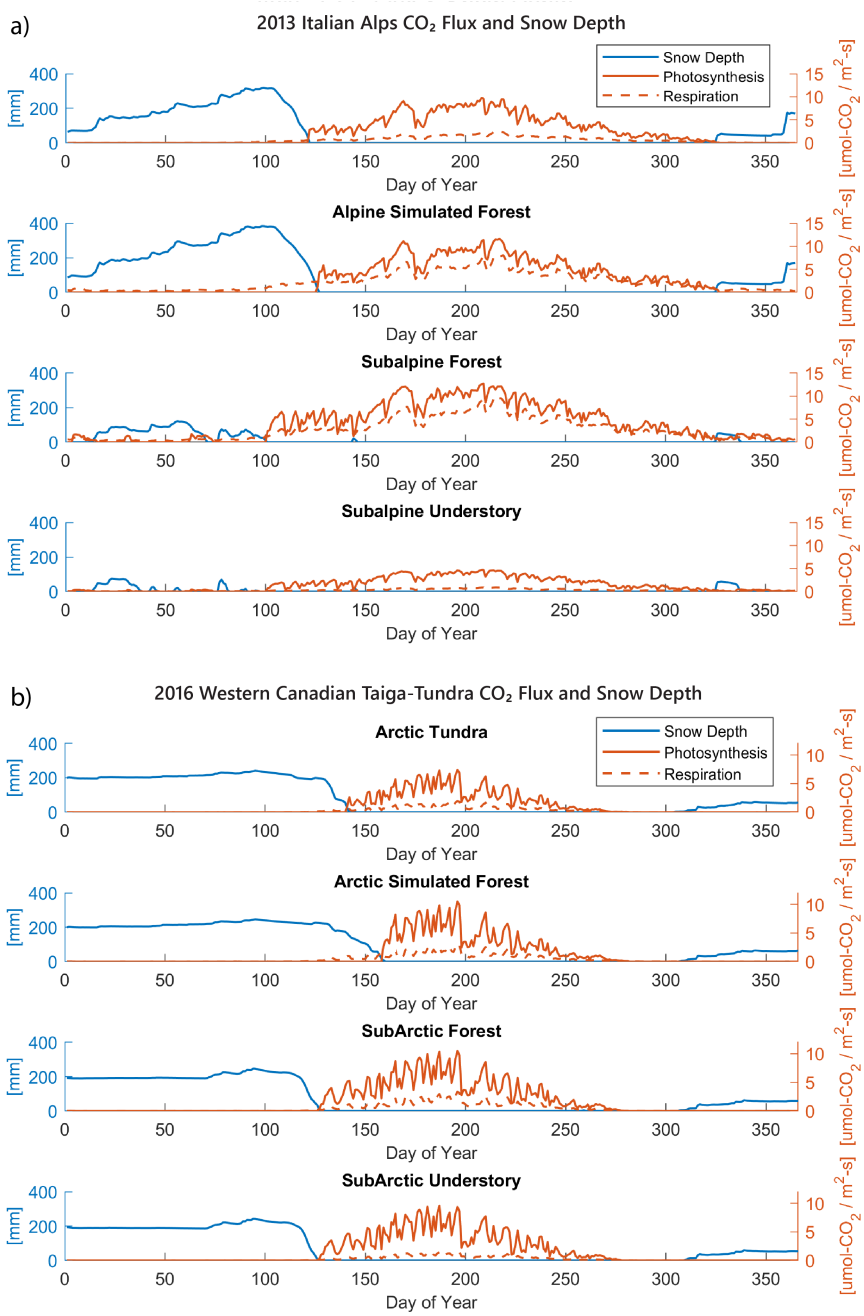

Figure A.11: Average daily leaf CO_2 flux and snow depth for representative years at the Italian Alps and Western Canadian Taiga-Tundra. Refer to Figure 5 of the main text for information on the United States Rocky Mountains scenarios. (a) 2013 daily timeseries of snow depth (*blue*) and leaf CO_2 flux – the averaged daily photosynthetic CO_2 uptake (*orange solid line*) and above-ground autotrophic respiration (*orange dotted line*) – for the Italian Alps scenarios. (b) 2013 daily timeseries of snow depth (*blue*) and leaf CO_2 flux – the averaged daily photosynthetic CO_2 uptake (*orange solid line*) and above-ground autotrophic respiration (*orange dotted line*) – for the Italian Alps scenarios.

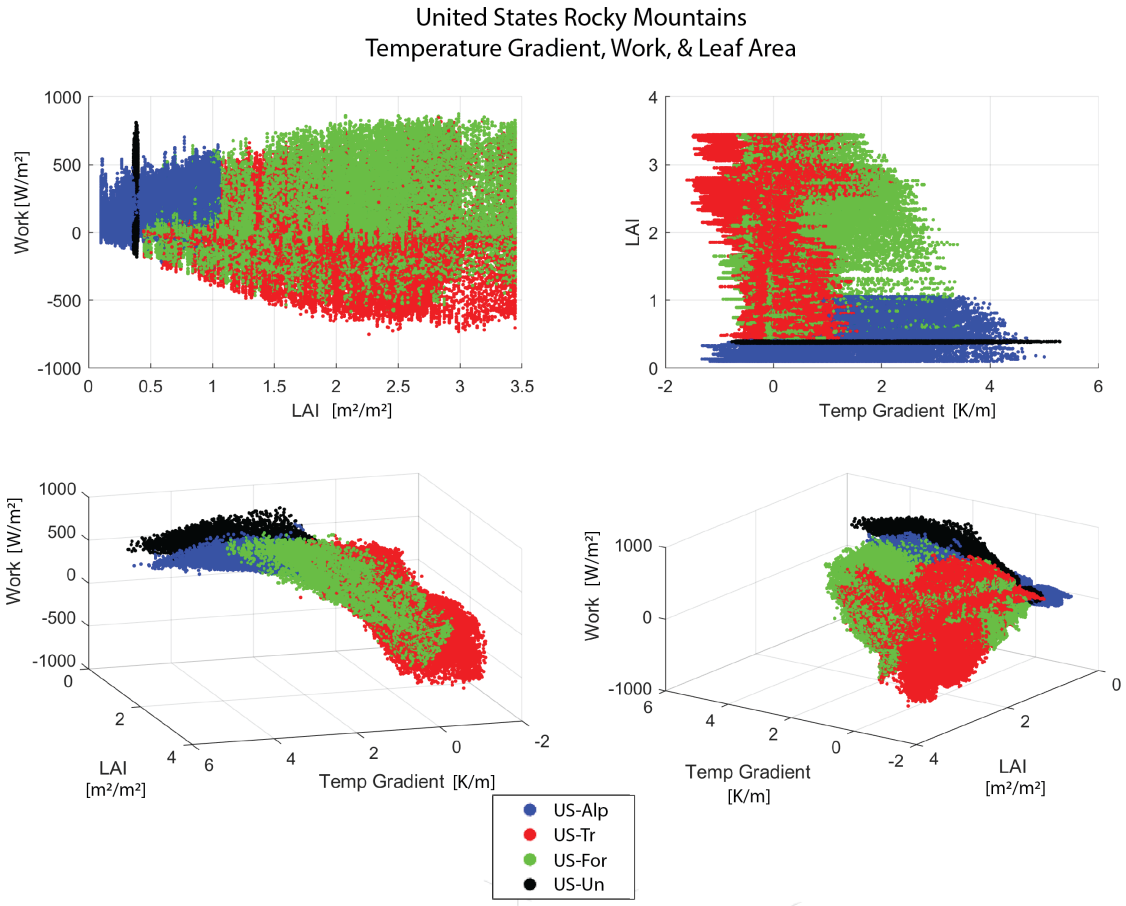

Figure A.12: Four projected views of the work, temperature gradient, leaf area index (LAI) 3D plot for the (a) Italian Alps and (b) United States Rocky Mountains scenarios. Refer to Figure 3.6 of the main text for information on the Western Canadian Taiga-Tundra scenarios. The 3D views show the transition from flatter curves to greater marginal increases in work with increases in temperature gradient as more LAI is modeled for each set of environmental conditions (i.e., alpine, subalpine). The simulated alpine forest scenario exhibits considerable negative work values since the LAI is beyond the supported limit of the local environmental conditions.